"Complete" Models of Young Stellar Objects: The Spectral Energy Distributions of Embedded YSO's With and Without Disks

Harold M. Butner
Center for Star Formation
UC Berkeley/NASA Ames Research Center

Abstract

Current star formation theories contain three components: the central source, a disk, and the collapsing envelope. In order to test star formation theories, it is necessary to study what are the observable consequences of each of the the different components. To date, most radiative transfer models have focused on a central source and either an envelope or a disk. We discuss a technique that allows us to combine all three elements (star, disk, and envelope) into a single radiative transfer model. The technique, which we refer to as the "spherical disk" approximation, allows us to assess the possible contributions of disks around embedded young stars to the overall spectral energy distribution.

We present models where disks have been added to the central source function of L1551-IRS 5, a source we have previously modeled with star and envelope alone. We discuss the implications for both the overall spectral energy distribution and the millimeter interferometer data. In addition, we discuss what effects an envelope can have on the disk and how this might change conclusions about the overall disk properties. Finally, we point out the possible effect warm envelopes can have on T Tauri systems.

1 Introduction

Terebey, Shu, and Cassen (1984-henceforth TSC) described a simple star formation model that has emerged as the standard picture in recent years. A centrally condensed core, with an initial density distribution $n(r) = n_i(r/r_i)^{-2}$, begins an "inside-out" collapse at the center. The region where infall occurs expands and inside this zone a density profile characteristic of infall, $n(r) \propto r^{1.5}$, developes as the collapse continues. If the core is rotating very slowly, centrifugal forces causes the infalling material not to collapse directly onto the central star, but instead to fall onto a disk. The material in the disk is then presumed to migrate through the disk, eventually accreting onto the star. At some point, due either to depletion of the parent molecular core or to disruption by an outflow, accretion onto the star+disk system stops. The TSC model is able to make specific testable predictions about the relationship between the young star, the disk, and the surrounding molecular envelope.

A number of authors have used spectral energy distributions to test the TSC picture. For example, Adams, Lada, and Shu (1987-ALS) modeled a number of nearby low mass young stellar objects. They found generally good agreement between the observed spectral energy distribution and the spectral energy distribution predicted using the envelope properties predicted by the TSC model. Butner *et al.* (1990, 1991) made use of high spatial resolution far-infrared data to further test the TSC model. Using a spherical radiative transport code developed by Egan, Leung, and Spagna (1988), Butner *et al.* modeled not only the spectral energy distribution but also the far-infrared spatial emission. They found that NGC 2071 and L1551-IRS 5 had density distributions similar to that expected from ALS models,ie. $r^{-1.5}$.

However, for L1551, one of the best studied protostars, Butner *et al.* (1991) pointed out two important problems for the ALS L1551 model. First, to adequately match the far-infrared flux, the total envelope column density had to be increased by a factor of two over what ALS predicted. The higher column density made the mid-infrared emission woefully inadequate compared to the observed spectra. ALS, however, had argued that a disk, not the envelope, was primarily responsible for the mid-infrared flux, since a disk would produce more mid-infrared emission than an envelope alone. It was possible that a "hot" disk, radiating in the mid-infrared, could be seen through the thick envelopes required by the far-infrared observations. If true, mid-infrared observations could be used study disk properties even in deeply embedded systems such as L1551-IRS 5.

An alternate possibility investigated by Butner *et al.* (1991) is that the dust in the envelope surrounding L1551 IRS 5 has a different dust extinction law than assumed by ALS. In Figure 1, we illustrate how two different dust extinction

laws can reproduce the far-infrared data, but predict dramatically different mid-infrared emission. Draine and Lee (1984) dust opacities (DL in figure 1) are similar to that used in the ALS models. The dust opacity law proposed by Mathis, Mezeger, and Panagia (1983, MMP in Figure 1) has more extinction in the far-infrared for the same amount of visual extinction. Alternatively, for a given amount of far-infrared extinction, the mid-infrared extinction is higher for DL dust than for MMP dust. As a result, though both radiative transfer models use similar far-infrared optical depths to match both the total flux and spatial extent of the 100 micron emission, the corresponding mid-infrared opacities are very different. The model with DL dust has significantly less mid-infrared emission escaping the envelope. Hence, any interpretation of the mid-infrared emission would appear to be highly dependent on the envelope dust properties.

The second problem was that the millimeter interferometer flux predicted by Butner *et al.* (1991) was much too small. The only way to simultaneous match the interferometer and big beam millimeter continuum fluxes appeared to be to add a disk that would radiate all the interferometer flux. Emission from the envelope would then account for the remaining flux seen in the big beam observations. However, such a disk might have sufficient far-infrared flux to alter conclusions about the envelope properties.

To address these questions, Butner, Natta, and Evans (1992) added a central disk to their L1551 model. We will outline some of their results and see what limits can be placed on the physical properties of the disk. A full discussion of the L1551 results is presented in Butner, Natta, and Evans (1992).

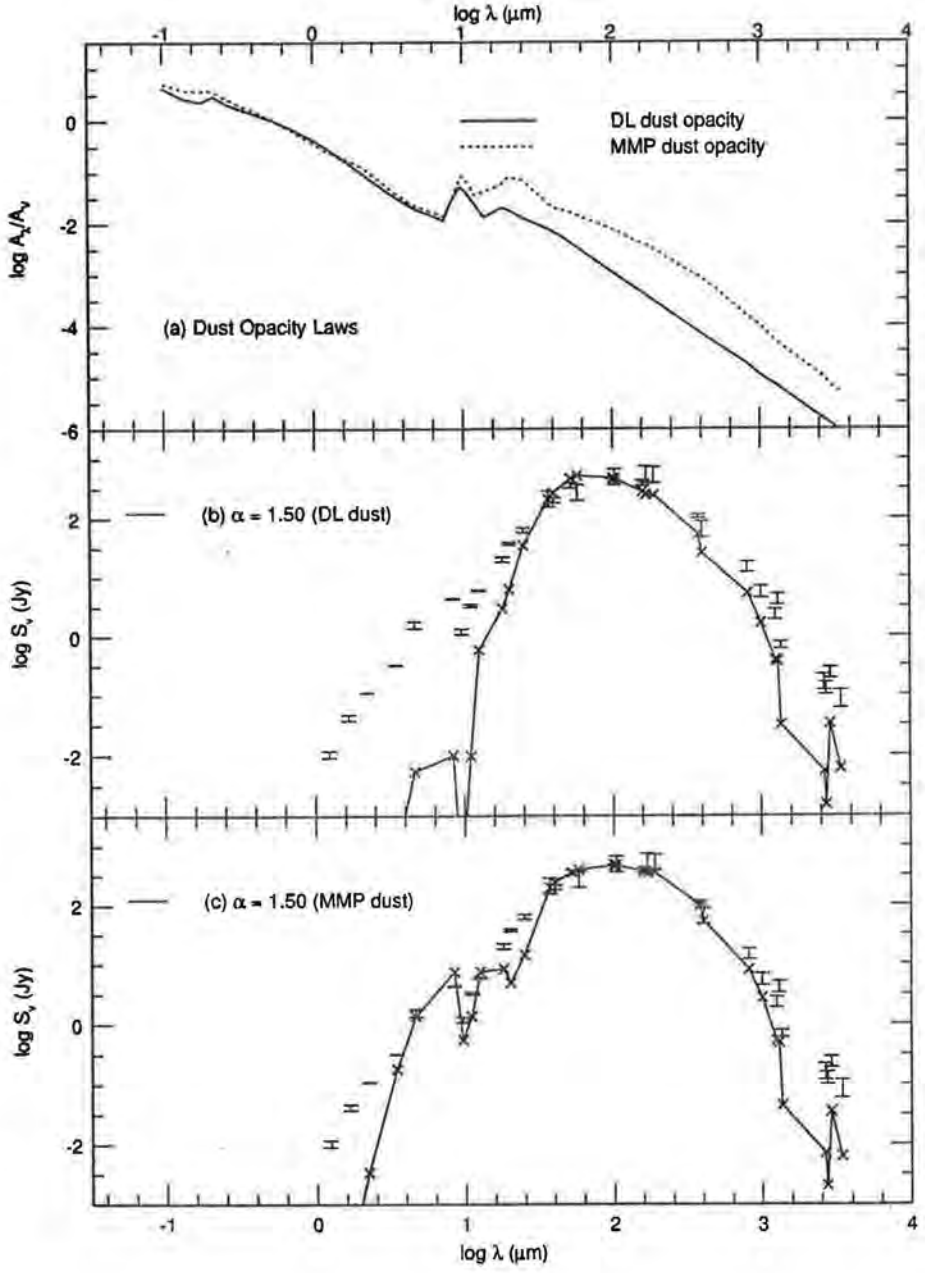

Figure 1: (a) Comparison of two different dust opacity laws: Draine and Lee (1984-DL) and Mathis, Mezger and Panagia (1983-MMP). (b) A star+envelope model for L1551 IRS 5, where a Draine and Lee (1984) type dust has been adopted. The model is fixed to reproduce the 100 micron flux and observed spatial distribution. The model fluxes have been beam-matched for comparison with the observations. (c) A star+envelope model for L1551 IRS 5, where a Mathis, Mezger and Panagia (1983) dust model has been adopted. The model fluxes have been beam-matched for comparison with the observations. Taken from Butner *et al.* (1991).

2 The Spherical Disk Model

In both Adams, Lada, Shu (1988) and Beckwith *et al.* (1990), a simple model for a disk temperature structure is presented. They consider the case of a spatially thin accretion disk. Effectively the disk surface temperature can be modeled as:

$$T(r) = T_i(r/r_i)^{-\beta} \quad (1)$$

where β is 0.75 for viscous accretion disks or simple reprocessing disks. $\beta = 0.50$ has been found by Beckwith *et al.* (among others) for T Tauri systems. (The physical mechanism responsible for such high β is not well understood.) We refer to β =0.5 systems as "active disks" in the discussion that follows.

The radiative transport code used by Butner *et al.* 1991 is a spherical radiative transport code. To handle a true disk in such a code is impossible, but we can estimate the effect of the disk's AVERAGE radiation field on the envelope. We refer to this assumption as the "spherical disk" approximation. Provided we do not attempt to model the spatial emission on size scales small compared to the inner radius of the envelope, we can use an spherically averaged disk radiation field inside the spherical radiative transport code. See Butner, Natta and Evans (1992) for details of how the models are calculated.

In Figure 2, we present the results for three different disks, a reprocessing

disk alone, a viscous accretion disk, and an "active" disk. All disk models must reproduce the observed 2730 micron interferometer flux. The total source luminosity is 28 solar luminosities, with the viscous and active disk models both splitting the intrinsic luminosities evenly between the star and disk. The viscous and active disk models include the effects of reprocessing the central star's luminosity. We also require that the source's 100 micron flux match the observations. The 100 micron flux includes contributions from star, disk and envelope. In addition, to set a minimum disk size, we treat all the disks as optically thick and determine the minimum disk size to match the observed 2730 micron interferometer flux of Keene and Masson. With these constraints, the disk radius and other parameters are presented in Table 1.

The intrinsic disk luminosities show very different profiles with the active disk producing more far-infrared flux. All the models produce a substantial amount of mid-infrared flux. However, the amount of mid-infrared flux that escapes the envelope is still small. Interestingly the cooler disks (reprocessing and viscous) have more emission escape. This is because they have larger sizes, hence larger envelope inner radii, and this leads to a lower total dust column density necessary to match the far-infrared observations. None of the disk models can contribute to the observed mid-infrared emission unless the ratio of the mid-infrared to far-infrared optical depth of the envelope is small. However, Butner *et al.* (1991) pointed out that with such dust opacity laws, a disk is not necessary to explain the observed L1551 mid-infrared emission. We are thus forced to the conclusion that the *observed* mid-infrared emission for a deeply embedded protostar is highly dependent on the *envelope properties* and not the disk properties as ALS have argued, even if the mid-infrared emission originates from the disk.

The millimeter emission from the disks all agree (by definition). However, following the lead of Keene and Masson (1990), we investigate the predicted uv visibilities from the interferometer data (Figure 3).

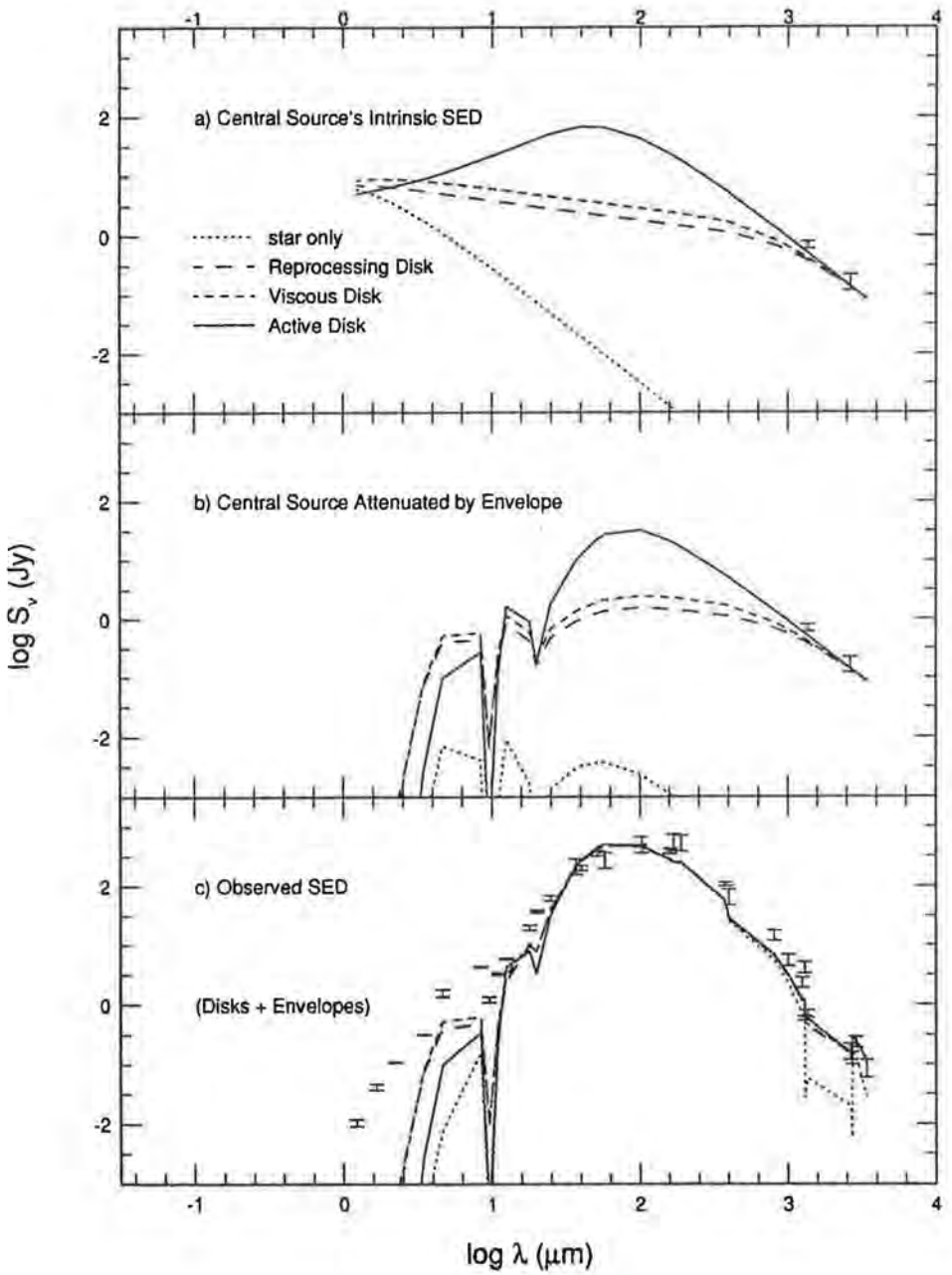

Figure 2: The top panel (a) shows the spectral energy distributions of different central sources: the dash-dotted line is a star only; the long dashed line is a reprocessing disk ($L_{int} = 0$); the short dashed line is a viscous disk ($L_{int} = 14$ solar luminosities and $q = 0.75$); and the solid line is an active disk ($L_{int} = 14$ solar luminosities and $q = 0.5$). The properties of the disks are given in Table 1. The two data points are interferometric observations at 1.3 mm (Sargent 1991) and 2.73 mm (Keene and Masson 1990). The middle panel (b) shows the spectral energy distributions of these disks (lines coded in the same way) *attenuated* by the envelopes with the properties described below. The bottom panel (c) shows the full spectral energy distributions of the central source plus envelope, for envelopes with $n(r) \propto r^{-\alpha}$ and inner radii (R_{inner}) given by the outer radii of the disks (see Table 2). For the models with disks, we have retained $\alpha = 1.5$, but we have adjusted τ_{100} to match the flux density at 100 microns and the dust opacity law at long wavelengths so that the model predictions for fluxes in big beams matches the observations at $\lambda > 1$ mm. The bottom panel also shows the observed spectral energy distribution with uncertainties. Taken from Butner, Natta, and Evans 1992.

Disk Type	q	L_{int} ($L_\odot$)	R_d (AU)	min R_d^a (AU)	min M_d^b ($M_\odot$)	$T(R_d)$ (K)
Reprocessing	0.75	0	167	>130	>1.6	5.4
Viscous	0.75	14	135	>106	>1.1	7.6
Active	0.50	14	45	>37	>0.14	69
Reprocessing[c]	0.75	0	59	>47	>0.28	95
Viscous[c]	0.75	14	48	>40	>0.19	103
Active[c]	0.50	14	43	>36	>0.15	108

Table 1: Disk Parameters

[a]Minium R_d determined by decreasing R_d of an opeque disk until the model flux density was 1σ below the observations.
[b]Minium M_d determined by keeping R_d fixed and decreasing the surface density (Σ_0) until the model flux density was 1σ below the observations.
[c]These disks include backwarming from the envelope, as discussed in the text.

Central Source	α	R_{inner} (AU)	T_{inner} (K)	T_{eff} (K)	τ_{100}
Stellar (G3)	1.5	42	240	...	0.30
Reprocessing	1.5	167	130	...	0.15
Viscous	1.5	135	135	...	0.16
Active	1.5	45	200	...	0.28
Reprocessing[a]	1.5	59	197	94	0.23
Viscous[a]	1.5	48	205	101	0.26
Active[a]	1.5	43	202	104	0.28

Table 2: Envelope Parameters

[a]These models include backwarming from the envelope in calculating the spectrum of the disk.

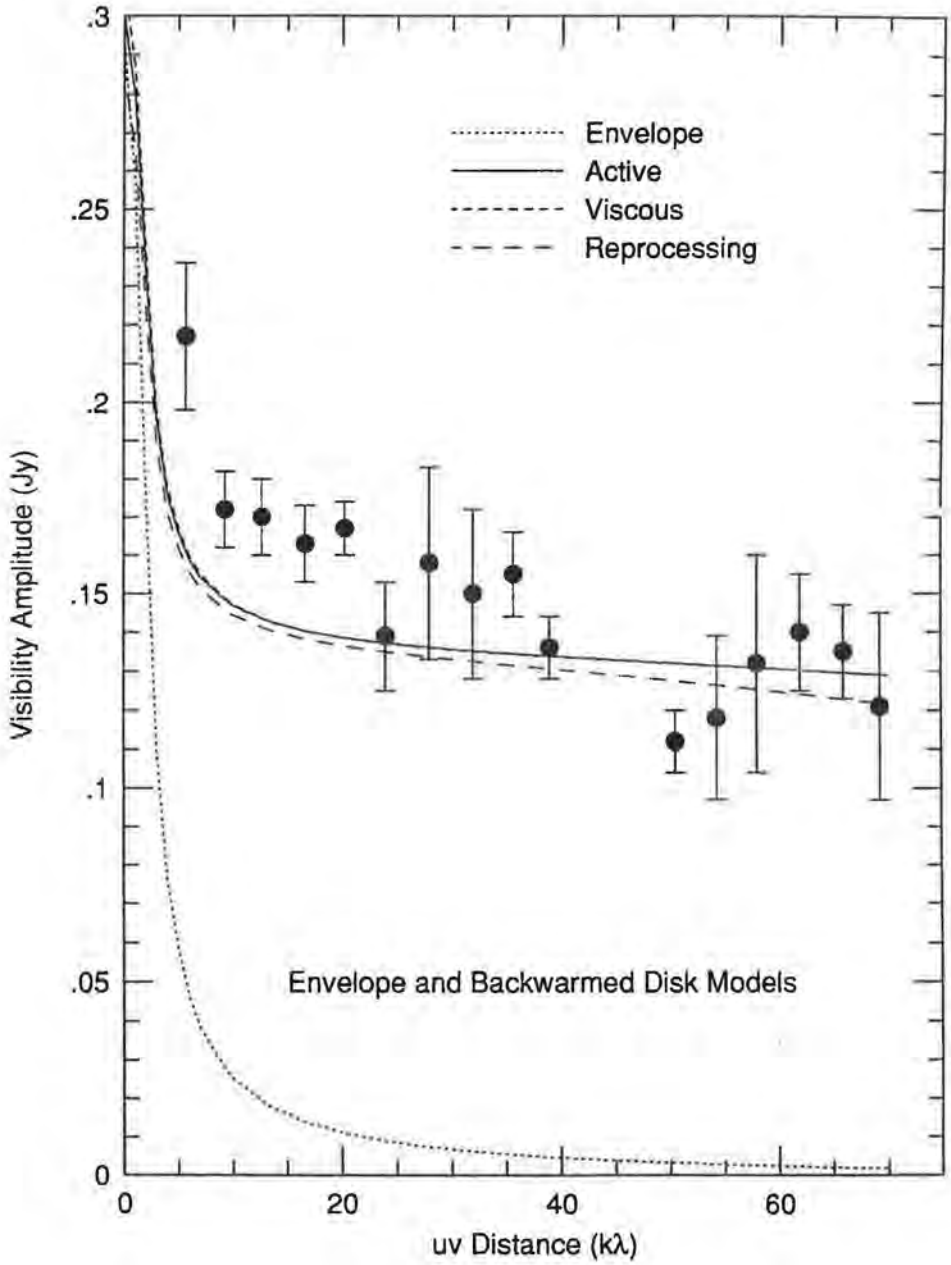

Figure 3: The visibility amplitudes at 2.73 mm, taken from figure 3 of Keene and Masson (1990) are plotted versus projected baseline. The predicted visibility amplitudes from models with various central sources and envelopes are shown as lines, with the line coding shown in the upper part of the figure. The envelope model contains only a star for a central source, but its flux has been scaled up to match the observed big beam flux. The models with active, viscous, and reprocessing disks are those whose spectral energy distributions are shown in figure 1c. Taken from Butner, Natta, and Evans 1992.

(The visibilities are a measure of the size scales where flux is detected in the interferometer beam. Small visibilities correspond to large size scales). While a pure envelope model fails, models which include the various disks do reproduce the higher visibility data moderately well. The best fit is for the active disk (which happens to be the most compact). None of the models fit the 5-25 kλ zone well, which suggests the envelope models beyond about 10-20 arcseconds radius are not complete. From Figure 3, one would conclude that some sort of disk (or other compact structure) is necessary and that an active disk is the best fit to the largest uv spacing data (smallest spatial scales).

In all cases, the derived envelope density gradient is not changed. The far-infrared emission is dominated by the envelope to such an extent that even an active disk model contributes only about one-fifth the total 100 micron flux. As a result, the envelope properties are relatively insensitive to the disk model adopted.

3 Backwarming of Disks

Keene and Masson (1990) invoked backwarming of the disk by the envelope in their source model. They argue that the disk would have a minimum temperature equal to the inner edge of the envelope. However, that is almost certainly an overestimate since the envelope's inner edge is not optically thick even in the case of L1551. The idea of a minimum disk temperature, however, seems reasonable, particularly in light of the fact that the predicted temperatures for the outer parts of a reprocessing disk could be as cold as 10 K. Using the temperature profile from our radiative transport models, we estimated the effective temperature (T_{eff}) of the cavity inside the envelope.

By constraining the disk's temperature to remain above T_{eff}, we calculated a new disk model where we determined the minimum disk radius to match the 2730 micron observed flux. We then used the new disk model as an input to a new envelope. We conserved the total system luminosity. The outer portions of the cooler disks are heated by the envelope and produce more millimeter emission. To match the observed millimeter flux, the disks must shrink. Eventually a disk size is reached such that the envelope's T_{eff} matchs the disk's temperature at the disk's outer radii. The β =0.75 disks become dramatically smaller as Table 2 illustrates. In addition, the various disk spectral energy distributions become very similar (Figure 4).

The backwarming effect also results in similar uv visibilities for all the disk models (Figure 5). The envelope properties

predicted by the various models are still similar to the conclusions reached by Butner *et al.* (1991).

Backwarming by an envelope onto the disk can dramatically alter the temperature structure of the outer disk. T_{eff} is about 50% of the inner envelope temperature for L1551, and is many times what the classic viscous or reprocessing models would predict for the outer disk temperatures. While T_{eff} is not as high as Keene and Masson envisioned, it is a significant effect for deeply embedded envelopes.

Backwarming severely constrains our ability to distinguish between different disk models given our limited knowledge of dust opacities and limited spatial resolutions.

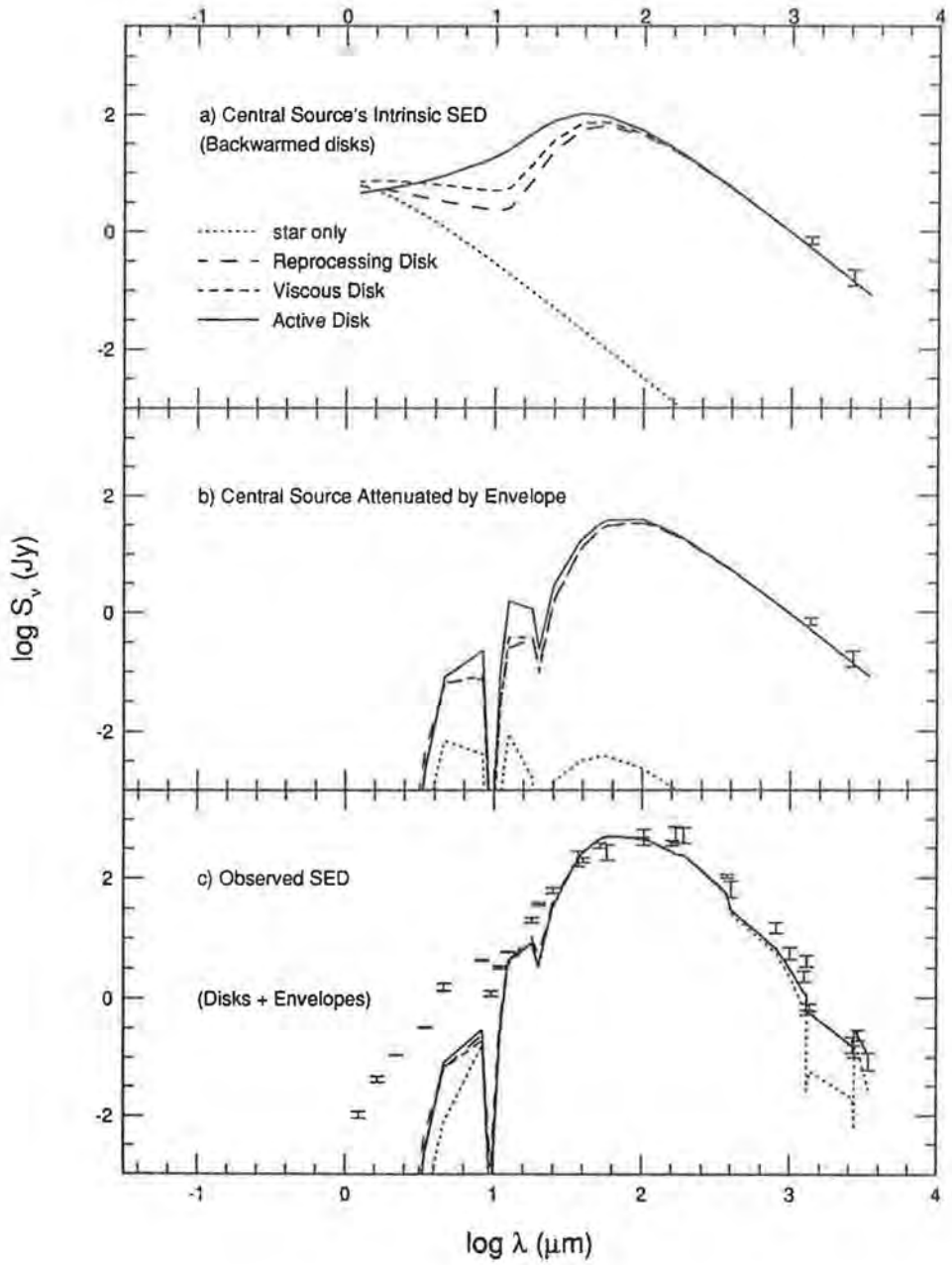

Figure 4: The same as figure 2, except that the disk temperature distributions have been calculated including backwarming by the envelope. Disk and envelope parameters are given in tables 1 and 2. Taken from Butner, Natta, and Evans 1992.

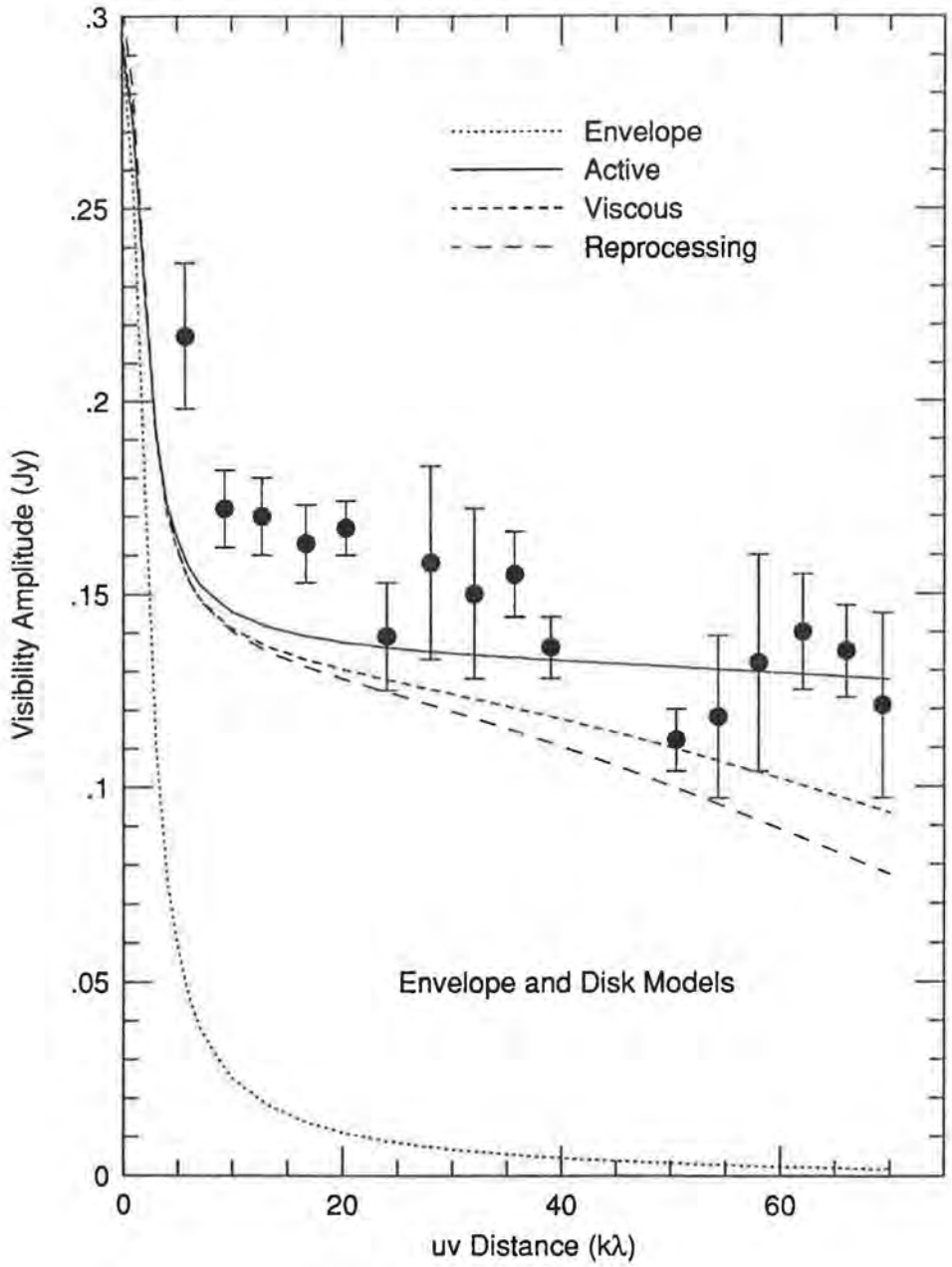

Figure 5: The same as figure 3, except that the disk temperature distributions have been calculated including backwarming by the envelope. The viscous disk model is virtually identical to the active disk model. Taken from Butner, Natta, and Evans 1992.

4 Implications for T Tauri systems

At first, the local optical depths of the dust around many T Tauri systems would seem to rule out a significant role for backwarming in heating disks. A typical line-of-sight extinction in the Beckwith *et al.* (1990) study was 2 or 3 A_V. However, as we have seen, backwarmed disks tend to look like active disks.

Since Beckwith *et al.* found 40% of the T Tauri stars they studied appeared to have disks, and most of those disks appeared to have β =0.50, it is worth exploring what effects a backwarming envelope can have on the T Tauri type disks. We consider a central source with a total luminosity of 1 solar luminosity, and an outer disk radius of 100 AU. Figure 6 shows the predicted disk temperature

profiles for a purely reprocessing disk, a viscous disk with half the luminosity intrinsic to the disk and half the total luminosity of 1 solar luminosity intrinsic to the star. An active disk model (0.5 solar luminosities in the disk and 0.5 solar luminosities for the star) is also shown.

These models are typical of the Beckwith et al. (1990) T Tauri sample.

We also calculate T_{eff} for various envelope models whose inner edge is at the radius shown (between 5 and 250 AU). The total optical depth is 2 A_V for the envelope, and the central source luminosity is 1 solar luminosity. We plot T_{eff} for two different density gradients ($n \sim r^{-\alpha}$). There is little difference in the T_{eff} for different density gradients. The important thing to note is that the viscous and purely reprocessing disks would be warmed by the envelope. Hence a β =0.75 disk could produce as much millimeter emission as the intrinsically warmer active disk model.

There is another implication in the presence of a surrounding envelope about a disk. Such envelopes are very efficient at producing far-infrared flux. For the T Tauri sources, the FIR data is from IRAS, which has a large beam. For the A_V under consideration, and for the models we describe, a few Jy of flux is predicted for the IRAS beamsize. This is comparable to what an active disk might produce. Why is this crucial? *Beckwith et al. use the MIR/FIR ratio to calcaculate β. If some fraction of the FIR is coming from an envelope and not the disk, then their estimate of β is too high.* This criticism can be applied to *any* disk analysis that uses MIR/FIR ratios to set β and assumes the absence of a surrounding dust envelope.

Natta (1992) has also considered the effects of scattered light from an envelope and found that scattered light alone could modify a classic viscous accretion disk spectrum to resemble the β =0.5 models. When both scattering and backwarming are considered, it seems that many of the spectral energy distribution features attributed to β =0.5 models can be accounted for by more traditional disk models *surrounded* by envelopes.

A more detailed discussion of the implications of envelopes on the question of disk properties around T Tauri stars is in preparation. (Natta 1992, Butner 1992).

5 Conclusions

1. The dust opacity properties assumed for the dust in envelopes has a profound effect on the predicted spectral energy distribution of young stellar objects. Dif-

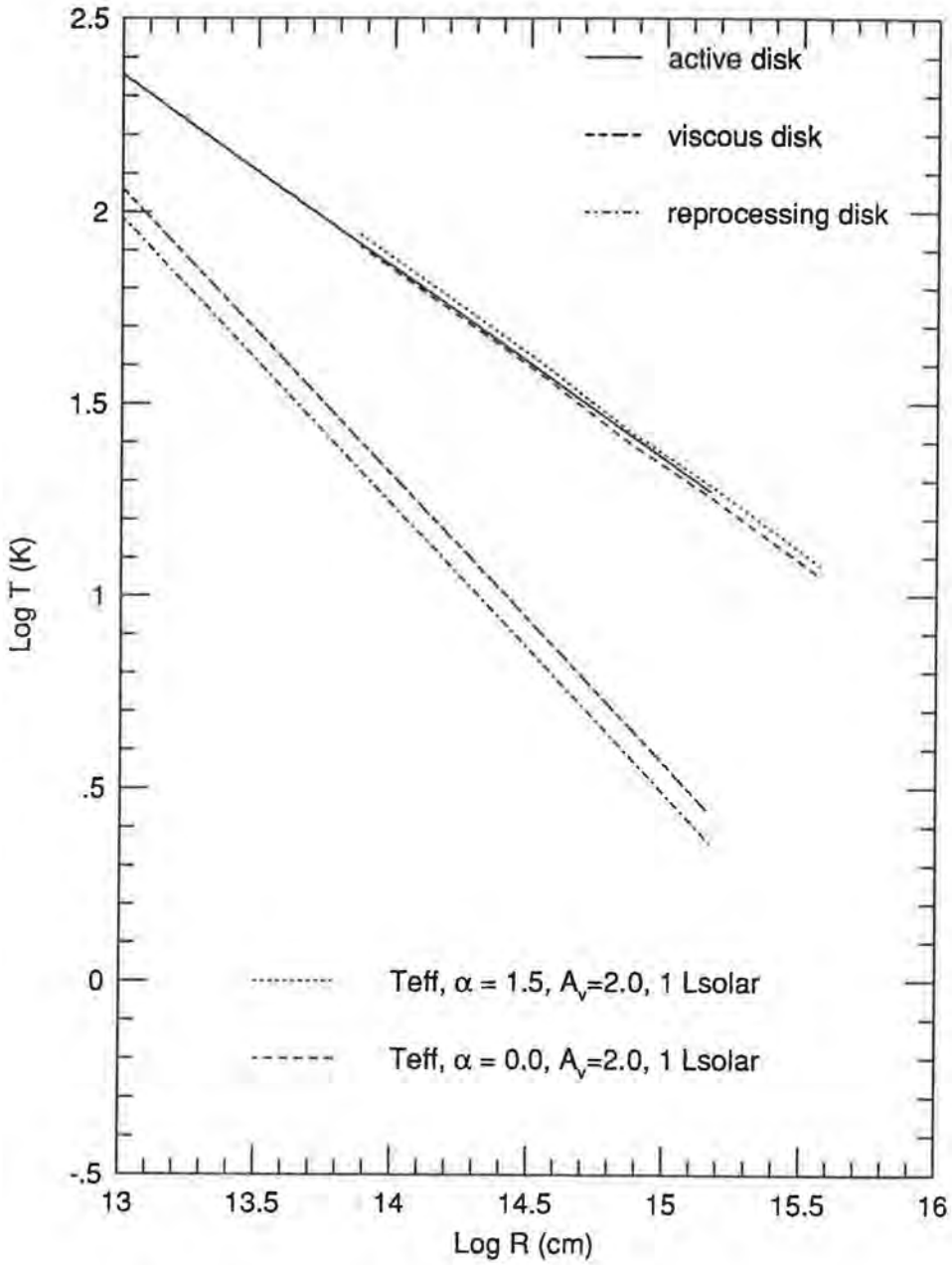

Figure 6: We present the temperature profiles for three disk models: an active disk (0.5 solar luminosities for the disk and 0.5 solar luminosities for the star), a viscous disk (same luminosity as the active disk), and a reprocessing disk (stellar luminosity equal to 1.0 solar luminosities). In addition, we plot the T_{eff} for two different sets of envelopes surrounding a central source of 1 solar luminosity and temperature 5500 K. The envelope's total visual extinction is fixed at 2 A_V. These parameters are typical of the Beckwith *et al.* 1990 T Tauri sample.

ferent source models will be favored depending on the dust model adopted. As a result, the presence of mid-infrared emission from deeply embedded sources cannot be used as a unique signpost for the presence of disks.

2. In the absence of backwarming from the envelope, L1551's interferometer millimeter emission seems best explained by an active (β=0.5) disk.
3. Backwarming can be important in moderating the disk temperature profile. If backwarming is important for L1551, then available data can not distinguish between different β disk models.
4. The presence of the disk does not alter the derived density gradient for the envelope surrounding L1551 IRS 5. The envelope has a density gradient $r^{-1.5}$ based on the far-infrared data, consistent with infall.
5. Envelopes can have important implications for the derivation of disk properties due to backwarming or scattering by the envelope, even around systems where the total envelope optical depth is quite low. Hence, T Tauri systems may contain classic viscous disks surrounded by a thin envelope and have a β =0.5 spectral energy distribution.

References

Adams, F. C., Lada, C. J., Shu, F. H. 1987, Ap. J., 312, 788 (ALS).

Adams, F. C., Lada, C. J., Shu, F. H. 1988, Ap. J., 326, 865.

Beckwith, S. V. W., Sargent, A. I., Chini, R. S., & Güsten, R. 1990, AJ, 99, 924.

Butner, H. M., Evans, N. J. II, Lester, D. F., Levreault, R. M., and Strom, S. E. 1991, Ap. J., 376, 636.

Butner, H. M., Natta, A., and Evans, N. J. II 1992, Ap. J., in press.

Butner, H. M., 1992, Ap. J., in preparation.

Egan, M. P., Leung, C. M., and Spagna, G. F. Jr. 1988, Comput. Phys. Comm., 48, 271.

Draine, B. T., and Lee, H. M. 1984, Ap. J., 285, 89.

Keene, J., and Masson, C. 1990, Ap. J., 355, 635.

Ladd, E. F., Adams, F. C., Casey, S., Davidson, J. A., Fuller, G. A., Harper, D. A., Myers, P. C., and Padman, R. 1991, Ap. J., 366, 203.

Mathis, J. S., Mezger, P. G., and Panagia, N. 1983, A.& A., 128, 212.

Natta, A., Palla, F., Butner, H. M., Evans, N. J. II, and Harvey, P. M. 1992, Ap. J., submitted.

Natta, A., 1992, Ap. J., in preparation.

Sargent, A. I. 1991, private communication.

Terebey, S., Shu, F. H., and Cassen, P. 1984, Ap. J., 286, 529 (TSC).

Numerical Simulations of the Formation of Protostellar Discs

H. Pongracic, S.J. Chapman, J.R. Davies, J.A. Turner,
M.J. Disney, A.H. Nelson & A.P. Whitworth
Department of Physics and Astronomy,
University of Wales, College of Cardiff,
PO Box 913, Cardiff CF2 3YB

Abstract

We report here the results of the first computer simulations capable of following the condensation of protostars out of turbulent interstellar gases. These protostars are rotationally supported discs with masses in the range $2 - 20$ $M_\odot$ and diameters from $100 - 4000$ AU. In many of our simulations multiple protostellar systems were formed.

1 Introduction

Observations show that stars form predominantly in Giant Molecular Clouds (GMCs). These GMCs have been resolved into a fractal hierarchy of clouds within clouds on scales ranging down to ~ 0.01 pc (Blitz & Thaddeus (1980), Scalo (1987), Perault, *et al.* (1985), Falgarone & Phillips (1991)). The clumpiness is thought to have been generated by turbulent motions within the GMC. The level of the fractal hierarchy that we explore in our computer simulations have a scale-length of ~ 1 pc and masses $\sim 10^2$ $M_\odot$. These lumps of the GMC we shall refer to as subclouds.

What could trigger regions within a GMC to become locally unstable and to contract under their own self-gravity and form stars? There are several mechanisms that may cause such a gravitational collapse. Thermal instabilities can result due the formation of molecular coolants or the decline of a local heat source (Chieze & Boisanger (1991)). Tidal stresses induced by passing field stars or subclouds (de Felice & Sigalotti (1991)) can cause regions of enhanced density to form and then fragment and collapse. A collapse will also result when the magnetic support of a region is gradually removed via ambipolar diffusion (Shu *et al.* (1987)). The mechanism that we have investigated is the shock compression which can occur in the supersonic collision of the subclouds described above (Scoville *et al.* (1986), Vallée & Avery (1990)).

We are also interested in finding an answer to the question of why it is that most stars are part of a binary and multiple system (Zinnecker (1989)). To this end, we have developed a computer program using some efficient numerical algorithms. This has enabled us to simulate the processes involved in the star formation regions within a GMC.

We use spherical random distributions of particles to represent the subclouds, and give them parameters that are similar to those obtained by observations (see below). These computer subclouds are then fired at one another with differing impact parameters, velocities etc. and the subsequent evolution of the system followed. We present here just

a few examples of our results to date. Section 2 describes the computer algorithms that we have used, Section 3 describes our results, and the final section, Section 4, presents some concluding remarks.

2 Method

To perform realistic simulations, we require a computer code that can accurately handle the highly disordered gas flows present in star formation regions, and can follow the large dynamical changes that occur when interstellar gas ($\rho \sim 10^{-21}$ g cm^{-3}) gets converted into stars ($\rho \sim 1$ g cm^{-3}). We have developed such a code (Pongracic *et al.* (1991)) by combining the particle techniques of Tree Code Gravity, TCG (Barnes & Hut (1986), Hernquist (1987)) with that of Smoothed Particle Hydrodynamics, SPH (Lucy (1977), Gingold & Monaghan (1977)).

In TCG, the gravitational force experienced by a particle due to all the other particles is calculated by carrying out a direct summation over near particles, while more distant particles are grouped into successively larger collections (clusters) and their contribution to the force found by performing a multipole expansion about the centre of mass of each cluster. This is done for all the particles in the computational domain. This has great savings over the more traditional direct summation approach, due to the approximations made in performing the multipole expansion. A tolerance criterion determines whether a group of particles at a given distance gets resolved into individual particles and subclusters, or remains a single entity. The clustering information in this method is stored in a tree data structure — hence the name Tree Code. Our code makes full use of the intrinsic vector functions available with modern CRAY compilers, to build this tree structure, and to extract information from it when evaluating the force on a particle.

In SPH, the particles represent extended fluid elements, which overlap in such a way that they have continuum properties rather than corpuscular properties. The pressure-force at any point within this continuum is calculated by performing a summation over nearby particles — the contribution from each particle being weighted according to some distribution function (known as a kernel). The near-neighbours of each particle are found by examining the data stored in the tree structure created by the TCG. Thus this method is as fast as the TCG algorithm, and we have again used the intrinsic CRAY vector functions to make the extraction of the near-neighbour data more efficient. The kernel used in the evaluation of the pressure forces has a finite size. There are a number of reasons why we require it to be finite. One is that if it were too large, then we would need to perform a direct summation over a sizeable fraction of the computational domain — hence making the time required to perform the simulations unacceptably large. Another reason is that in real fluids, quantities are localized and information travels with the sound speed of the fluid. A final reason however is that the resolution of the code is the size of the kernel, and by making it vary as a function of the density, such that in regions of high density we have a small kernel, and *vice-versa*, we have been able to simulate large changes in the density and linear size of regions within a fluid. Typically we chose the size of the kernel such that there are around 50 near-neighbours in the summation.

The advantage of such a code is that it is three-dimensional, fully Lagrangian and there are no geometric constraints (*i.e.* no restrictions to spherical or cylindrical problems, or clumsy interpolation onto grids). Due to the use of a tree-structure, the computational

cost goes as $\sim O(N \log N)$, where N is the number of particles used in the simulation and $\log N$ a measure of the number of levels in the cluster hierarchy. (Compare this with direct summation methods that have computational times that scales as $\sim O(N^2)$.) The code has been comprehensively checked using a number of different test problems.

The gas in our simulations has a piecewise polytropic equation of state which mimics the expected behaviour of real interstellar gas. This equation of state is given by

$$\begin{aligned} P = &\quad a_0^2 \rho_0^{2/3} \rho^{1/3} + a_1^2 \rho \quad \rho > \rho_0 \\ P = &\quad a_0^2 \rho \qquad\qquad\qquad\quad \rho < \rho_0 \end{aligned}$$

where $a_0 = 0.57$ km s^{-1} is the sound speed representative of molecular hydrogen at 100 K for densities less than $\rho_0 = 300$ cm^{-3} and where $a_1 = 0.18$ km s^{-1} is the sound speed representative of molecular hydrogen at 10 K for densities greater than $\sim 10^4$ g cm^{-3} . For intermediate densities the gas cools as the density increases. The radiative cooling implicit in this equation of state greatly increases the compression factors that can occur, even when the subclouds collide at relatively modest supersonic velocities. When the protostellar discs that we form in the simulations become rotationally supported, the trapping of cooling radiation is just beginning to occur. If we were to evolve the discs further we would need to take this effect into account.

Using this code we have been able to follow density increases of up to factors of $\sim 10^{10}$ times that of the initial density. Compare this with previous authors who have obtained increases of only, at most, 10^4 (*e.g.* Stone (1970), Hausman (1981), Gilden (1984), Lattanzio *et al.* (1985), Hunter *et al.* (1986), Nagasawa & Miyama (1987), Monaghan & Varnas (1988)).

3 Results

We will discuss here just four examples of our work. We have chosen these particular examples because they illustrate the variety of initial conditions that we feel that our code can accurately model. The first and second simulations describe the collisions between two subclouds at different impact parameters. The third treats the effects of another level of the fractal hierarchy of a subcloud. Whereas the fourth simulation collides three subclouds in an attempt to form the ridge-like star formation structures found by some observers. The first three simulations use around 4000 particles, the fourth uses around 8000 in total.

3.1 Head-on collision

The first simulation starts with two equal, uniform density , uniform temperature, spherical subclouds. These subclouds approach one another head on (*i.e.* impact parameter, $b = 0.0$ pc) at a relative speed of 1.62 km s^{-1} (Mach 2.8). (Mach numbers are quoted relative to the sound speed of the gas that has just entered the cooling portion of the equation of state at the low density end (0.57 km s^{-1}).) The subclouds each have mass 75 M$_\odot$, radius 1 pc, and density 300 cm^{-3} and are stable against contraction. They are not however in detailed hydrostatic balance and immediately start to expand; they are therefore only transient, which we presume turbulent features would be. Calculations where the subclouds have been in detailed hydrostatic balance and are contained by a

hotter, more rarefied (inter-subcloud) gas which entirely encompasses the subclouds have been performed. They are qualitatively similar — they form protostars.

Figures 1a-d show a sequence in the evolution of the collision. Figure 1a displays the initial condition of the simulation. The next figure, Figure 1b, shows the particle positions after 0.96×10^6 years. Notice the formation of a dense shocked layer, which is even more evident in Figure 1c. It is around the time of Figure 1c (1.45×10^6 years) that a protostellar object has condensed out of the shocked layer — although it cannot be seen on the scale of Figure 1. This object reaches a density of 10^{10} times the initial density of the subclouds, and its collapse is halted in two dimensions by rotation — this results in the formation of a protostellar disc. (The presence of small amount of angular momentum is due to the centers of mass of the two subclouds being slightly off-axis at the start. This is due to the random way in which the particles were initially positioned.) Figure 1d shows the system at the end of the simulation (1.60×10^6 years). To demonstrate that we are able to model large density contrasts, we display in Figure 2 the logarithm of the density at each particle projected along the collision axis ($t = 1.6 \times 10^6$ years). In Figures 3a-c we zoom in (by a factor of ~ 200) and show this high density region in more detail, and along the other axes. Notice the flattening along the y-axis indicating that this is a disc rotating about this axis. To best display the nature of the object formed we show in Figures 4a-c velocity vectors for the particles projected onto the (x,y), (x,z) and (y,z) planes respectively. The fact that the object is rotating about the y-axis is fortuitous; we have performed a number of simulations in which the rotation axis makes an arbitrary angle to the axes. The disc formed here has a radius of ~ 400 AU and a thickness of ~ 80 AU. When it first forms it has a mass of 16.5 $M_\odot$ and it is still accreting material at a rate of 1.4×10^{-3} $M_\odot$ yr^{-1} at the end of the simulation.

3.2 Non-zero impact parameter

The next model that we shall describe has a non-zero impact parameter ($b = 0.4$ pc). The two subclouds again have a uniform density, a uniform temperature and are spherical in shape. They each have a mass of 75 $M_\odot$ and radii 1 pc. The formation mechanism of the protostellar discs in this simulation is described in more detail in Chapman *et al.* (1992a), but we will briefly sketch their evolution. In a similar way to the head-on collision, a dense shocked layer is formed. This layer then breaks up into a number of fragments, and a complex series of mergers and orbit mixing occurs to form the end result — a stable binary system. We show this in Figures 5a-d. Figures 5a and 5b shows the initial ($t = 0.0$) and the final particle positions ($t = 2.82 \times 10^6$ years) on the same scale. Figure 5c displays the point in the simulation ($t = 2.12 \times 10^6$ years) at which the shocked layer fragments, while Figure 5d show the end result after a number of mergers have taken place ($t = 2.82 \times 10^6$ years). Figure 5d is zoomed in by a factor of 50. The two discs formed have masses of 12.8 and 5.6 $M_\odot$, and diameters 4,000 and 300 AU respectively. The two objects are separated by 11,500 AU. Due to the large amount of rotational angular momentum in the bigger disc, it retains quite a large size. When the simulation ends, the protostellar discs have undergone two orbits and appear to have stabilized.

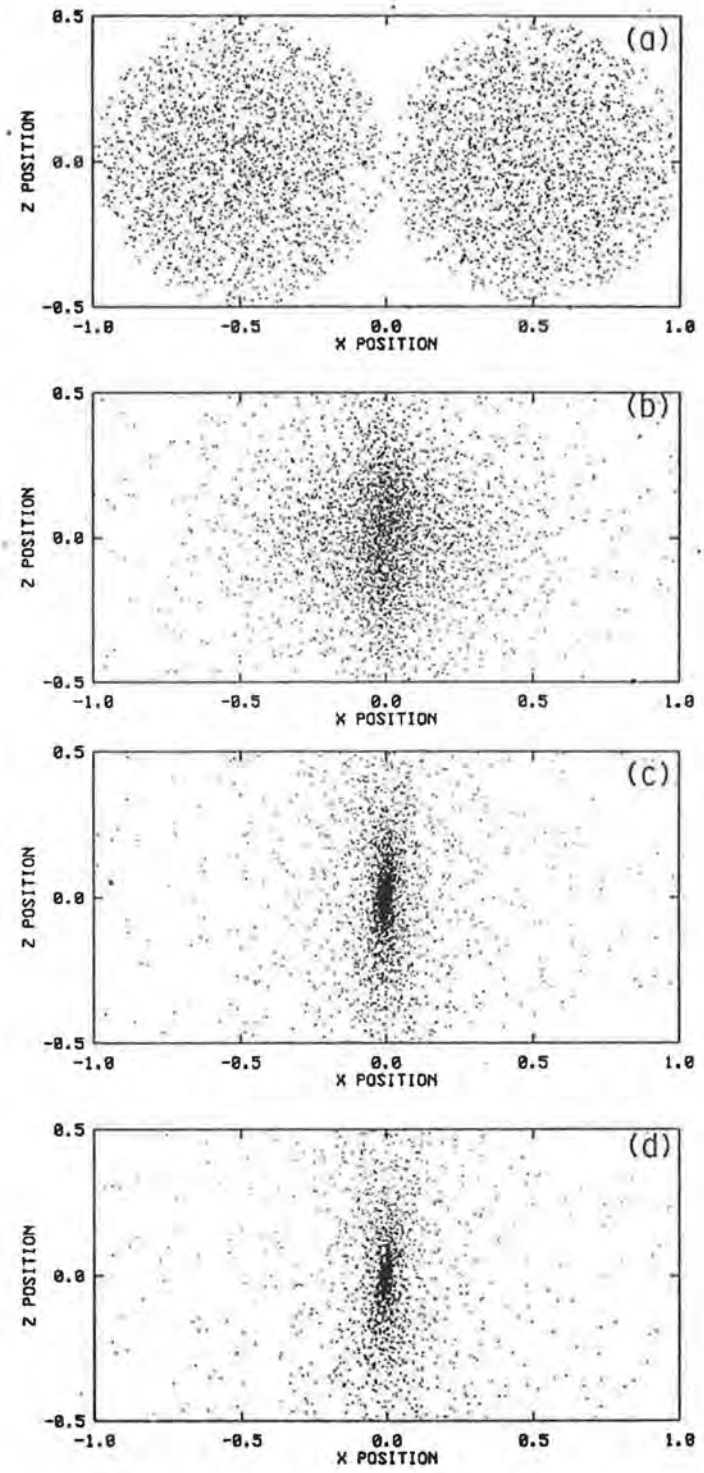

Figure 1: Head-on (b = 0.0 pc) collision. Particle positions are plotted on the (x,z)-plane at times: (a) t = 0.0; (b) $t = 0.96 \times 10^6$ year; (c) $t = 1.45 \times 10^6$ years; and, (d) $t = 1.60 \times 10^6$ year. The length unit is 2 pc.

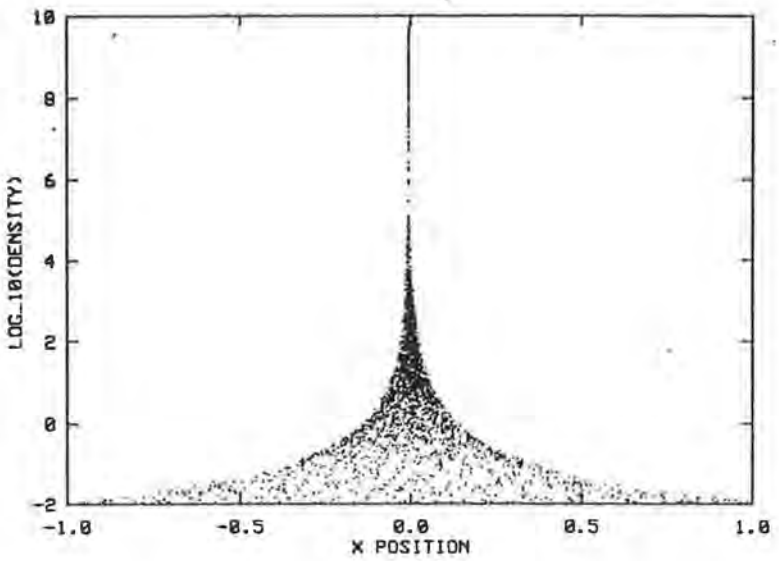

Figure 2: Head-on ($b = 0.0$ pc) collision. The logarithm of the density is plotted for each particle against the x-axis at time 1.60×10^6 years. The density unit is 200 cm^{-3}

3.3 A subcloud with internal structure

Again this simulation is described in Chapman *et al.* (1992a), so only a brief description is given. The initial conditions correspond to just one of the subclouds in the previous example. We were interested in what would happen if we descended one more level down the fractal hierarchy of a GMC. Therefore the subcloud in this simulation is made up of 20 sub-subclouds. These sub-subclouds are moving randomly with respect to one another within the subcloud and are approximately virialized. Each sub-subcloud has mass 4 $M_\odot$ and radius 0.2 pc with a mean separation of 0.6 pc. The regions between the sub-subclouds is occupied by 20 $M_\odot$ of a hot rarefied gas. The initial conditions are shown in Figure 6a. The sub-subcloud collisions are highly inelastic, and their bulk kinetic energy is quickly dissipated — the dense layer that results is shown in Figure 6b (this is at a time 0.78×10^6 years). In Figure 6c we zoom in by a factor of 30 at the point in time when the protostars first form ($t = 0.78 \times 10^6$ years). As can be seen, there are four discs — each having their rotation axes oriented in different directions. They are orbiting one another in a hierarchical manner (*i.e.* two protostar pairs each orbiting their center of mass while they in turn orbit the center of mass of the whole system). After a number of orbits one of the pairs merge to form a single disc surrounded by a spherical halo of accreting material. At the end of the simulation ($t = 0.82 \times 10^6$ years) 80% of the mass in the region shown in Figure 6d is in the protostars and the surviving close binary pair has completed six orbits, and appears to be quite stable. The third component of the system has also completed an orbit, which is circular and also appears to be stable. The masses of the close pair are 11.2 and 4.9 $M_\odot$ and they have diameters 600 and 150 AU with a separation of 1200 AU. The third protostar has mass 8.8 $M_\odot$ and diameter 400 AU with the surrounding halo extending out to 800 AU from the center of the disc. This third component orbits at a distance of 7500 AU from the close pair.

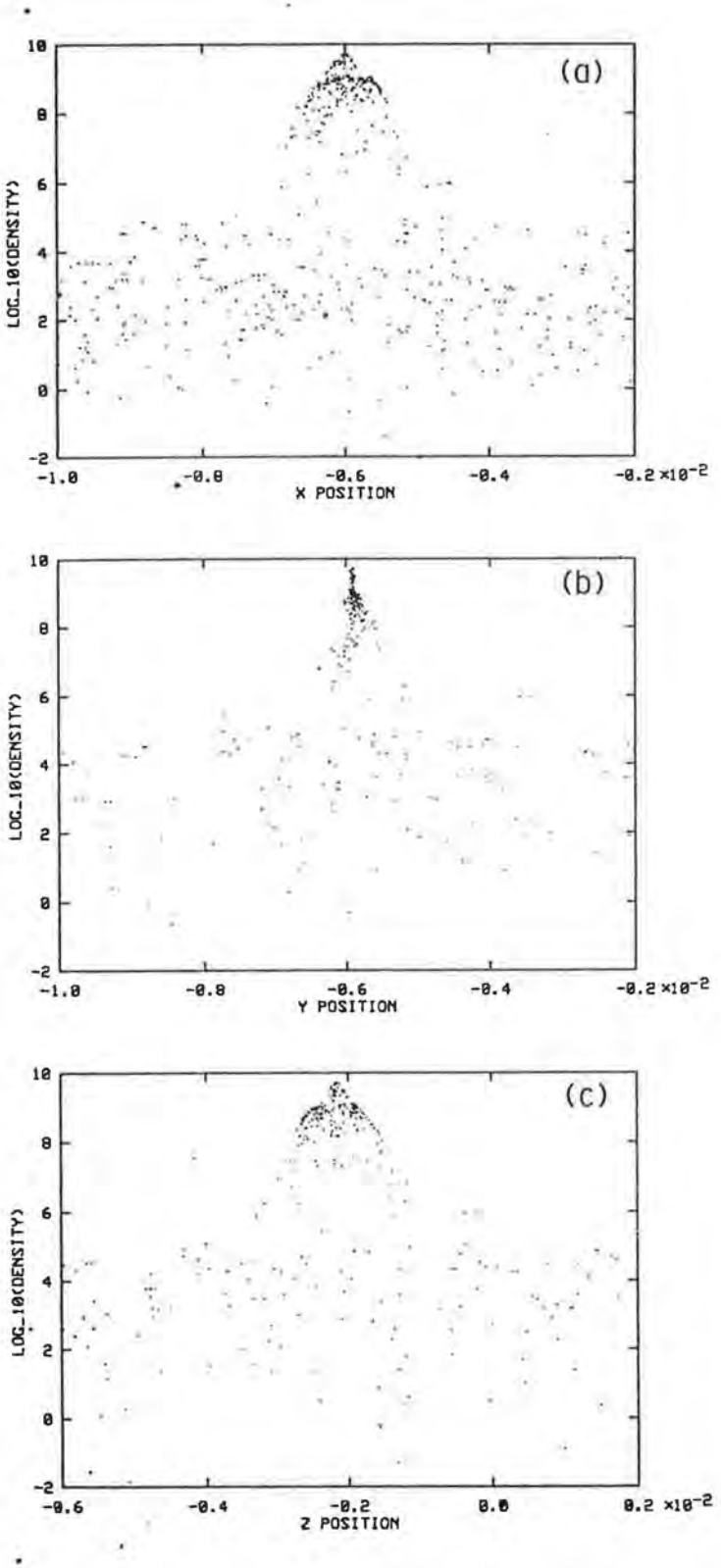

Figure 3: Head-on ($b = 0$ pc) collision. Close-up of the protostar formed in the collision at $t = 1.60 \times 10^6$ years. The logarithm of the density is plotted for each particle against: (a) its x-coordinate; (b) its y-coordinate; and (c) its z-coordinate. The apparent core-halo structure is a transient feature. The density unit is 200 cm^{-3}

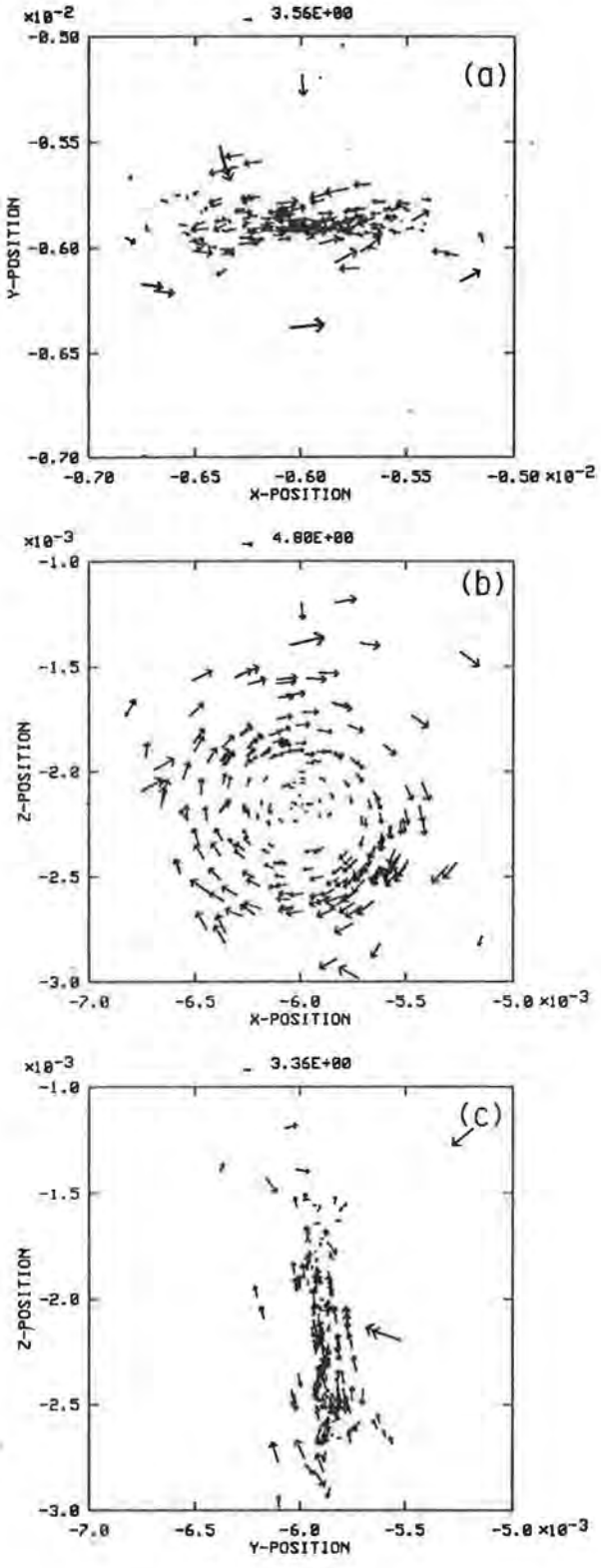

Figure 4: Head-on ($b = 0$ pc) collision. Close-up of the protostellar disc ($t = 1.60 \times 10^6$ years) formed in the collision. The particles are represented by vectors — the size and direction giving the velocity of the particle in the (a) (x,y), (b) (x,z), and (c) (y,z) plane. The largest velocities shown are ~ 7 km s^{-1} .

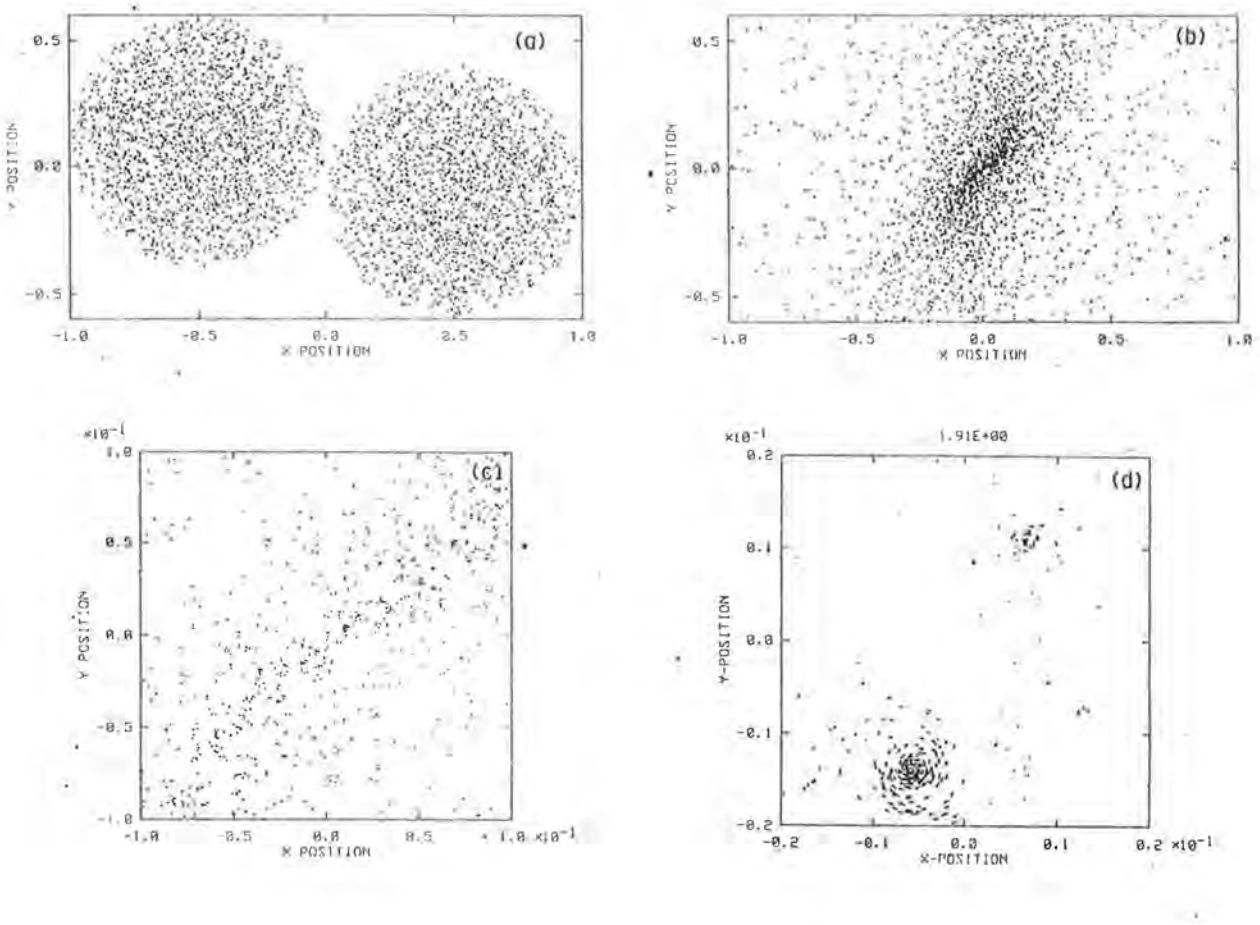

Figure 5: Non-zero impact parameter ($b = 0.4$ pc) collision. (a) and (b) show the particle position projected onto the (x,y)-plane at $t = 0.0$ and $t = 2.03 \times 10^6$ years. (c) is a factor of 10 enlargement of the compressed layer shown in (b) — notice how it has broken up into a number of fragments. (d) is another enlargement (this time a factor of 50) showing the binary pair of protostars at $t = 2.82 \times 10^6$ years. In this figure, we plot velocity vectors at the particle positions (largest velocities are ~ 2.4 km s^{-1}). The length scale in these figures is 2 pc.

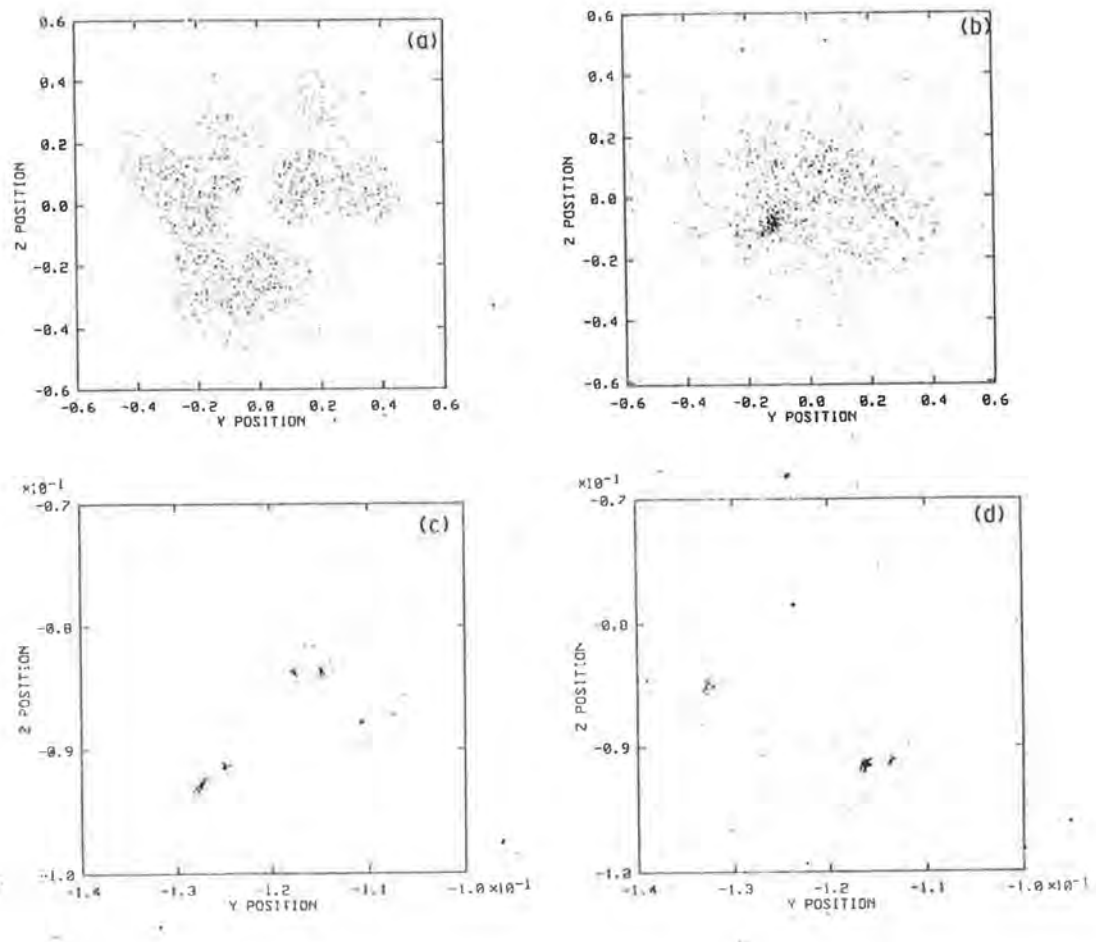

Figure 6: A subcloud with internal structure. Particle positions in all the figures are projected onto the (y,z)-plane. (a) The subcloud at $t = 0.0$. Notice that it no longer has a uniform density. (b) The subcloud at $t = 0.78 \times 10^6$ years plotted on the same scale as (a). (c) Close-up (zoomed in by a factor 30) of the hierarchical binary formed at $t = 0.78 \times 10^6$ years. (d) Close-up on the same scale as (c) showing the final stable hierarchical binary system ($t = 0.82 \times 10^6$ years). The length unit is 2 pc.

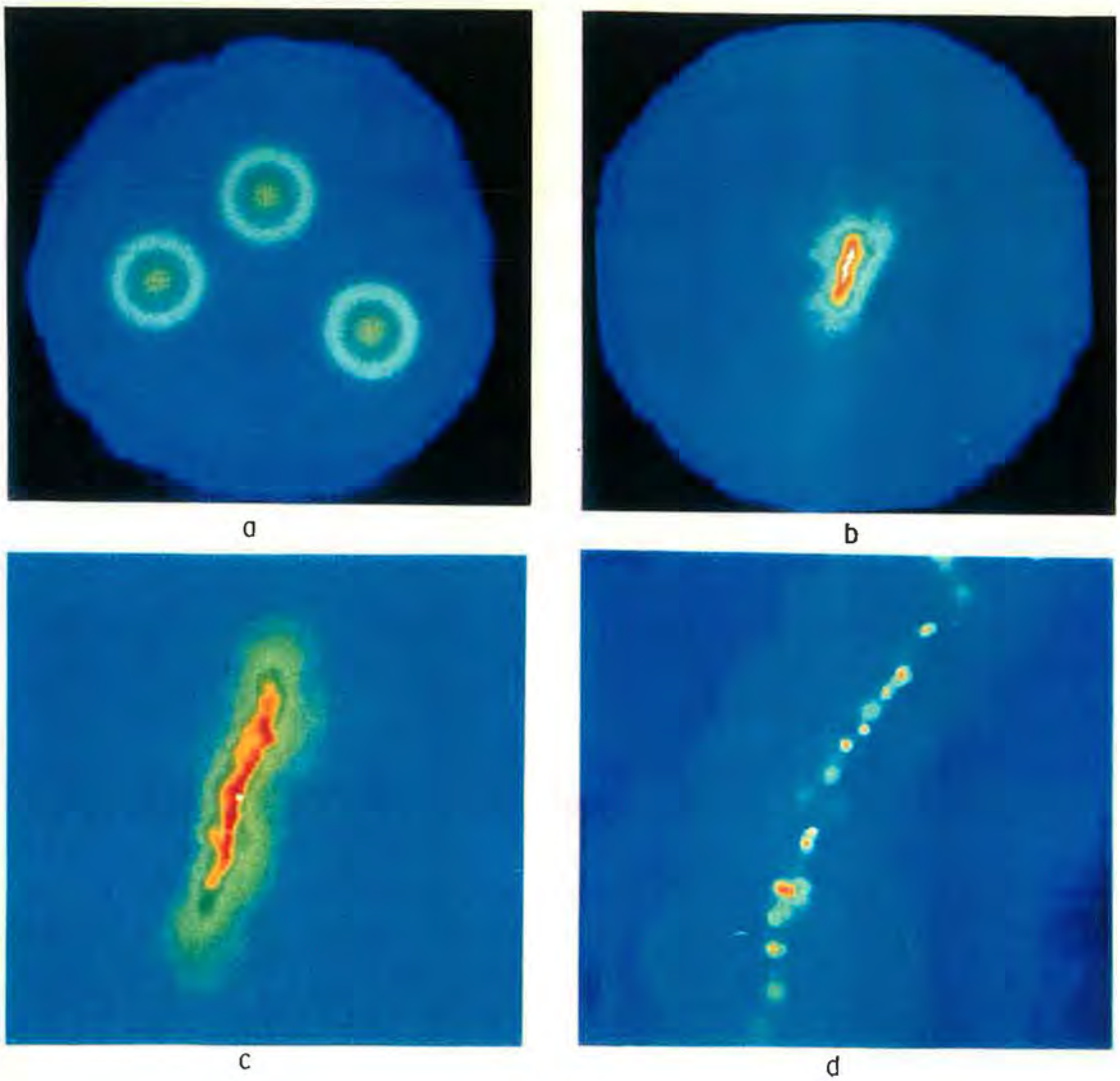

Figure 7: Three-subcloud collision. In this set of figures, instead of displaying particle positions we plot the column-density, σ, through the computational domain using a grey scale representation ($\Delta \log_{10}(\sigma) = 5$). (a) shows the initial configuration — three subclouds about to collide. (b) shows the result of such a collision after a time $t = 1.02 \times 10^6$ years. (c) and (d) are zoomed-in (by factors 3 and 10 respectively) views of the extended linear feature shown in (b). (d) displays ~ 10 protostellar discs. The region shown in (a) is 6×6 pc.

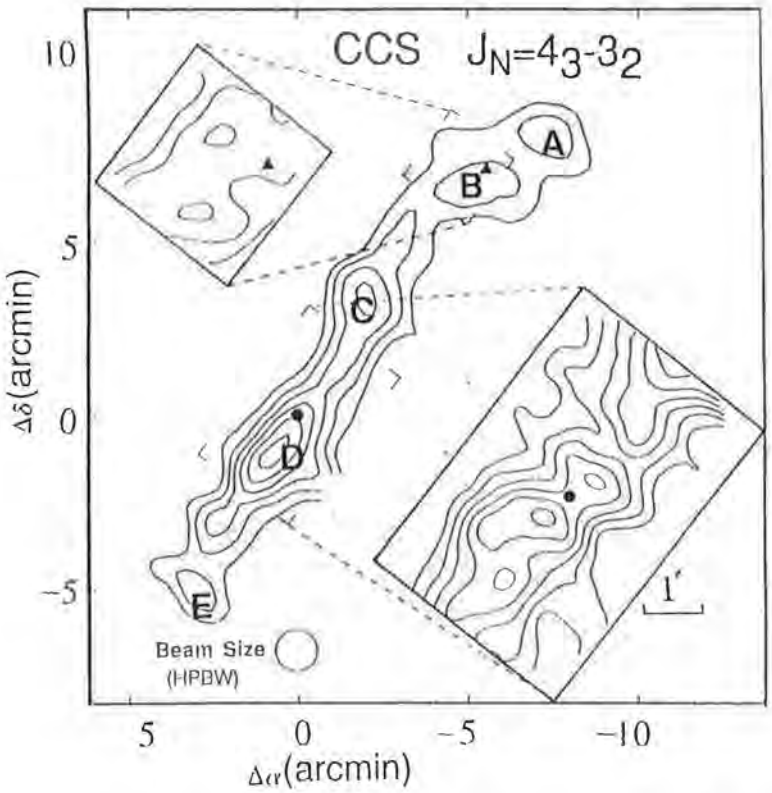

Figure 8: Integrated intensity map of CCS line ($J_N = 4_3 - 3_2$) of a region in Taurus Molecular Cloud-1. Taken from Hirahara *et al.* (1992).

3.4 Three-subcloud collision

We have increased the number of subclouds in the system to three with the eventual goal of increasing it to many. These subclouds have radii 1.4 pc, masses 75 $M_\odot$ and have a random separation (between 1.4 and 3.0 pc). The subclouds are then fired toward the center of mass of the system with relative velocities of 3.4 km s^{-1} (Mach 5.9). The outcome of this collision is described in Chapman *et al.* (1992b). The initial conditions are shown in Figure 7a, and after 1.02×10^6 years a bar-like compressed region is formed (Figure 7b). This structure undergoes a Rayleigh-Tayler-like instability (*e.g.* Hunter *et al.* (1986)) and break up into ~ 10 protostars (Figures 7c and 7d). Each of the protostellar discs shown in Figure 7d have similar properties — mass, size, etc. — to the discs in the previous examples (*i.e.* masses $2 - 20$ $M_\odot$ and radii $100 - 1000$ AU). The length of the structure is 120,000 AU and it has a thickness of 16,000 AU. The individual stars are separated by between 16,000 and 2,000 AU. These values are very similar to the observations made by Hirahara *et al.* (1992). Figure 8 shows a region of the Taurus Molecular Cloud-1 (TMC-1) mapped with a high resolution CCS line ($J_N = 4_3 - 3_2$). This ridge has broken up into a number of cores and bears a striking resemblance to our simulation.

4 Conclusion

We have demonstrated the flexibility of our computer code. The combination of TCG and SPH is very effective and enables us to resolve density peaks of around 10^{10} times the initial density.

The protostars we have found have similar dimensions to those inferred from observations. We also find that multiple systems seem to arise naturally.

References

[1] J. Barnes and P. Hut. *Nature*, **324**:446–449, 1986.

[2] L. Blitz and P. Thaddeus. *Astrophys. J.*, **241**:676, 1980.

[3] S.J. Chapman, H. Pongracic, M.J. Disney, A.H. Nelson, J.A. Turner, and A.P. Whitworth. *Nature*, **359**:207, 1992.

[4] S.J. Chapman, J.A. Turner, M.J. Disney, A.H. Nelson, H. Pongracic, and A.P. Whitworth. Multiple subcloud collisions. In preparation, 1992b.

[5] J.P. Chieze and C. Boisanger. In E. Falgarone, F. Boulanger, and G. Duvert, editors, *Fragmentation of Molecular Clouds and Star Formation*. Dordrecht, 1991.

[6] F. de Felice and L.G. Sigalotti. *Mon. Not. R. astr. Soc.*, **249**:248, 1991.

[7] E. Falgarone and T.G. Phillips. *Astrophys. J.*, **359**:344–354, 1991.

[8] D.C. Gilden. *Astrophys. J.*, **279**:335, 1984.

[9] R.A. Gingold and J.J. Monaghan. *Mon. Not. R. astr. Soc.*, **181**:375–389, 1977.

[10] M.A. Hausman. *Astrophys. J.*, **245**:72, 1981.

[11] L. Hernquist. *Astrophys. J. Suppl. Ser.*, **64**:715–734, 1987.

[12] Y. Hirarhara, H. Suzuki, S. Yamamoto, K. Kawaguchi, N. Kaifu, M. Ohishi, S. Takano, S. Ishikawa, and A. Masuda. Mapping observations of sulfur-containing carbon-chain Molecules in Taurus Molecular Cloud-1 (TMC-1). Technical Report 295, Nobeyama Radio Observatory, 1992.

[13] J.H. Hunter, Jr., M.T. Sandford II, R.W. Whitaker, and R.I. Klein. *Astrophys. J.*, **305**:309, 1986.

[14] J.C. Lattanzio, J.J. Monaghan, H.Pongracic, and M.P. Schwarz. *Mon. Not. R. astr. Soc.*, **215**:125, 1985.

[15] L.B. Lucy. *Astron. J.*, **82**:1013–1024, 1977.

[16] J.J. Monaghan and S.R. Varnas. *Mon. Not. R. astr. Soc.*, **231**:515, 1988.

[17] M. Nagasawa and S.M. Miyama. *Prog. theor. Phys.*, **78**:1250, 1987.

[18] M. Perault, E. Falgarone, and J.L. Puget. *Astron. Astrophys.*, **152**:371, 1985.

[19] H. Pongracic, S.J. Chapman, J.R. Davies, A.H. Nelson, and A.P. Whitworth. *Mon. Not. R. astr. Soc.*, **256**:291–299, 1992.

[20] J.M. Scalo. In D.J. Hollenbach and H.A. Thronson, Jr., editors, *Interstellar Processes*. Dordrecht, 1987.

[21] N.Z. Scoville, D.B. Sanders, and D.P. Clemens. *Astrophys. J. Lett.*, **310**:L77, 1986.

[22] F.H. Shu, F.C. Adams, and S. Lizano. *Ann. Rev. Astron. Astrophys.*, **25**:23–81, 1987.

[23] M.E. Stone. *Astrophys. J.*, **159**:293, 1970.

[24] J.P. Vallée and L.W. Avery. *Astron. Astrophys.*, **233**:553, 1990.

[25] H. Zinnecker. In B. Reipurth, editor, *Low Mass Star Formation and Pre-main Sequence Objects*, pages 447–469, 1989. (European Southern Observatory, Garching, 1989).

ISO Science - Observations of Dusty Discs

A. Heske
ISO Science Operations Team / ESA
P.O.Box 299
2200 AG Noordwijk zh
The Netherlands

Abstract

ISO, the Infrared Space Observatory, will be an infrared observing facility in space. Via submission of observing proposals, use of this facility will be open to the astronomical community. The scientific payload consists of two spectrometers, a camera and a photo-polarimeter.

Following an overview of the ISO mission, this paper describes the highlights of the Central Programme - proposals which are being prepared by the instrument groups, the mission scientists and the astronomers of the ISO Science Operations Team - with special emphasis on the proposals concerned with dusty discs.

1 ISO MISSION

1.1 OBJECTIVES

ISO, the Infrared Space Observatory, will be the first true infrared observatory in space. Equipped with four highly sophisticated instruments it will carry out observations in the wavelength range between 2.5 and 200 microns. The ISO spacecraft and its instruments have been designed to provide a new observing facility that allows:

- to explore new wavelength ranges,
- to explore fainter sources,
- to achieve better spatial and spectral resolution throughout the whole ISO wavelength range.

1.2 OVERVIEW OF OPERATIONS

ISO will be operated in a pre-planned way. This means that all observations to be carried out have to be fully specified in advance (by the proposer) before they can be considered for being scheduled (by the Science Operations Team) in a way that maximises the expected scientific return from the mission.

Observing time on ISO will be 'allocated' on a 'per observation' basis as was the case for EXOSAT and not on a 'per night' or 'per shift' basis as is the case for IUE and most ground-based observatories.

The expected high sensitivity of the ISO instruments leads to observations of relatively short duration, typically in the order of minutes up to a few hours. This means that a large number of observations must be properly sequenced and executed in ISO's limited lifetime of nominally 18 months. To handle the large number of proposed observations and to achieve the high throughput required in the production of daily observing schedules under numerous constraints requires automation of most processes between proposal submission and the generation of satellite commands that cause a recommended observation to be carried out.

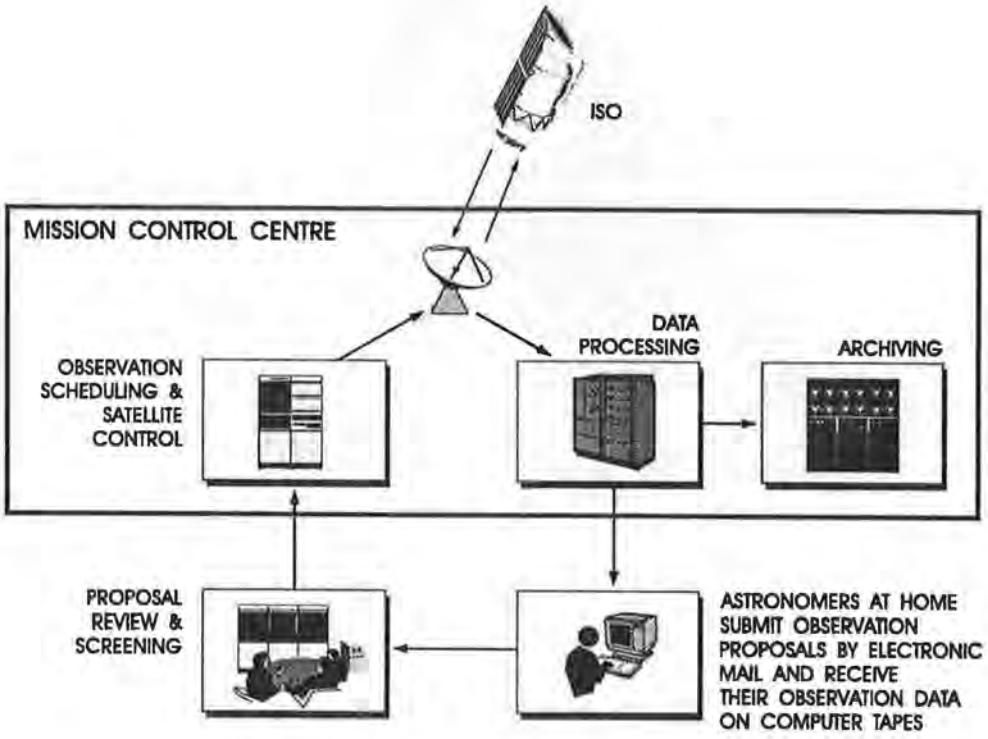

Figure 1: Schematic overview of ISO operations.

Astronomers will prepare their proposals and submit them electronically using a special software tool provided and developed by the ISO Science Operations Team at ESA/ESTEC, the Proposal Generation Aids (PGA). The setup of proposal processing in the Scientific Operations Centre (SOC) does not permit any input in the 'classical' paper form.

All proposals submitted by the astronomical community for open time observations will go through peer review by the ISO Observing Time Allocation Committee (OTAC). The observations recommended by OTAC form the basis from which the mission planning process generates a chain of individual observations. Because this time-line can only be frozen a few days in advance of the corresponding revolution, the actual time when a recommended observation is carried out cannot be determined far in advance. Scheduling observations and archiving/processing of the data returned by the on-board instruments

will be done at the Science Operations Centre SOC at Villafranca, where the ground station is located. The proposer does not have to be present during the observation.

After a one year proprietary period the data become open to all astronomers.

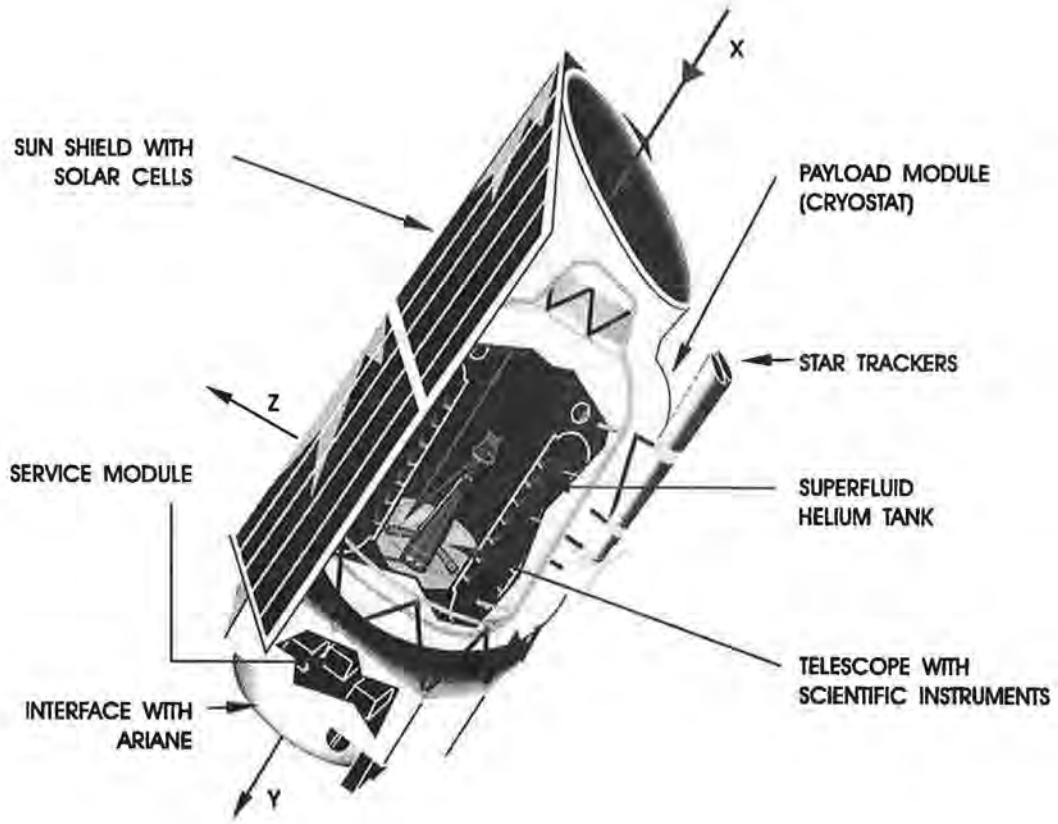

Figure 2: Cutaway view of the ISO satellite.

1.3 SPACECRAFT AND ORBIT

The satellite is essentially a large cryostat containing 2140 litres of superfluid helium to maintain the telescope and scientific instruments at temperatures between 2 and 8 Kelvin for an orbital life time of nominally 18 months. The toroidal helium tank surrounds the telescope, with a primary mirror of 60 cm diameter and an overall f/ratio of 1/15, and the complement of the four scientific instruments.

ISO's operational orbit is highly elliptical with a perigee height of 1000 km, an apogee height of 70,000 km and a period of 24 hours. The spacecraft will spent 16 hours outside the main parts of the Earth's radiation belts. Since ISO lacks the capability to record a large volume of data on-board it needs to be in continuous contact with the ground station for scientific use.

ESA will provide one ground station, enabling ISO to make astronomical observations for 12-13 hours per day. The mission's scientific return could be greatly increased by the

addition of a second ground station, which would permit ISO to be operated scientifically for about 16 hours per day, i.e. the entire time that the satellite will spend outside the trapped-particle belts. An international collaboration is being sought by ESA to provide this second ground station. In return ESA's partner would receive guaranteed observing time.

1.4 SKY VISIBILITY

There are a number of constraints on the allowed pointing directions of ISO. These constraints are due to thermal and power reasons and also to prevent celestial straylight from reaching the instruments and degrading their performance. In particular, the solar panels must always point in the direction of the Sun, and ISO may never point in the direction of the strong infrared emitters, the Earth, Moon and Jupiter, unless, of course, Jupiter or one of its moons itself is a target.

Due to these viewing constraints, only a limited area of the sky is available for observations with ISO at any moment. This accessible area changes with time as the Earth plus ISO moves around the Sun and as ISO's orbit precesses. However, during the 18 months of in orbit lifetime, approximately 15 percent of the sky is never accessible from ISO in particular due to the Earth constraint.

For other reasons, the launch must take place around midnight in a period of a few months in spring or autumn. The region of zero visibility is thus either in the Galactic Centre (spring launch) or in Orion (autumn launch). The diameter of this region is about 100 degrees in both cases. The following regions will be visible irrespective of the launch date:

- the poles of the ecliptic = Declinations higher than +60 or lower than –60 degrees
- two intervals in Right Ascension = R.A. between 10:00 and 13:30 hrs and R.A. between 20:00 and 3:30 hrs

1.5 CAPABILITIES OF THE SCIENTIFIC PAYLOAD

ISO's payload consists of four instruments:

- a camera (CAM, 2.5-18 μm),
- a long wavelength spectrometer (LWS, 45-180 μm),
- an imaging photo-polarimeter (PHT, 3-200 μm),
- a short wavelength spectrometer (SWS, 3- 45 μm).

The capabilities provided jointly by these instruments can be summarised in the following categories: imaging, photometry, polarimetry and spectroscopy.

Wavelength Range (μm)	No. of Pixels	Pixel f.o.v. (arc secs)
2.5 – 5	32 x 32	1.5, 3, 6, 12
5 – 17	32 x 32	1.5, 3, 6, 12
50 – 120	3 x 3	43.5
120 – 200	2 x 2	89.4

Table 1: ISO's Imaging Capability.

ISO will be capable of direct IMAGING using arrays in broad and narrow spectral bands across much of its entire wavelength range from 2.5 to 200 μm with CAM and PHT. Mapping will also be possible with the single pixel detectors of PHT by use of the satellite's raster pointing capability.

PHOTOMETRY and POLARIMETRY will be possible in broad and narrow spectral bands across the entire wavelength range with CAM and PHT. Observations using multiple apertures will be possible out to 100 μm. Both instruments are equipped with three polarisers which can be used with various pixel field of views (CAM) or spectral band/aperture combinations (PHT).

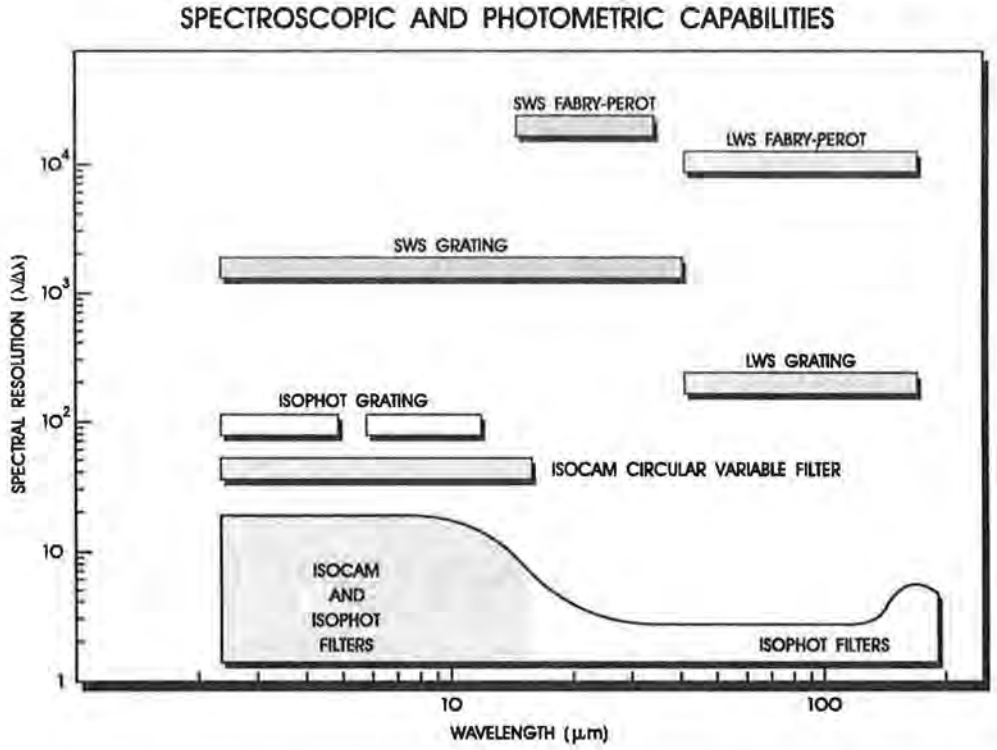

Figure 3: Photometry and spectroscopy with ISO.

For SPECTROSCOPY, various resolutions will be available. Each of two spectrometers have a grating mode, where a resolution of 1000 - 2000 for SWS and 200 for LWS can be achieved. By inserting a Fabry-Perot unit the resolution can be increased to 20,000, in the range from 15 to 35 μm (SWS), and to between 10,000 and 20,000 in the range from 45 to 180 μm (LWS).

Wavelength Range (μm)	Resolution ($\lambda/\Delta\lambda$)	Instrument
2.5–12	90	ISOPHOT-S
2.5–17	40	ISOCAM-CVF
2.5–45	2000	SWS-Grating
15–35	20000	SWS-Fabry-Pérot
45–180	200	LWS-Grating
45–180	15000	LWS-Fabry-Pérot

Table 2: ISO's Spectroscopic Capability.

With the expected high sensitivities of the instruments, it will be possible to make the following observations with a signal-to-noise ratio of 10 in less than an hour:

- Imaging between 2.5 and 17 μm of sources with a flux of the order of milliJanskies.
- Photometry of sources with fluxes of around 10 milliJansky out to 200 μm.
- Spectroscopy of a molecular band, e.g. around 12 μm, at a flux in the order of Janskies, where the resolution $\Delta\lambda$ is of the same order of magnitude as the separation of the rotational lines in a molecular band.
- A full grating spectrum between 45 and 200 μm of a source with a flux of the order of Janskies.

1.6 CALL FOR PROPOSALS

ESA will announce the opportunity for performing observations with ISO to the astronomical community via a "Call for Observing Proposals" one year before launch. The Call is embedded in the Proposal Generation Aids and contains all necessary information to prepare proposals. The Call will be similar to Calls for Proposals for ground-based/space-borne observatories which are issued as printed announcements, except that the ISO "Call for Observing Proposals" is not published in paper form.

From the point of view of the community proposing observations, ISO has the following novel features:

- All proposals must be finalised and submitted in electronic form.
- All proposed observations must be specified fully in advance by the proposer, at the time the proposal is finalised.
- The proposer specifies an observation by entering the target, instrument and observation parameters into pre-defined panels, so-called Astronomical Observation Templates, AOTs.

Each of the four instruments on the spacecraft has several possible operational modes. To simplify the user interface, Astronomical Observation Templates have been defined for the astronomically-useful operating modes of each instrument. Each AOT is designed

to carry out a specific type of astronomical observation and the proposer specifies an observation by entering the target, instrument and observation parameters into an AOT.

In addition to the pre-launch Call for Observing Proposals it is planned to issue two more Calls during the mission.

1.7 OBSERVING TIME

Approximately two thirds of the observing time will be open to the general scientific community via the "Calls for Observing Proposals". This time is called Open Time. The remaining one third of the time - the Guaranteed Time - is reserved for the scientists in the four instrument teams, the Mission Scientists and the astronomers in the ISO Science Operations Team (ESA). These teams are preparing a coherent co-ordinated programme of ISO observations, the Central Programme. Details of this programme (including targets and observation parameters) will be published with the first Call for Observing Proposals.

2 ISO SCIENCE

Due to the sophistication and the expected high sensitivity of its instruments ISO will have an impact on almost every field of astronomical research, from studies of the solar system to cosmology. It will be possible to study objects in wavelength ranges not accessible from the ground and to explore new objects.

2.1 THE CENTRAL PROGRAMME – TARGETS FOR ISO

The Central Programme consists of about 130 proposals from the four instrument teams, the mission scientists and the Science Operations Team. These proposals are being co-ordinated in terms of scientific objectives and target lists to define a coherent programme.

Many of the proposals in the Central Programme contain observations of several samples from different classes of objects to investigate their spectral characteristics, their morphologies and their evolution. The highlights of the Central Programme can be summarised as follows:

SOLAR SYSTEM

Photometric and spectroscopic studies of comets and comet trails, giant planets and their atmospheres, Asteroids and Titan are proposed. The zodiacal light and its seasonal variation will be studied.

INTERSTELLAR MATTER

The different components of the interstellar medium, such as HII regions, molecular clouds, Cirrus, will be studied in photometry, polarimetry and line spectroscopy to reveal physical and chemical conditions.

STAR FORMATION

The studies include searches for protostars at early phases, physics and chemistry of bipolar outflows, stellar jets and discs around young low mass stars.

STELLAR AND CIRCUMSTELLAR PHYSICS

Main sequence stars, Vega-type stars, eruptive variables and evolved stars, including planetary nebulae will be studied. Their environment such as expanding envelopes and discs will be observed to investigate morphology of the circumstellar matter and its evolution.

EXTRAGALACTIC SYSTEMS

The targets range from nearest neighbours, the Magellanic Clouds, via normal galaxies, active and interacting galaxies to the most distant objects. Interdisciplinary studies include investigations of interstellar matter, star formation and starbursts in galaxies.

COSMOLOGY

The studies include extragalactic infrared background radiation, deep exposures of selected areas, search for brown dwarfs in galactic haloes and gravitational lenses.

SURVEYS

Spectral classification of bright IRAS sources and spectra across the entire ISO wavelength range of selected sources (2.5 - 200 μm) is propsed.

2.2 DUSTY DISCS IN THE CENTRAL PROGRAMME

A substantial fraction of proposals in the areas interstellar matter, star formation and stellar physics aim at investigating circumstellar material and its morphology. In most objects the structure of the circumstellar environment is not clear and no observations exist which could distinguish between spherically symmetric envelopes or disc-like structures. Accordingly, there is a number of proposals which are related to studies of circumstellar discs but do not aim at it explicitly.

Eight proposals in the central programme are explicitly devoted to investigations of dusty discs. The range of targets include young stars, Vega-type and main-sequence stars, evolved stars and post-AGB stars. The majority of the proposals (five) deals with investigations of Vega-type systems.

The scientific objectives concentrate on three different areas: The search for new discs, the survey of objects with known infrared excess and the detailed spectroscopic and photometric study of discs.

DISCS AROUND YOUNG STARS

Two proposals aim at studying the energy distributions of the discs around young stars based on multiband photometry. The targets are young stars of different ages and T Tauri stars of different classes, where each class is characterised by specific spectral features. The aim is to investigate evolutionary characteristics of the discs and to derive their evolution and the timescales for the different evolutionary phases.

Another study plans to map photometrically and spectroscopically a small sample of pre-main sequence stars and Vege-type systems to investigate the structures of these discs and to create a scenario of the evolution from pre-main sequence to Vega-type stars.

VEGA-TYPE SYSTEMS

Two proposals aim at detailed photometric and spectroscopic studies of known Vega-like systems. Photometric multi-aperture scanning observations are proposed to investigate the structure and the energy distributions in the discs. Five systems are suitable for observations of ice bands in the discs. In addition, Beta Pictoris will be also searched for ionic fine structure lines.

Three proposals plan to search for new Vega-like stars based on the following samples: a distance limited sample of main-sequence stars between B5 and M0, in order to investigate how widespread the Vega-phenomenon is; the Hyades and Pleiades, in order to derive the fraction of stars at intermediate ages surrounded by discs; a sample of stars with known infrared excess, in order to search for discs of Vega-type morphology.

EVOLVED STARS

Two proposals plan to investigate the circumstellar environment of evolved stars. One conducts a survey of objects with infrared excess detected by IRAS in order to investigate the continuum emission in more detail. The other will study the morphology of the circumstellar environment of a number of post-main sequence stars with imaging and spectroscopy.

RELATED STUDIES

Around 1/7 of the Central Programme proposals plan to investigate circumstellar material of pre-main sequence and post-main sequence stars; in particular they comprise imaging of the dust envelopes, spectroscopic mapping of outflows and photometric investigations of the infrared continuum. The targets are outflows of low and high mass protostars, accretion discs of novae, outflows of evolved stars and dust in (pre-)planetary nebulae. These studies complement those mentioned above.

CONCLUSIONS

The large number of observation modes of the ISO instruments offers a variety of possibilities to study known dusty discs and to explore new ones. With the new wavelength ranges and the spatial and spectral resolution offered by ISO it will be possible to carry out observations, which were impossible up to now. More details can be observed. However, to make full use of ISO's scientific capabilities the questions ISO may help to answer must be formulated very precisely. For a proposer this means that each observation must be prepared and specified to a level of detail which far exceeds the level normally required in observing proposals for ground-based or air-borne facilities.

FURTHER READING

- *"Infrared Astronomy with ISO, Les Houches*, Encrenaz, Th. and Kessler, M.F. (eds.) 1992, Nova Science Publ. Co., 1992
- *"The ISO Mission - A Scientific Overview"*, Kessler, M.F., Heske, A., Metcalfe, L., Salama, A. in: ESA Bulletin 67, p.8, 1991

Radiative Transfer in Dusty Discs: Models of Bipolar Flow Sources

A. Efstathiou
School of Mathematical Sciences
Queen Mary & Westfield College
University of London
London, E1 4NS.

Abstract

We present a generalisation of the method of Efstathiou & Rowan-Robinson (1991) for modelling low-mass protostars that takes into account a distribution of grain species and sizes. The method includes treatment of multiple scattering from grains. We apply this method to protostellar systems which are in the bipolar flow phase.

1 INTRODUCTION

The exact mechanism that produces bipolar flows in young stellar objects is not very well understood yet. It has been suggested that sources like L1551 IRS5 are examples of low-mass protostars in which inflow is accompanied by outflow along the rotation axis of the star (Adams, Lada & Shu 1987 and references therin.) Efstathiou & Rowan-Robinson (1991; herafter ER91) presented models of rotating protostars with pure inflow and showed how the emergent spectrum depends on orientation. The density distribution was assumed to be that resulting from the semi-analytic collapse calculations of Terebey, Shu & Cassen (1984.) In this paper we generalise their method in the sense that we calculate the radiative transfer in the axisymmetric envelope by taking account of a distribution of grain species. We also assume that the polar regions are completely dust free in order to investigate the effect of bipolar geometry on the appearance of the source.

2 OUTLINE OF THE METHOD

The physics of the star, disc and envelope is described in detail in ER91 (see also Adams & Shu 1986). The density distribution in the envelope, effective temperature of the star T_*, maximum temperature of the accretion disc T_{D^*} and other quantities of interest are determined self consistently by assuming three parameters: the sound speed α, the rotation rate Ω and the protostar mass M. The first two may be seen to define the initial state of the molecular cloud core and the protostar mass the evolutionary state of the system.

The method of solution of the radiative transfer problem is a generalisation of the method of Efstathiou & Rowan-Robinson (1990; herafter ER90.) We assume that the cloud consists of l species of dust with number density distributions $n^i(r,\Theta)$ and temperatures $T^i(r,\Theta)$. We also assume that the relative abundances of all grains remain

constant throughout the cloud except in the inner part where the sublimation radii of different species may be different. The equation of radiative transfer may then be written in the form

$$\frac{dI_\nu}{ds} = -\sum_{i=1}^{l} C^i_{\nu,ext}\, n_i(r,\Theta)\, I_\nu + \sum_{i=1}^{l} C^i_{\nu,abs} n_i(r,\Theta) B_\nu(T_i(r,\Theta)) + \frac{1}{4\pi}\int I'_\nu \sum_{i=1}^{l} C^i_{\nu,sc}(\theta') n_i(r,\Theta)\, d\omega' \tag{1}$$

where all symbols have their usual meaning with the superscript i denoting properties of the i^{th} grain species. With the usual notation we also express the absorption and scattering cross-sections as

$$C^i_{\nu,abs} = \pi(\alpha^i)^2 Q^i_{\nu,abs} \tag{2}$$

and

$$C^i_{\nu,sc} = \pi(\alpha^i)^2 Q^i_{\nu,sc} \zeta^i(\theta') \tag{3}$$

where α^i is the grain radius and $\zeta^i(\theta')$ is its phase function, and

$$C^i_{\nu,ext} = C^i_{\nu,abs} + C^i_{\nu,sc} \tag{4}$$

The solution to equation (1) is carried out with the ray tracing method i.e. by defining a grid of rays and for each one following the interaction of radiation with dust both in the form of absorption and scattering. In the notation of ER90 the intensity I_ν is given by the superposition of radiation directly from the central source(s) $I^{(1)}_\nu$, thermal emission from grains $I^{(2)}_\nu$ and scattered light from grains $I^{(3)}_\nu$. At a general point $P(r,\Theta)$ in the cloud, $I^{(1)}_\nu$ is the sum of contributions from the star and disc ie

$$I^{(1)}_\nu = I^{(1)}_{\nu_*} + I^{(1)}_{\nu D} \tag{5}$$

where

$$I^{(1)}_{\nu_*} = B_\nu(T_*) \quad e^{-\tau_\nu(r,\Theta)} \tag{6}$$

and

$$I^{(1)}_{\nu D} = 2\, exp(-\tau_{uv}(r,\Theta)) sin\Theta \int_{r_s}^{r_{out}} \int_0^\pi \frac{B_\nu(T_D(R)) r R\, dR\, d\Phi}{\sqrt{R^2 + r^2 - 2Rr cos\Theta cos\Phi}} \tag{7}$$

where T_D follows the Lynden-Bell and Pringle (1974) form for $R >> r_s$

$$T_D(R) = T_{D^*}(R/r_s)^{-3/4} \tag{8}$$

where R is the distance from the centre of the star. The disc is assumed to extend from r_s to an outer radius r_{out} (at temperature lower than T_1.)

The optical depth to the central source $\tau_\nu(r,\Theta)$ is given by,

$$\tau_\nu(r,\Theta) = \int_{r_1}^{r} a_{\nu,ext}(r',\Theta) dr' \tag{9}$$

where now

$$a_{\nu,ext} = \sum_{i=1}^{l} \quad C^i_{\nu,ext} \quad n^i(r', \Theta) \tag{10}$$

The contributions to the intensity by thermal emission from grains and scattering $I_\nu^{(2)}$ and $I_\nu^{(3)}$ are given by

$$I_\nu^{(2)}(r, \Theta, \theta, \phi) = \int_0^S exp(-\int_0^{S'} a_{\nu,ext} ds') \sum_{i=1}^{l} C^i_{\nu,abs} n^i(r', \Theta') B_\nu(T^i(r', \Theta')) ds \tag{11}$$

and

$$I_\nu^{(3)}(r, \Theta, \theta, \phi) = \int_0^S exp(-\int_0^{S'} a_{\nu,ext} ds') \sum_{i=1}^{l} C^i_{\nu,abs} n^i(r', \Theta') J^i_{sc}(r, \Theta, r', \Theta', \theta) ds \tag{12}$$

where

$$J^i_{sc}(r, \Theta, r', \Theta', \theta) = J_\nu(r', \Theta') - b^i_1 cos\psi H_\nu(r', \Theta') \tag{13}$$

and where J_ν and H_ν are the first and second moments of the intensity respectively. S is the distance from P to the edge of the cloud along s, and S' is the distance of the point $P'(r', \Theta')$ from P.

In the last equation we allow for the fact that different grain components may have different scattering anisotropy factors b^i_1. In practice, however, we will assume here that all grains scatter isotropically.

As in ER90 the solution proceeds iteratively with the temperature corrections for each grain species now given by

$$\Delta T^i(r, \Theta) = \frac{\int_0^\infty Q^i_{\nu,abs}[J_\nu - B_\nu(T^i(r, \Theta))] d\nu}{\int_0^\infty Q^i_{\nu,abs} \frac{\partial B_\nu}{\partial T^i} d\nu} \tag{14}$$

until the radiative balance equation

$$\int_0^\infty Q^i_{\nu,abs} J_\nu(r, \Theta) d\nu = \int_0^\infty Q^i_{\nu,abs} B_\nu(T^i(r, \Theta)) d\nu. \tag{15}$$

is satisfied to within a few percent for every grain species and at every point in the cloud. The flux constancy condition

$$r^2 \int_0^{\pi/2} H cos\Theta d\Theta = \text{const.} \tag{16}$$

where $H = \int_0^\infty H_\nu d\nu$ provides an additional test for the accuracy of the solution.

3 GRAIN PROPERTIES

The grain mixture adopted for the calculations in this paper is that of Rowan-Robinson (1992) that leads to a very good agreement with the interstellar extinction curve and observations of interstellar clouds. The mixture invokes the minimum number of grain types that could explain most of the observational evidence. It includes (i) $0.1\mu m$ amorphous

carbon grains with optical properties derived from models of circumstellar dust shells around carbon stars, (ii) $0.1\mu m$ amorphous silicate grains with properties derived from circumstellar dust shells around M stars, (iii) $0.03\mu m$ graphite grains, (iv) $0.03\mu m$ silicate grains, (v) $0.01\mu m$ graphite grains (vi) $0.01\mu m$ silicate grains and (vii) $30\mu m$ amorphous grains. The optical properties of the $0.03\mu m$ and $0.01\mu m$ grains have properties as calculated by Draine and Lee (1984). Evidence for the $30\mu m$ grains comes from observations of interstellar dust by COBE and balloon-borne experiments.

The model of Rowan-Robinson (1992) also includes two species of very small graphite grains of 0.002 and $0.0005\mu m$ in radius. The difficulties associated with treating the out-of-equilibrium behaviour of the small grains have prevented us from including them in the present calculations. In the high optical depth models we are considering in this paper, however, the small grains should have a negligible effect on the continuum spectrum (Rowan-Robinson 1986). For the purpose of the calculations in this paper the mass of the small grains is included in the $0.01\mu m$ graphite particles.

4 BIPOLAR FLOW MODELS

Our model for a bipolar flow source is based on those presented in ER90 and ER91. We start from the density structure predicted by the formalism of ER91 but assume that the cloud is completely dust free above Θ_1 (where Θ_1 is measured from the equator.) Needless to say that the interaction of the outflow with the envelope will produce a more complicated structure than the one assumed here but provided the outflow has swept away most of the dust in the polar region our assumption should not be too restrictive.

We assume that the outer radius of the cloud r_2 is 2×10^{17}cm (a value typical for sources in Taurus and ρ Oph.) The stellar radius is also assumed to scale as

$$\frac{r_s}{r_2} = 1.5 \times 10^{-6}(\frac{\alpha}{0.35\text{km s}^{-1}}) \tag{17}$$

The value of inner to outer cloud radii necessary to give rise to a temperature of 1000K at the inner boundary is found to be 4×10^{-5}. The melting temperature of each grain species is of course different. The above value is that corresponding to the $0.1\mu m$ silicate (coldest) grains.

In Fig. 1 we plot the emergent spectrum from different viewing angles for a model that assumes $\alpha = 0.35Kms^{-1}$, $\Omega = 5 \times 10^{-13}s^{-1}$ and $M = 0.5M_{\odot}$. We also assume that $\Theta_1 = 70°$, a situation that is thought to exist in the prototypical bipolar flow source L1551 IRS5.

The bottom four specra correspond to views from $\theta_v = 0, \pi/16, \pi/6$ and $\pi/4$ (in order of increasing mid-infrared νH_ν.) The A_V to the central star and disc is in the range 120-40 and the silicate features are therefore deeply in absorption. The decrease of the depth of the absorption features (notably that of the 10μm feature) as θ_v increases is discussed in detail in ER90. They are qualitatively understood as due to variations in the optical depth to the dust whose emission peaks at that particular wavelength.

The model also predicts bumps due to scattering centred at around 1μm similar to those obtained in ER90. Note that this effect depends crucially on the assumed geometry. As demonstrated in ER91 this effect disappears completely if the whole sphere around the star is surrounded by dust.

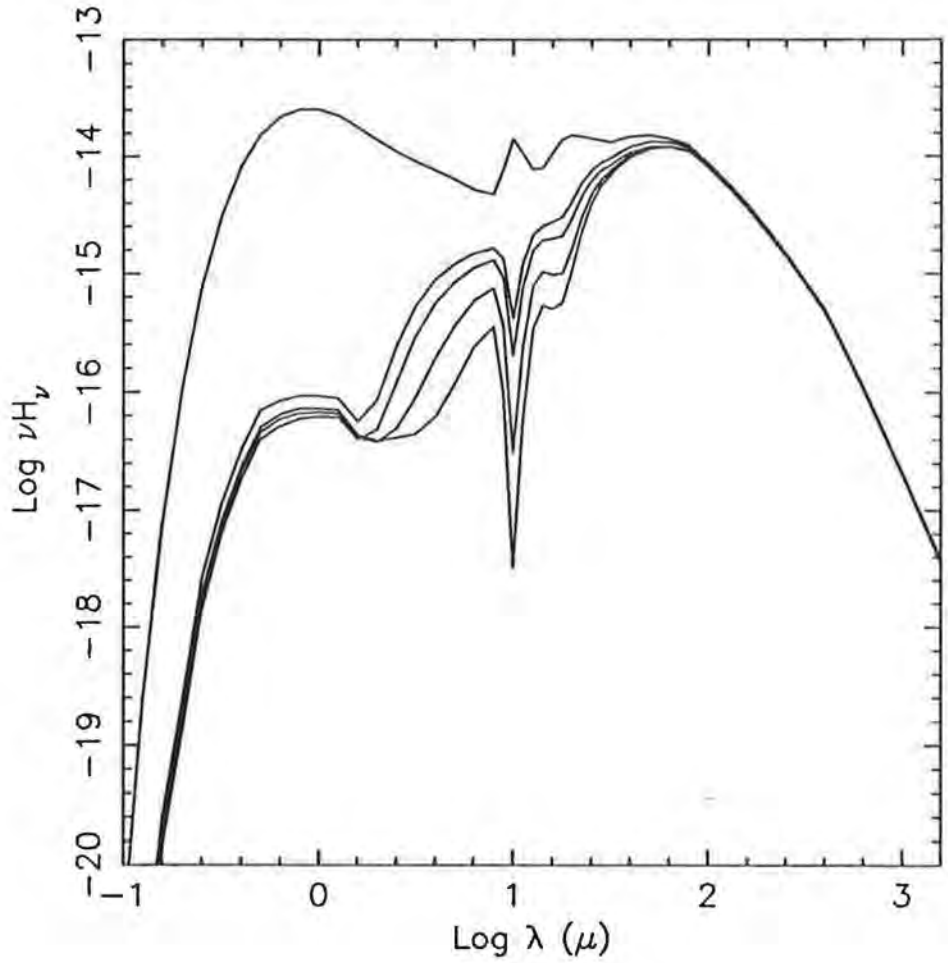

Figure 1: Emergent spectra from different viewing angles predicted from a model that assumes $\alpha = 0.35\ Kms^{-1}$, $\Omega = 5 \times 10^{-13}\ s^{-1}$ and $M = 0.5 M_\odot$. The model also assumes that the disk opening angle $\Theta = 70°$. The spectra corresponding to views from $\theta_v = 0, \pi/16, \pi/6, \pi/4$ and $\pi/2$ (in order of increasing mid-infrared νH_ν)

The top spectrum in Fig. 1 corresponds to a viewing angle of $\pi/2$. It is dominated by direct stellar and disc radiation but also shows a complete reversal of the silicate features. This effect was demonstrated by ER90 but for much lower equatorial optical depths.

CONCLUSIONS

A method of solving the radiative transfer problem in the type of geometry appropriate for bipolar flow sources is presented. The mid- and far-infrared spectra are similar to those obtained for protostars in earlier phases of evolution for views close to the equatorial plane. In shorter wavelengths scattering dominates completely over emission and the model predicts a prominent bump centred at around 1μm. This is a potentially observable effect although reddening from local or interstellar material will tend to weaken it. The polar view is dominated by direct stellar and disc radiation and strong silicate features in emission.

Acknowledgement: The author acknowledges receipt of an SERC research fellowship and is grateful to the RAL for their hospitality during the workshop.

References

Adams, F.C., & Shu, F.H., 1986. *Astrophys.J.*, 308, 836.
Adams, F.C., Lada, C.J., & Shu, F.H., 1987. *Astrophys.J.*, 312, 788.
Draine, B.T., & Lee, H.M., 1984. *Astrophys.J.*, 285, 89.
Efstathiou, A., & Rowan-Robinson, M., 1990. *Mon.Not.R.astr.Soc.*, 245, 275.
Efstathiou, A., & Rowan-Robinson, M., 1991. *Mon.Not.R.astr.Soc.*, 252, 528.
Lynden-Bell, D., & Pringle, J.E., 1974. *Mon.Not.R.astr.Soc.*, 168, 603.
Rowan-Robinson, M., 1986. *Mon.Not.R.astr.Soc.*, 219, 737.
Rowan-Robinson, M., 1992. *Mon.Not.R.astr.Soc.*, (in press)
Terebey, S., Shu, F.H., & Cassen, P. 1984. *Astrophys.J.*, 286, 529.

The Stability of a Magnetized Disc

E. Szuszkiewicz and J. Papaloizou
Astronomy Unit,
School of Mathematical Sciences
Queen Mary and Westfield College,
Mile End Road, London E1 4NS.

Abstract

The present state of our knowledge of the stability of a magnetized differentially rotating disc is reviewed here. Balbus and Hawley recently concluded that in a weakly magnetized accretion disc there is an instability which might be important in understanding of the nature of viscosity. They used a local approach similar to that by Fricke, applied to a case of a rotating star. They found that toroidal field is not important for stability. Then, Hawley and Balbus performed for the first time nonlinear calculations to study the evolution of such an instability. Knobloch questions validity of the local approach showing by means of a global analysis that, for cylinders, the toroidal field has an important effect on stability. Finally, Papaloizou and Szuszkiewicz have shown, using full global analysis, that for a disc there is a purely growing mode with a poloidal field, as in Balbus and Hawley. In the case of an externally imposed poloidal magnetic field Papaloizou and Szuszkiewicz estimated the strength of the field above which the disc will become stable to axisymmetric modes. To give such an estimate, a global analysis of the type given in their paper is necessary. The estimated field strength was found to be such that the typical Alfvèn speed is proportional to the product of the orbital velocity and the square root of the ratio of the disc thickness to radius. The stability of a disc in the more general case, with a non zero toroidal field is still an open problem.

1 Introduction

Magnetic fields may play an important role in the dynamics of accretion discs circulating around either a compact object or a protostar, (see Pringle, 1981, for a review). The field may arise from the central object, (Ghosh and Lamb, 1979), or background material if a disc-like configuration forms during the process of star formation, (Mestel and Ray, 1985). In discussing the structure and evolution of such objects linear stability analysis in the ideal MHD approximation has played an important role (for example see Moss and Tayler, 1969, and Pitts and Tayler, 1985).

Recently, Balbus and Hawley (1991) pointed out that the instability to axisymmetric modes found in the case of magnetized rotating stars might be important in accretion disc theory. Such instabilities would be expected because accretion discs have approximately Keplerian rotation, so that although the angular momentum increases outwards, the angular velocity decreases outwards, violating the stability condition if there is a weak poloidal magnetic field. The instability of the Keplerian disc appears as an instability of

the flow which moves under constraints modified by the presence of the field. The non-linear development of unstable modes might lead to angular momentum redistribution in the disc and provide a reason for the anomolous viscosity of Shakura and Sunyaev (1973), Hawley and Balbus (1991). Stability analyses that are applicable to compressible differentially rotating discs use local approximations. The results of such analyses suggest that instability always occurs for a wavelength in the vertical direction longer than a critical value (Balbus and Hawley, 1991). This critical value becomes arbitrarily small, enabling some justification of local analysis, only in the small field limit. However, the global stability analysis of the incompressible cylinder done by Chandrasekhar (1960) indicates that stability to axisymmetric modes might be recovered if an imposed magnetic field is large enough, and a global analysis is indeed necessary to resolve this issue.
Papaloizou and Szuszkiewicz (1992) gave a rigorous global stability analysis of a non self-gravitating, differentially rotating gaseous system with a poloidal magnetic field. Their approach is to derive a variational principle from which rigorous stability criteria may be obtained.

2 Local stability analysis for a rotating star and the global one for an incompressible cylinder

In the stellar case, the results of a stability analysis of differentially rotating configurations is relevant to the selection of physically realizable rotation laws. Fricke (1969) performed a local stability analysis for axisymmetric modes, allowing for the possible presence of a poloidal and a toroidal magnetic fields, which used a Boussinesq approximation. He found that the stability criteria obtained when the magnitude of the magnetic field was allowed to tend to zero differed from those obtained for non magnetic stars. In particular, for the stability of a constant entropy differentially rotating star threaded by a uniform vertical magnetic field, the angular velocity, Ω, must be monotonic increasing function of the cylindrical polar radius r,

$$\nabla \Omega^2 > 0.$$

For a non magnetic star the corresponding condition is the well known Rayleigh criterion that the specific angular momentum, $J = \Omega r^2$, should increase outwards

$$\nabla J^2 > 0.$$

In order to understand the way this difference occurs we may consider the perturbed motion of a particle initially in circular orbit neglecting pressure forces as these do not affect the stability criterion. In the non magnetic case, specific angular momentum is conserved for fluid elements and the elementary criterion for stability of the particle motion is that the specific angular momentum of the circular orbits increase outwards. In the magnetic case the effect of the field is to tend to enforce isorotation (Ferraro, 1937), so that a fluid element conserves its angular velocity as it moves. In that case the stability of the particle motion requires that the angular velocity of the circular orbits increase outwards. It was first noted by Chandrasekhar (1960) that the latter criterion applied to the special case of an incompressible cylinder threaded by a uniform vertical field no matter how weak the field may be. As he used a global analysis his results were rigorous and he was able to conclude that for sufficiently large fields there would be stability to axisymmetric modes.

3 Local stability analysis for a disc and nonlinear evolution of the instability found in this analysis

The instability found in the case of weakly magnetized rotating stars might naturally appear in the magnetized accretion discs. It is expected because the rotation law of accretion discs is approximately Keplerian. The specific angular momentum and angular velocity are given by

$$J(r) = r^2\Omega(r) = GMr^{1/2},$$

$$\Omega(r) = \left(\frac{GM}{r^3}\right)^{1/2}.$$

where G is the gravitational constant, M is the mass of a central object and r is the cylindrical polar radius. It is clear that if the criterion for stability is such that $\nabla\Omega^2 > 0$, the disc is unstable.

Balbus and Hawley (1991) using local analysis give a critical wavenumber in the vertical direction

$$|k_z| \sim v_A^{-1}\left|r\frac{d\Omega^2}{dr}\right|^{1/2},$$

v_A being the Alfvèn speed, below which stability is expected. From this we expect the scale lengths associated with the instability to increase with field strength to the point where local analysis may break down. But no rigorous estimate of the breakdown point may be obtained from the local analysis. The rigorous estimates of field strengths sufficient to provide stability to axisymmetric modes are possible only if a global analysis is carried out.

Even if a local analysis cannot give us any details about the nature of the instability it is justified to assume its existence. Balbus and Hawley performed axisymmetric numerical calculations in order to find an evolution of this instability in nonlinear regime. For simplicity they used periodic boundary conditions in the vertical direction and reflecting boundary conditions on the radial walls of the box, which represents a small region within a Keplerian disc. As they have said, their simulations are consistent with the linear analysis and can be regarded as a test of the code. They stated that neither compressibility nor toroidal field have a significant effect on the instability for the range of parameters in which Boussinesq approximation holds. They pointed out the importance of this instability for the presence of self-sustaining dynamo activity but they were very careful about any conclusions because one must study the nature of nonaxisymmetric disturbances. This can be easily understood in terms of Cowling's theorem saying that a magnetic field symmetric about the axis cannot be maintained by a symmetric motion (Cowling, 1976). In fact, under such conditions the field ultimately decays.

4 Global stability analysis for a cylinder in a more general magnetic field configuration

Knobloch questions validity of a local stability analysis of shear flows showing by means of a global analysis that in a case of incompressible cylinders, the toroidal field has an important effect on stability. This is quite different from the Balbus and Hawley (1991) conclusion. Knobloch discussed three particular cases:

1) $B_z = 0$, $B_\varphi \neq 0$
2) B_z = constant, $(\neq 0)$, $B_\varphi = 0$
3) B_z = constant, $(\neq 0)$, $B_\varphi \neq 0$

He shows that the presence of an azimuthal magnetic field alters the character of the instability. In the case when both the azimuthal magnetic field and the angular velocity are non-zero and of one sign, he expects that a basic equilibrium state is not unstable to exponentially growing axisymmetric perturbations. Instead, the instability takes the form of overstable oscillations. Knobloch's results depend on the boundary conditions used on the perturbation velocity.

5 Global stability analysis for a disc with a poloidal magnetic field

The complete discussion and all details of this subject can be found in Papaloizou and Szuszkiewicz (1992). Here we would like to define the problem and present our results.

5.1 Formulation of the problem

The basic equations are the conservation laws of momentum, mass and Maxwell's equations in the ideal MHD approximation in SI units:

$$\frac{\partial \mathbf{v}}{\partial t} + \mathbf{v} \cdot \nabla \mathbf{v} = \frac{1}{\rho}(-\nabla P + \mathbf{j} \times \mathbf{B}) - \nabla \Phi, \tag{1}$$

$$\frac{\partial \rho}{\partial t} + \nabla \cdot (\rho \mathbf{v}) = 0, \tag{2}$$

$$\nabla \times \mathbf{B} = \mu_0 \mathbf{j}, \quad \text{and} \tag{3}$$

$$\frac{\partial \mathbf{B}}{\partial t} = \nabla \times (\mathbf{v} \times \mathbf{B}). \tag{4}$$

Here P denotes the pressure, ρ the density, $\mathbf{B}$ the magnetic field, $\mathbf{j}$ the current density, Φ the gravitational potential, and $\mathbf{v}$ the flow velocity. In addition we assume that time dependent changes are governed by the adiabatic condition

$$\frac{\partial P}{\partial t} + \mathbf{v} \cdot \nabla P = -\Gamma_1 P \nabla \cdot \mathbf{v}, \tag{5}$$

where Γ_1 is the usual adiabatic exponent.

We shall be considering the stability of steady state axisymmetric configurations for which the disc is in a state of differential rotation such that in cylindrical coordinates (r, φ, z), $\mathbf{v} = (v_r, v_\varphi, v_z) = (\ 0\ ,\ r\Omega\ ,\ 0)$.

We assume that there is an axisymmetric magnetic field which can be expressed in the general form

$$\mathbf{B}(r, z) = \mathbf{B_p}(r, z) + \mathrm{B}_\varphi(r, z)\boldsymbol{\varphi} \tag{6}$$

where $\mathbf{B_p} = (\mathrm{B}_r, \mathrm{B}_z)$ is the poloidal component of the field and B_φ is the toroidal (φ) component. Because $\mathbf{B}$ and $\mathbf{B_p}$ are solenoidal one can express $\mathbf{B_p}$ in terms of a flux function ψ and write

$$\mathbf{B} = \frac{1}{r}(\nabla \psi) \times \boldsymbol{\varphi} + \mathrm{B}_\varphi \boldsymbol{\varphi}, \tag{7}$$

(Bernstein et *al.*, 1958).
The lines of the magnetic force lie in the surfaces ψ = constant. Therefore it is convenient to introduce an orthogonal coordinate system (ψ, φ, χ), where the surfaces of constant χ are orthogonal to the surfaces of constant ψ and φ. In these coordinates the magnetic field has no component in the ψ direction so that it has the form:

$$\mathbf{B} = (0, \mathrm{B}_\varphi, \mathrm{B}_\chi),$$

with

$$\mathrm{B}_\chi = \frac{|\nabla\psi|}{r}.$$

Here we shall be mainly concerned with systems for which only the poloidal component is non zero so that $\mathrm{B}_\varphi = 0$. Then no torques are exerted between the magnetic field and disc. Examples of such systems have been considered in the thin disc limit by Mestel and Ray (1985).

We assume that in the steady state the following equilibrium conditions hold:

$$\frac{1}{\rho}(-\nabla P + \mathbf{j} \times \mathbf{B}) - \nabla\Phi + r\Omega^2\nabla(r) = 0, \tag{8}$$

$$\nabla \times \mathbf{B} = \mu_0\mathbf{j}, \quad \text{and} \tag{9}$$

$$\nabla \times (\mathbf{v} \times \mathbf{B}) = 0. \tag{10}$$

For an axisymmetric field equation (10) reduces to

$$\mathbf{B_p} \cdot \nabla\Omega = \mathrm{B}_\chi|\nabla\chi|\frac{\partial\Omega}{\partial\chi} = 0. \tag{11}$$

From this we deduce that Ω must be a function of ψ alone, which is just an expression of the law of isorotation, (Ferraro, 1937). This simply states that every field line must rotate at constant angular velocity in a steady state. For a thin disc with near Keplerian rotation and with field lines penetrating perpendicular to the equatorial plane, the isorotation condition implies that the angular velocity is approximately a function of r alone. We shall suppose that any magnetosphere above the disc corotates with the disc material out to sufficient distances and the field there is curl free so that it can be treated like a vacuum field through all space. Thus any interaction with a central object which causes this corotation condition to breakdown is supposed to be sufficiently far away that it can be neglected. Such an assumption is necessary to make the problem tractable. We thus define a simple global equilibrium in which there are no torques acting between disc and magnetic field and discuss its global stability to axisymmetric modes of the type that have been suggested might lead to toroidal field production, angular momentum transport and an effective viscosity by Balbus and Hawley (1991). Because the analysis is global we are able to provide rigorous criteria which cannot be obtained from a local treatment.

As it is usual in stability problems, we suppose that a small Lagrangian displacement $\boldsymbol{\xi} = (\xi_\psi, \xi_\varphi, \xi_\chi)$ in flux surface coordinates, $\equiv (\xi_r, \xi_\varphi, \xi_z)$ in cylindrical coordinates, occurs to fluid elements whose dependence on time occurs through a factor $\exp(\sigma t)$. Then we have an instability when the real part of σ is positive.

The perturbed equation of motion is:

$$\rho\left(\sigma^2\boldsymbol{\xi} + 2\Omega\sigma\hat{\mathbf{z}} \times \boldsymbol{\xi} + 2\Omega r(\boldsymbol{\xi} \cdot \nabla\Omega)\hat{\mathbf{r}}\right) = \rho' r\Omega^2\hat{\mathbf{r}} - \nabla P' - \rho'\nabla\Phi + \mathbf{F}'_{\mathbf{M}}, \tag{12}$$

where $\hat{\mathbf{r}} = \nabla(r)$ and $\hat{\mathbf{z}}$ are unit vectors in the r and z directions respectively. The perturbations to the density and pressure are given in terms of $\boldsymbol{\xi}$ by

$$\rho' = -\nabla \cdot (\rho \boldsymbol{\xi}) \text{ and}$$
$$P' = -\Gamma_1 P \nabla \cdot \boldsymbol{\xi} - \boldsymbol{\xi} \cdot \nabla P$$

respectively. The perturbation in the force per unit volume due to the magnetic field is then given by

$$\mathbf{F}'_{\mathbf{M}} = \mathbf{j}' \times \mathbf{B} + \mathbf{j} \times \mathbf{B}'.$$

Because of the coriolis terms proportional to σ in equation (12) it is not possible to derive a convenient variational principle of the type employed by Bernstein *et al.* (1958) (see Frieman and Rotenberg, 1960). However, by using the azimuthal component of the equation of motion to eliminate ξ_φ, it is posssible to derive an effective variational principle from which necessary and sufficient conditions can in principle be derived for stability to axisymmetric modes. It should be noted that the eigenvalue equation from which we derive our variational principle differs from that of Bernstien *et al.* in the way the eigenvalue is contained. We can eliminate ξ_φ from the poloidal components of the equation of motion which will then give two equations for ξ_ψ and ξ_χ. These can be written in the operator form:

$$\mathbf{O}(\boldsymbol{\xi}\ ) = \mathbf{L}(\boldsymbol{\xi}) \tag{13}$$

where, discarding the φ component

$$\mathbf{O}(\boldsymbol{\xi}) = \rho\sigma^2\boldsymbol{\xi} + \sigma^2\mu_0 \int G(\chi, \chi', \psi) 2\Omega r \rho \left[\frac{2\Omega r^2 \rho \xi_r}{|\nabla\chi||\nabla\psi|}\right]_{\chi=\chi'} d\chi' \hat{\mathbf{r}} \tag{14}$$

and

$$\mathbf{L}(\boldsymbol{\xi}) = -2\rho\Omega r(\boldsymbol{\xi} \cdot \nabla\Omega)\hat{\mathbf{r}} - \nabla \cdot (\rho\boldsymbol{\xi}) \left(r\Omega^2\hat{\mathbf{r}} - \nabla\Phi\right) + \nabla\left(\Gamma_1 P \nabla \cdot \boldsymbol{\xi} + \boldsymbol{\xi} \cdot \nabla P\right) + \mathbf{F}'_{\mathbf{M}}, \tag{15}$$

where $G(\chi, \chi', \psi)$ is a Green's function (which depends on σ^2).

Solutions of the equations of motion must be sought which satisfy the appropriate boundary conditions. If the fluid density is considered to vanish smoothly at a well defined disc boundary, while the field in exterior regions is taken to be curl free, the only condition other than regularity that we require is that the perturbed flux $\psi' = r\xi_\psi B_\chi$ related to the azimuthal displacement interior to the disc fluid match on to a vacuum solution.

If there is no matter other than that contained in the disc we must have $\psi' \to 0$ at ∞. If there are any additional perfect conductors, which could be sources of the field applied to the disc, we must have $\psi' = 0$ on their boundaries.

We proved that any eigenvalue, σ^2, must be real. Thus there can be no overstable axisymmetric modes.

5.2 Necessary and sufficient conditions for stability

The fact that the operator $\mathbf{O}$ is positive definite for an unstable mode which must have σ^2 real and positive enables us to assert that a necessary and sufficient condition for stability is that for any trial $\boldsymbol{\xi}$:

$$\int \boldsymbol{\xi}^* \cdot \mathbf{L}(\boldsymbol{\xi}) dV < 0. \tag{16}$$

In order to see this; sufficiency follows from the fact that for an unstable mode the positive definite nature of $\mathbf{O}$ requires that the condition (16) be violated for the appropriate eigenfunction. This condition is also necessary for stability to density perturbations with odd symmetry with respect to reflection in the equatorial plane. This follows from the fact that if (16) is violated for some $\boldsymbol{\xi}$, the eigenvalue equation

$$\lambda \mathbf{O}(\boldsymbol{\xi}) = \mathbf{L}(\boldsymbol{\xi}),$$

where λ is the eigenvalue, must have at least one positive eigenvalue or point in the spectrum as long as σ^2 is real and positive; a fact that follows from application of the standard variational principles as applied to self adjoint problems. By considering the way $\mathbf{O}$ depends on σ^2, the maximum value of λ in the spectrum must $\to \infty$ as $\sigma^2 \to 0$ and must $\to 0$ as $\sigma^2 \to \infty$. From continuity arguments, it then follows that there must be a positive value of σ^2 for which this must be unity, giving a spectral point for the required eigenvalue problem and hence instability.
Multiplying the $\mathbf{L}$ operator in equation (15) by $\boldsymbol{\xi}^*$, and integrating over the system, we have after some integrations by parts

$$\int \boldsymbol{\xi}^* \cdot \mathbf{L}(\boldsymbol{\xi}) dV = -\int \left(\frac{|P'|^2}{\Gamma_1 P} + \rho Q(\boldsymbol{\xi}, \boldsymbol{\xi}^*) - \frac{j_\varphi}{r} (\boldsymbol{\xi} \cdot \nabla(\psi')^* + \boldsymbol{\xi}^* \cdot \nabla \psi') + \frac{|\nabla \psi'|^2}{\mu_0 r^2} \right) dV = \mathbf{I_L}. \tag{17}$$

Here, for a fluid with smoothly vanishing density and pressure at the boundary, all integrals other than the last involving μ_0 are taken over the fluid volume V. The last integral which is in fact the magnetic energy associated with the perturbation must be taken over the whole of space excluding any perfect conductors.
The quadratic form $Q(\boldsymbol{\xi}, \boldsymbol{\xi}^*)$ includes both rotational and magnetic effects

$$Q(\boldsymbol{\xi}, \boldsymbol{\xi}^*) = r(\boldsymbol{\xi}^* \cdot \nabla r)(\boldsymbol{\xi} \cdot \nabla \Omega^2) - \boldsymbol{\xi}^* \cdot \frac{\nabla P}{\rho} \boldsymbol{\xi} \cdot \left(\frac{\nabla P}{\Gamma_1 P} - \frac{\nabla \rho}{\rho} \right) - (\psi')^* \boldsymbol{\xi} \cdot \nabla \left(\frac{j_\varphi}{r \rho} \right). \tag{18}$$

5.2.1 Stability criteria in case of a weak magnetic field

As explained above, the general necessary and sufficient condition for stability is that $\mathbf{I_L}$ given by equation (17) be negative definite. In the limit of vanishing magnetic field, all terms in equation (17) except the first two become negligible, while the first term involving P' is always negative definite. Thus it is sufficient that the quadratic form $Q(\boldsymbol{\xi}, \boldsymbol{\xi}^*)$ be positive definite for all trial functions $\boldsymbol{\xi}$ evaluated at any location. Because of the self-adjoint character of the operators $\mathbf{L}$ and $\mathbf{O}$ for an unstable mode, we can restrict ourselves to trial functions that are purely real. It is clear that we can write down a sufficient condition for stability to axisymmetric modes in the limiting case of a weak magnetic field in the form of the requirement that for any arbitrary vector $\mathbf{e}$,

$$Q(\mathbf{e}, \mathbf{e}) = r(\mathbf{e} \cdot \nabla r)(\mathbf{e} \cdot \nabla \Omega^2) - \mathbf{e} \cdot \frac{\nabla P}{\rho} \mathbf{e} \cdot \left(\frac{\nabla P}{\Gamma_1 P} - \frac{\nabla \rho}{\rho} \right) \geq 0. \tag{19}$$

If $\nabla(\Omega^2)$ in the above criterion is replaced by $2r^{-2}\Omega\nabla(r^2\Omega)$ we obtain the Hoiland criterion which one obtains for a system with no magnetic field directly, (see Tassoul, 1978). In the limit of zero rotation the condition (19) reduce to the Schwarzschild criterion,

$$-\mathbf{e}\cdot\frac{\nabla P}{\rho}\mathbf{e}\cdot\left(\frac{\nabla P}{\Gamma_1 P}-\frac{\nabla\rho}{\rho}\right)\geq 0,$$

implying that the entropy always increases in the direction of decreasing pressure for stability. In the case of rotating fluid, assuming that the vector $\mathbf{e}$ is tangent to surfaces of constant pressure or of constant entropy, the stability condition becomes

$$r(\mathbf{e}\cdot\nabla r)(\mathbf{e}\cdot\nabla\Omega^2)\geq 0.$$

This is the Solberg criterion (compressible fluid version of the Rayleigh criterion) that applies in the limiting case of a weak magnetic field, requiring that the angular velocity must increase outward for stability.
The condition (19) can be shown to be necessary as well as sufficient for stability in the limiting case of very small magnetic field. The proof of this is included in Papaloizou and Szuszkiewicz (1992).

5.2.2 Sufficient conditions for stability for the case of an externally imposed curl free magnetic field ($j_\varphi = 0$)

For a system with externally imposed magnetic field such that the current density in equilibrium is zero, using equation (17) the general condition for stability (16), $\mathbf{I_L} < 0$, reduces to

$$-\int\left(\frac{|P'|^2}{\Gamma_1 P}+\rho Q(\boldsymbol{\xi},\boldsymbol{\xi}^*)+\frac{|\nabla\psi'|^2}{\mu_0 r^2}\right)dV<0. \tag{20}$$

The quadratic form $Q(\boldsymbol{\xi},\boldsymbol{\xi}^*)$ is given by

$$Q(\boldsymbol{\xi},\boldsymbol{\xi}^*)=r(\boldsymbol{\xi}^*\cdot\nabla r)(\boldsymbol{\xi}\cdot\nabla\Omega^2)-\boldsymbol{\xi}^*\cdot\frac{\nabla P}{\rho}\boldsymbol{\xi}\cdot\left(\frac{\nabla P}{\Gamma_1 P}-\frac{\nabla\rho}{\rho}\right). \tag{21}$$

The first two terms in (20) are the same as in the case of a very weak magnetic field. The third one, which differentiates the present case from the previous one increases with the strengh of the magnetic field, B_χ. This being positive definite acts to stabilize the system, so if we replace it by a lower bound for its magnitude in equation (20), we obtain a sufficient condition for stability.
To construct a lower bound we determine the minimum possible value of the real number ζ defined by

$$\zeta=\frac{\int\frac{1}{r^2}|\nabla\psi'|^2dV}{\int g|\psi'|^2dV}, \tag{22}$$

with respect to variation over functions ψ' which vanish at ∞, where g is for the moment an arbitrary positive definite function which vanishes outside the region occupied by the disc matter.
The integral should be taken over all space excluding any external conductors but it is easy to see that if these are ignored the minimum ζ decreases because the range of possible

trial functions increases. Thus for the purposes of obtaining a lower bound and a sufficient condition for stability, we may ignore any possible external conductors.

Then we find that

$$\zeta = \frac{\int \frac{1}{r^2}|\nabla\psi'|^2 dV}{\int g|\psi'|^2 dV} \geq \frac{1}{\sqrt{\int\int \mathcal{K}^2(\mathbf{r},\mathbf{r}')gg'(rr')^2 dV dV'}} = \zeta_0, \tag{23}$$

where the kernel $\mathcal{K}(\mathbf{r},\mathbf{r}')$ has the form:

$$\mathcal{K}(\mathbf{r},\mathbf{r}') = \frac{1}{2\pi}\int_0^\pi \frac{\cos\varphi d\varphi}{(r^2+r'^2-2rr'\cos\varphi+(z-z')^2)^{1/2}}. \tag{24}$$

The use of the inequality (23) to estimate the last term on the right hand side of the condition (20) allows us to give a sufficient condition for stability in the form similar to the condition (19), which applies in the case of an arbitrary weak magnetic field. With the choice of the function g to be unity inside the matter and zero otherwise, this takes the form that for any vector $\mathbf{e}$ we require that

$$Q_{j=0} = r(\mathbf{e}\cdot\nabla r)(\mathbf{e}\cdot\nabla\Omega^2) - \mathbf{e}\cdot\frac{\nabla P}{\rho}\mathbf{e}\cdot\left(\frac{\nabla P}{\Gamma_1 P} - \frac{\nabla\rho}{\rho}\right) + \frac{\zeta_0}{\mu_0}\frac{(\mathbf{e}\cdot\nabla\psi)^2}{|\nabla\psi|^2}\frac{r^2 B_\chi^2}{\rho} \geq 0, \tag{25}$$

where we have used the fact that $\psi' = -\boldsymbol{\xi}\cdot\nabla\psi$ and the subsequent replacement of $\boldsymbol{\xi}$ by $\mathbf{e}$. This condition is that the quadratic form in the components of $\mathbf{e}$, $Q_{j=0}$, must be positive definite. These criteria generalize the conditions for stability derived from a local analysis given by Fricke (1969) so that they apply to the full global problem which has so far only been treated in the special case of an incompressible cylinder with a vertical magnetic field by Chandrasekhar (1960).

When there is no rotation or magnetic field we find Schwarzschild's criterion to be sufficient for stability. When rotation and a magnetic field are present if Schwarzschild's condition is to be satisfied along every field line, then there is a magnitude of the magnetic field above which we are guaranteed stability to axisymmetric modes for any differentially rotating system threaded by an externally applied field. However, we should note that satisfaction of Schwarzschild's criterion may not be necessary for stability since it has been shown that the presence of a magnetic field can provide increased stability to convection, (Moss and Tayler, 1969).

In the case of a geometrically thin ring or disc, if the differentially rotating ring is threaded by an applied field such as one due to a dipole, in the limit when it is very thin the flux surface coordinates (ψ,χ) become equivalent to the cylindrical coordinates (r,z). Provided Schwarzschild's criterion is satisfied in both the radial and vertical directions, then it was shown that it is sufficient for stability that at any point in the ring

$$\frac{\zeta_0}{\mu_0}\frac{r^2}{\rho}\mathrm{B}_\chi{}^2 > -r\frac{d\Omega^2}{dr}.$$

We use equation (23) to evaluate ζ_0 and hence find a magnitude for the magnetic field above which there should be stability to axisymmetric modes. The kernel $\mathcal{K}(\mathbf{r},\mathbf{r}')$ can be expressed in terms of the elliptic integrals K and E. Integrating over the volume of the disc which is taken to have local vertical thickness, $H(r) << r$, we have

$$\zeta_0 = \frac{1}{\sqrt{\int_{R_0}^{R_1}\int_{R_0}^{R_1}\mathcal{K}^2(\mathbf{r},\mathbf{r}')(rr')^3 HH' dr dr'}} = \frac{1}{\alpha\epsilon R_1^4}.$$

Here R_1, R_0, ϵ and α are the outer radius of the disc, the inner radius of the disc , a dimensionless measure of H/r, and a constant of order unity respectively.
The strength of the magnetic field sufficient to stabilize the flow is then given by

$$B_\chi^2 \geq \mu_0 \rho \alpha \epsilon R_1^4 \left(\frac{1}{r}\right) \left|\frac{d\Omega^2}{dr}\right|. \tag{26}$$

In physical terms this means that, to within a factor of order unity, the Alfvèn velocity must exceed the product of the orbital velocity and the square root of the ratio of the thickness to radius.
We comment that the minimizing perturbed flux varies on a length scale comparable to the disc radius and note that it extends into the vaccuum region also varying on this length scale. Thus contributions to the perturbed magnetic energy come from a volume which is larger than that of the disc by a factor that is measured by the ratio of the disc radius to thickness. It is for this reason that our estimates of the stabilizing field magnitude vary as the square root of the disc thickness.
To get an idea of the strength of a magnetic field sufficient to give stability of the accretion discs, which are expected to exist in many astrophysical systems, we consider a case of a accreting neutron star. A star of one solar mass typically accretes matter from a disc of size 10^{10} cm at a rate of 10^{16} g/s. The standard, Shakura-Sunyaev (1973), thin disc model gives at the outer edge of the disc the density $\rho \approx 3 \cdot 10^{-8}$ g/cm^3 and the relative thickness $\epsilon \approx 2 \cdot 10^{-2}$. (The viscosity parameter, α, is taken to be 1). Inserting those values into the formula (26) we find the magnetic field to be of the order of 10^3 Gauss.

5.2.3 Sufficient conditions for stability for the case of a magnetic field with non-zero current density in equilibrium ($j_\varphi \neq 0$)

In order to find a sufficient condition for stability in this case we use the condition (16) but now all the terms in (17) and (18) must be taken into account. In order to obtain a criterion in the same form as that given in the previous section, we find a lower bound for the magnitude of the last two terms in equation (17). The last two terms can be written as follows

$$\int \left(\frac{j_\varphi}{r} (\boldsymbol{\xi} \cdot \nabla (\psi')^* + \boldsymbol{\xi}^* \cdot \nabla \psi') - \frac{|\nabla \psi'|^2}{\mu_0 r^2} \right) dV =$$

$$- \int \left(\mu_0 \left| \frac{j_\varphi \boldsymbol{\xi}}{\theta} - \frac{\nabla \psi'}{\mu_0 r} \theta \right|^2 - \mu_0 \frac{j_\varphi^2 |\boldsymbol{\xi}|^2}{\theta^2} + \frac{|\nabla \psi'|^2 (1-\theta^2)}{\mu_0 r^2} \right) dV$$

where $0 < \theta < 1$ is an arbitrary constant. The first term in the integral on the right hand side of the above is negative definite and may be ignored for the purposes of determining a sufficient condition for stability. Doing this and using equation (23), the sufficient condition for stability, $\mathbf{I_L} < 0$, will be satisfied if at any location, $\mathbf{r}$, and for any vector $\mathbf{e}$

$$\begin{aligned} Q_{j \neq 0} \;=\; & r(\mathbf{e} \cdot \nabla r)(\mathbf{e} \cdot \nabla \Omega^2) - \mathbf{e} \cdot \frac{\nabla P}{\rho} \mathbf{e} \cdot \left(\frac{\nabla P}{\Gamma_1 P} - \frac{\nabla \rho}{\rho} \right) + \frac{(\mathbf{e} \cdot \nabla \psi)}{|\nabla \psi|} r B_\chi \left(\mathbf{e} \cdot \nabla \left(\frac{j_\varphi}{r \rho} \right) \right) \\ & + \frac{\zeta_0 (1-\theta^2)}{\mu_0} \frac{(\mathbf{e} \cdot \nabla \psi)^2}{|\nabla \psi|^2} \frac{r^2 \mathrm{B}_\chi^2}{\rho} - \mu_0 \frac{j_\varphi^2 |\mathbf{e}|^2}{\theta^2} \geq 0 \end{aligned} \tag{27}$$

Setting $j_\varphi = 0$ and θ to be arbitrarily small, the condition for stability (25) is recovered. When there is a non-zero current density, the sufficient condition for stability is more complicated. However, the magnitude of the current density cannot be arbitrary large. This is guaranteed by a property of the equilibrium itself. In fact from equation (8) it follows that for large B_χ, j_φ varies as $1/B_\chi$. In this limit the effect of the equilibrium current density becomes small, and as before, we conclude that if a large enough magnetic field threads the system and Schwarzschild's criterion is satisfied along the field lines, there will be stability to axisymmetric modes.

6 Final remarks

The problem of the stability of a non self-gravitating differentially rotating system with an externally imposed poloidal magnetic field to axisymmetric modes was solved by Papaloizou and Szuszkiewicz (1992). They obtained global criteria in a rigorous way using a variational principle without the necessity of introducing incompressibility or Boussinesq approximations. A general necessary and sufficient condition for stability was given for the limiting case when the magnetic field was weak. Then the system is dynamically stable with respect to axisymmetric motions if and only if condition (19) is satisfied. This shows that there will be instability if on any surface of constant entropy or pressure, the angular velocity decreases outwards. This implies that a thin rotating disc in a state of near Keplerian rotation is unstable.

For a system with externally imposed magnetic field such that the current density in equilibrium is zero they obtained a sufficient condition for stability (25) which generalizes the conditions for stability given by Fricke (1969) on the basis of a local analysis which used a Boussinesq approximation.

If Schwarzschild's criterion along every field line is satisfied then there is always a magnitude of the magnetic field above which the system is stable. For a geometrically thin ring or disc, they found that the strength of the magnetic field is sufficient to stabilize the flow if locally, to within a multiplicative factor of order unity, the Alfvèn speed is greater than the product of the rotational velocity and the square root of the ratio of the disc thickness to radius.

They also gave a sufficient condition for stability (27) when the system has azimuthal currents in addition to a poloidal magnetic field. The equilibrium conditions for a differentially rotating system show that for very strong fields, the current density has to decrease in magnitude with increasing field strength. This means that stability to axisymmetric modes is guaranteed if an externally applied magnetic field is strong enough. These results are in the full agreement with those obtained by Knobloch (1992) for the case of a constant vertical field (the second particular case listed in Section 4). The stability of a disc in the more general case is still an open question. A study of the type presented by Papaloizou and Szuszkiewicz (1992) should be extended to the case of non-zero toroidal field.

References

Balbus, S. A., and Hawley, J. F., "A Powerful Local Shear Instability in Weakly Magnetized Disks: I. Linear Analysis", preprint, (1991)

Bernstein, I. B., Frieman, E. A., Kruskal, M. D., and Kulsrud, R. M., "An Energy Principle for Hydromagnetic Stability Problems", *Proc. R. Soc.* **A244**, 17, (1958)

Chandrasekhar, S., "The Stability of Non-Dissipative Couette Flow in Hydromagnetics", *Proc. Nat. Acad. Sci.* **46**, 253, (1960)

Cowling, T. G., *Magnetohydrodynamics* (2nd ed.) Hilger, Bristol, (1976)

Ferraro, V. C. A., "The Non-Uniform Rotation of the Sun and its Magnetic Field", *Mon. Not. R. astr. Soc.* **97**, 458, (1937)

Fricke, K., "Stability of Rotating Stars II. The Influence of Toroidal and Poloidal Magnetic Fields", *Astron. Astrophys.* **1**, 388, (1969)

Frieman, E., and Rotenberg, M., "On Hydromagnetic Stability of Stationary Equilibria", *Rev. Mod. Phys.* **32**, 898, (1960)

Ghosh, P., and Lamb, F. K., "Accretion by Rotating Magnetic Neutron Stars III. Accretion Torques and Period Changes in Pulsating X-ray Sources ", *Astrophys. J.* **234**, 296, (1979)

Hawley, J. F., and Balbus, S. A., "A Powerful Local Shear Instability in Weakly Magnetized Disks: II. Nonlinear Evolution", preprint, (1991)

Knobloch, E., "On the Stability of Magnetized Accretion Discs", *Mon. Not. R. astr. Soc.* **255**, 25P, (1992)

Mestel, L., and Ray, T. P., "Disc-like Magneto-gravitational Equilibria", *Mon. Not. R. astr. Soc.* **212**, 275, (1985)

Moss, D. L., and Tayler, R. J., "The Influence of a Poloidal Magnetic Field on Convection in Spherical Shells", *Mon. Not. R. astr. Soc.* **145**, 217, (1969)

Papaloizou, J., and Szuszkiewicz, E., "The Stability of a Differentially Rotating Disc with a Poloidal Magnetic Field", *Geophys. and Astrophys. Fluid Dynamics*, to appear, (1992)

Pitts, E., and Tayler, R. J., "The Adiabatic Stability of Stars Containing Magnetic Fields - VI. The Influence of Rotation", *Mon. Not. R. astr. Soc.* **216**, 139, (1985)

Pringle, J. E., "Accretion Discs in Astrophysics", *Ann. Rev. Astr. Ap.* **19**, 137, (1981)

Shakura, N. I., and Sunyaev, R.A., "Black Holes in Binary Systems. Observational Appearance", *Astron. Astrophys.* **24**, 337, (1973)

Tassoul, J.-L., "Theory of Rotating Stars", Princeton University Press, Princeton, (1978)

Dusty Discs as Tracers of Binary Star Formation

C. J. Clarke
Institute of Astronomy
Madingley Road, CAMBRIDGE,ENGLAND.

1. INTRODUCTION

In recent years, much effort has been expended on the modeling of circumstellar emission around pre-main sequence stars (Adams, Lada and Shu 1987, Beckwith et al. 1990). Such models consist, in general, of a central stellar source and a flattened, axisymmetric, distribution of gas and dust whose luminosity may be derived both from the re-processing of stellar radiation and an intrinsic (accretion) luminosity. Although such models have had some success in explaining the broadband spectral energy distributions of pre-main sequence stars, they are clearly incomplete in an important respect: implicitly they apply to *single* stars, whereas the majority of stars exist in binary systems, both during the main sequence and pre-main sequence stages (Abt and Levy 1976, Duquennoy and Mayor 1991). A recognition of this fact would complicate the models fits considerably, since one would then have to take into account not only the multiple stellar sources but also the discs around each of these sources, together with the possibility of further dusty disc material external to the entire system.Since it is by no means clear what the relative orientation of these components would be, the number of model parameters would become uncomfortably large.

There are, however, good reasons for studying the distribution of gas and dust around pre-main sequence binaries. Firstly, such distributions may contain valuable fossil evidence about the initial mechanism for binary formation: whether, for example, one should favour models in which residual gas is predominantly distributed around the individual components or those in which a substantial quantity ends up in circumbinary orbit. Secondly, recent theoretical work suggests that residual gas discs may play an important role in shaping the orbital parameters of binary systems: that is, in shaping the distribution of orbital periods and eccentricities. The magnitide of such an effect is however likely to depend on the location of the residual gas (i.e. circumbinary or circumstellar), again requiring an input from observational studies.

In this contribution, we review the recent observational and theoretical developments that make the study of circumbinary dust distributions particularly timely. In Section 2, we briefly describe the parameters of main sequence and of pre- main sequence binaries, paying particular attention to the properties of any associated gas/dust. In Section 3 we describe some recent theoretical work on binary-disc interactions and, in Section 4, we discuss some of the issues that can be settled by future observational programmes.

2. THE OBSERVATIONAL PROPERTIES OF BINARY SYSTEMS

2.1. Binary Parameters

2.1.1. Main sequence binaries

It has long been known that binaries are common among stars of solar type and earlier: although much controversy has surrounded precise estimates of the incidence of binary systems (e.g. Abt and Levy 1976, Morbey and Griffin 1987), there is a broad consensus that the binary fraction for solar type stars lies in the range $65 - 100\%$ (Duquennoy and Mayor 1991).

A striking feature of the binary parameter distribution is the enormous dynamic range of orbital separations: seven orders of magnitude from systems that are almost in contact to those so wide that they are destined to be dissociated by encounters with field stars. The distribution can be represented by a broad Gaussian in log period, with a median period of 180 years: for the present discussion the important feature of this distribution is the lack of a characteristic scale for binary formation.

Another notable chararcteristic of binary systems is their high orbital eccentricity. Apart from the closest systems (periods less than 10-20 days) which are circularised by tidal effects, eccentricities of several tenths are common, with a trend of increasing mean eccentricity with increasing period: although low eccenticities are encountered in long period systems, the converse is not true, so that observed systems lie beneath an upper envelope in the log period, eccentricity plane (Duquennoy and Mayor 1991, Duquennoy, Mayor and Mermilliod 1992). The existence of such an envelope is hard to ascribe to selection effects and is without explanation at present.

2.1.2. Pre-main sequence binaries

Although visual pairs of pre-main sequence stars have long been noted in objective prism surveys (e.g. Cohen and Kuhi 1979), it is only during the last ten years that there has been substantial progress in detecting pre-main sequence binaries through spectroscopic, lunar occultation and speckle techniques. It is difficult at present to make a reliable assessment of the relative incidence of binarity during the main sequence and pre-main sequence stages, but preliminary estimates indicate that binaries are at least as common during the pre-main sequnce stage as subsequently. Approximately one in ten T Tauri stars has a spectroscopic companion (Mathieu, Adams and Latham 1989), a figure in line with similar estimates for the main sequence population: when placed in the H-R diagram, such systems number among them some of the youngest objects that are optically visible, so that binaries can clearly form within a timescale of 10^5 years. Amongst somewhat wider systems (that is, those with separations in the range 1-100 A.U. that are detected by interferometric techniques) there have been a number of recent claims that the the binary fraction seems to be somewhat higher (by a factor 1.5 to 2) than on the main sequence (Ghez et al 1992, Simon 1992 Leinert et al. 1992). Such findings, although intriguing, should not however be over- interpreted pending a fuller understanding of the differential selection effects between main sequence and pre-main sequence surveys.

The number of systems with well determined orbital parameters is at present small, but when such systems are plotted in the log period, eccentricity plane they display an upper envelope qualitatively similar to that exhibited by main sequence systems (Mathieu 1992).

2.2. Gas and dust distributions around binaries

The direct spectral diagnostic of warm dust close to the surface of young stars is the incidence of excess emission at near infra-red wavelengths over purely photospheric emission (Adams, Lada and Shu 1989). Such a characteristic is usually associated with strong broad H α emission, a defining property of the so-called Classical T Tauri Stars (CTTS), which constitute about a quarter of low mass pre-main sequence stars. Thus H α equivalent width (which is available for many more systems than are broadband spectral energy distributions) is used as an indirect indicator of circumstellar material within a few stellar radii.

The relation between H α equivalent width and binary separation is striking: very few binaries closer than about an A.U. are classified as CTTS. Associated gas and dust is not necessarily absent from such systems, but appears to be excluded from size scales comparable with the binary orbit: thus close binaries, whilst lacking an excess at near infra-red wavelengths, may exhibit an excess in the far infra-red, a finding consistent with the binary being enclosed by a hollowed out disc (Jensen et al. 1991). (Note, however, that such cavities are common among Weak Line T Tauri Stars (Montmerle 1991) and cannot, therefore, be always ascribed to the presence of close binary companions). A notable system with evidence for both circumstellar and circumbinary emission is the CTT GW Orionis (separation of about an A.U.) in which the spectral energy distribution indicates excess emission at both 1 micron and again at 20-100 microns but with a spectral dip in between: such structure has been interpreted as indicating a disc around the primary, an annular gap, and then an enclosing circumbinary disc (Mathieu, Adams and Latham 1991).

In the case of millimetre emission,the connection with binarity is less clear. In the course of an extensive survey of T Tauri systems, Beckwith et al. 1991 found detectable millimetre emission (corresponding to dust masses greater than 0.01 solar masses) only in the case of binaries wider than 100 A.U.. The implication of such a result is that whereas millimetre emission (which arises from cool dust on scales of order 100 A.U. from the stellar source) is commonly found in discs around the individual components in binaries wider than this, it is rarely to be found as circumbinary material around a closer binary. However Beckwith et al stressed that their conclusions were provisional, based as they were on upper limits in many cases. Moreover, subsequent binary surveys have shown that a number of systems classified as single by Beckwith et al (and possessing detectable masses of cool dust) are in fact binaries, thus weakening the original correlation considerably.

Thus, to summarise the available data on dusty material around pre-main sequence binaries, it can be said that circumstellar material (that is, material surrounding the individual components) is common among wider binaries, but rare among closer systems. The transition between these two regimes occurs for separations of 1-10 A.U., that is, the region most readily accessible

through lunar occultation studies. The situation concerning the incidence and quantity of circumbinary material (that is, material enclosing the entire binary) is considerably less clear and, in view of the arguments presented in Section 3, in urgent need of clarification.

3. THE THEORY OF BINARY-DISC INTERACTIONS

What happens to a gaseous disc if it is set up with a binary (rather than a single star) at its centre? This question was investigated by Artymowicz, Clarke, Lubow and Pringle (1989) using a Smoothed Particle Hydrodynamic (SPH) code, with the aim of discovering both the disc response and the dynamical conseqeunces for the binary. The simulations showed that after a brief transient stage a cavity is swept in the inner disc, whose radius, for a binary whose components are not vastly different in mass, is roughly equal to twice the binary orbital separation. The cavity is a result of the lack of stable particle orbits deep in the binary potential: its rim is fixed by the requirement that at this point the rate of angular momentum transfer from binary to disc is equal to the rate at which viscous torques are able to transfer angular momentum outward through the disc. Although the disc viscosity thus plays an important role in establishing such a rim, the radius of the rim is however rather insensitive to the magnitude of the viscosity. This is because the interaction with the central binary falls off so steeply as a function of radius that a relatively minor adjustment to the cavity rim is able to compensate for variations in the viscosity.

A notable feature of this simulation is that after the transient clearing stage, the cavity rim is a stable phenomenon, with no leakage of particles through the tidal barrier set up around the binary.

An immediate consequence of the creation of such a cavity is that the material closest to the binary (and that, therefore, with which it is in strongest interaction) is rotating more slowly than the binary and therefore can extract both energy and angular momentum from the binary orbit. Clearly, then, the sign of the interaction is such that the binary orbit must shrink, but the sign of eccentricity changes depends on the ratio in which energy and angular momentum are removed. It turns out that the dominant coupling between binary and disc material is via an Outer Lindblad Resonance for which angular momentum transfer dominates energy transfer: consequently, the binary eccentricity *grows*. The magnitude of this effect depends on the magnitude of the surface density at the resonance: as an example, Artymowicz et al found that a disc that contained 1% of the binary mass within a few binary radii suffered fractional changes in eccentricity of order unity within 10^3 orbital periods. Clearly, therefore, this effect would be significant for binaries with periods less than about 10^3 years even for the case of rather modest circumbinary disc masses.

4. DISCUSSION

One consequence of the above simulation is that circumbinary discs, if deposited during the initial stages of binary formation, should be long lived phenomena. This is because, unlike the case of discs around single stars, they do not have the opportunity to rid themselves of most of their mass by accretion onto the central star, since this is prevented by the tidal barrier set up around the binary. This may imply, for example, that dusty discs around binaries are more likely to survive to the main sequence than are their counterparts around single stars, an effect that could be sought in samples of main sequence stars showing a Vega-like excess. (It should be stressed, however, that the mechanism for the dispersal of pre-main sequence disc material is poorly understood, and that the action of stellar winds may be the chief agent by which such structures are stripped away. Nevertheless, it may be argued that since circumbinary discs are unable to rid themselves of mass by accretion, they should be *at least as* likely to survive to the main sequence as are their counterparts around single stars. An observational study of the relative incidence of Vega-like excesses around single stars and around binaries could thus provide important information as to whether binaries are formed with circumbinary discs).

A more direct approach would be to continue the search for circumbinary material around pre-main sequence binaries as pioneered in the studies described above. Discs around single stars are known to survive for several million years (Strom et al 1990), and so, by the above argument, circumbinary discs should be at least as long lived. There are several motivations for wishing to know whether binaries are formed with material in circumbinary orbit. Firstly, the simulation of Artymowicz et al suggested that the presence of such material would have a dramatic effect on the orbital parameters of the binary, producing a significant growth in orbital eccentricity even for the case of rather modest disc masses. An immediate question, therefore, is to ask whether this effect is compatible with the observed distribution of binaries in the log period, eccentricity plane. Secondly, the presence or absence of circumbinary material may lend some clues as to the initial mechanism for binary formation. For, whereas the detailed predictions of the various models are not yet available, it is likely that contending mechanisms would result in differing fractions of the system mass ending up in circumbinary orbit. It is tempting to speculate, for example, that whereas the formation of a binary through disc fragmentation (e.g Adams, Ruden and Shu 1989) would leave a substantial reservoir of such material, this might not be the case for binaries formed either through capture or through the sort of 'prompt initial fragmentation' scenario described by Pongracic (this volume). In the latter cases, it is not necessarily straightforward to retain on bound orbits material that has sufficient angular momentum to orbit outside the binary. (It should be stressed, at this point, that not all circumbinary material qualifies as a circumbinary *disc*: material raining in on almost radial orbits would not encounter such a tidal barrier and could be readily accreted by the central components (e.g. Bonnell 1991). The longevity of material in circumbinary orbit only applies to the case of angular momentum supported (i.e. disc) material).

A further consequence of recognising the binary (or higher order multiple) nature of most pre-main sequence systems is that even cold circumstellar dust can assume a much more three-dimensional distribution than that assumed in the case of single star disc models. This is because the gas and dust around the system may be warped/ flared by the dynamical interactions between the components. For example, Clarke and Pringle (1992) computed the case of an eccentric binary in which the discs around the individual stars were not co-planar with the binary orbit, and in which the discs were initially set up so as to be intersected by the binary companion at pericentre. The result was that the discs were stripped, on the first periastron passage, to radii such that they would not intersect on subsequent passes, whilst the material retained around the individual components was highly warped after the encounter. Moreover, that material that was stripped from the system expanded away from the binary with a speed comparable with the binary orbital velocity at pericentre, and would therefore modify the appearance of longer period binaries over a substantial fraction of their pre-main seqeunce lifetimes. Thus, the optical extinction of visual pairs can place some constraints on the mechanism for binary formation.

Finally, we speculate that the results of Artymowicz et al may provide an explanation of the observed dearth of close spectroscopic binaries possessing the spectral diagnostics of material close to the individual components. For, if the cavity of a circumbinary disc is as stable as indicated by these calculations, the supply of material that can accrete onto the binary inside is thereby cut off. The interior discs (around each of the stars) are thereby starved of material with which to replenish that which they lose by viscous accretion onto their central stars. Consequently, such a binary would only possess the characteristics of a Classical T Tauri Star for a timescale of order the viscous accretion timescale of its interior discs (whose dimensions are necessarily less than the orbital separation of the binary). We might therefore use this argument to estimate the viscous diffusion timescale of such discs as a function of their radii, by noting that CTT characteristics start to be commonly observed for binaries wider than a few A.U.. This would suggest that discs of such a radius would have a viscous diffusion timescale comparable with the lifetime of T Tauri stars, i.e. $10^5 - 10^6$ years.

REFERENCES

Abt, H.A. 1987. *Ap. J.* **317**,353.

Abt, H.A. and Levy, S.G., 1976. *Ap. J. Suppl.* **30**,273.

Adams, F.C., Lada, C.J. and Shu, F.H.,1987. *Ap. J.* **312**, 788.

Adams, F.C., Ruden, S.P. and Shu, F.H., 1989. *Ap. J.* **347**,959.

Artymowicz, P., Clarke, C.J.,Lubow, S. and Pringle, J.E. 1991.*Ap. J.* **370**,L35.

Beckwith, S. et al., 1990. *Astr. J.* **99**,924.

Bonnell, I., 1992. in IAU Colloq. 135, ed W. Hartkopf & H. McAlister, (ASP San Francisco), in press.

Clarke, C.J. and Pringle, J.E., 1992. *MNRAS* in press.

Cohen, M. and Kuhi, L.V., 1979. *Ap. J. Suppl.* **41**,743.

Duquennoy, A. and Mayor, M., 1991. *A &A* **248**,485.

Duquennoy, A.,Mayor,M. and Mermilliod, J.-C. 1992. in IAU Colloq. 135, ed W. Hartkopf and H. McAlister (ASP, San Francisco), in press.

Ghez, A., Neugebauer, G. and Mathews, K. 1992. in IAU Colloq. 135, ed W. Hartkopf and H. McAlister, (ASP, San Francisco), in press.

Jensen, E.L. et al 1992. in preparation.

Leinert, C. et al 1992. in IAU Colloq. 135, eds W. Hartkopf & H. McAlister, (ASP, San Francisco), in press.

Mathieu, R.D. 1992. in 'Binary Stars as Tracers of Stellar Formation', ed. A. Duquennoy and M. Mayor (CUP), in press.

Mathieu, R.D., Adams, F. and Latham, D.W., 1991. it Astr. J. **101**, 2184.

Mathieu, R.D., Walter, F.M. and Myers, P.C., 1989 *Astr. J.* **98**,987.

Montmerle, T., 1991. in 'The Physics of Star Formation and Early Stellar Evolution', eds C.J. Lada and N.Kylafis, (Kluwer:Dordrecht),p.675.

Morbey, C.L. and Griffin, R.F., 1987. *Ap. J.* **317**, 343.

Simon, M. 1992. in IAU Colloq. 135, eds W.Hartkopf and H.McAlister, (ASP, San Francisco), in press.

Strom, S.E., Edwards, S. and Skrutskie, M.F. 1990. *AIP Conf. Proc.* **207**, p. 71.

What is a Vega-like Dust Disc?

H. J. Walker
Rutherford Appleton Laboratory,
Chilton, Didcot, Oxon, UK

Abstract

The main, common properties of the prototype Vega-like stars are defined. Using these properties, of the stars and dust discs, it is possible to determine search criteria for finding new Vega-like dust discs, and to determine new areas for refining the properties of the discs by further investigation, to establish more accurately their characteristics.

1 Introduction

One exciting discovery by the Infrared Astronomy Satellite (IRAS) was the dust disc around Vega (α Lyr), a normal main-sequence star. Vega was one of the stars used to calibrate IRAS, because it was well understood in the optical (if we ignore the pioneering work in the near infrared by Selby *et al*, 1983). Aumann *et al* (1984) reported that the star showed excess infrared emission (over that expected by a 10 000K black-body) at 60μm. They determined that the infrared excess was caused by thermal radiation arising from dust grains more than 1mm in radius, heated to 85K. The source profile of Vega at 60μm was broader than that of other stars (*e.g.* Acturus) and the disc diameter was deduced to be around 20 arcsec. They concluded 'that the radiating solid material is in orbit around the star and has been since the time of formation of the star'. Their evidence for this was that the dust grains were too large to be interstellar dust grains, and there was no sign of mass loss from Vega.

2 The properties of the prototypes

Gillett (1986) reported on four stars with Vega-like infrared excesses, namely Vega, β Pic, α PsA, and ϵ Eri. These four stars became the prototype Vega-like stars, with the infrared excesses called by many different names in the literature (*e.g.* cool excesses, cool matter, preplanetary discs, protoplanetary discs). The Vega disc was found to be viewed face-on, where as the β Pic disc was edge-on.

The main features the stars had in common were:—

- They were all very normal, main-sequence stars

- They were all bright, nearby stars
- They were all single stars
- They were all surrounded by cool dust (only β Pic had an excess at 12μm, the rest showed excess emission at 25μm, 60μm, and 100μm)
- The dust discs were small in size and mass

Wolstencroft & Walker (1988) showed the range of disc masses possible, in terms of Earth-masses, depending on whether the upper limit to the size of the dust grains was of the order 1mm or 100km (*i.e.* asteroid sized dust grains). They also noted one other common feature for the prototypes, that they have an inner dust free zone (apart from ϵ Eri).

There are two approaches to further investigation, one is to find more stars with the same type of dust characteristics, the second is to investigate the prototypes further, to refine the properties of those known dust discs.

3 The search for new Vega-like stars

As might be expected, several people have searched the IRAS catalogues and data for stars showing the same kind of cool excess. By studying the criteria selected for the search, it is possible to see which characteristics of the dust discs, and their associated stars, are regarded as most significant. Some examples are given in Table 1, showing the variety of searches undertaken.

Table 1. Search criteria for new Vega-like stars

1. Aumann (1985): criteria —
   - Used Gliese and Woolley catalogues of nearby stars
   - IRAS source must be associated with dwarf or sub-giant
   - IRAS catalogued flux at 12μm, 25μm, 60μm
   - 'Statistically significant' excess at 60μm
   - Spatial extent less than 90 arcsec
2. Sadakane & Nishida (1986): criteria —
   - Used Bright Star Catalog, no K or M giants, no emission lines
   - IRAS catalogued fluxes at 12μm, 25μm, 60μm
   - Significant excess at 60μm
   - $|\ b\ | > 10^{\circ}$
3. Backman & Gillett (1987): criteria —
   - Used Gliese Catalog

- Only 12μm flux need be in IRAS Catalog, other fluxes found from raw data
- Excess at 25μm, 60μm, or 100μm

4. Walker & Wolstencroft (1988): criteria —
   - Used SAO Catalog, no peculiar or emission line stars
   - IRAS catalogued flux at 12μm, 25μm, 60μm, + 100μm
   - 60μm/100μm 'like' prototypes
   - IRAS Confusion status = 3, for any wavelength (showing source very slightly extended)

Aumann (1985) followed the characteristics of the prototypes most closely, and found 12 stars which fulfilled his criteria (including the four prototypes). None of the new stars had flux detected by IRAS at 100μm. Sadakane & Nishida (1986) and Walker & Wolstencroft (1988) dropped the criterion that the stars must be nearby. Sadakane & Nishida focussed, partly by chance, on A stars, and found 12 new candidates. Walker & Wolstencroft found 18 new candidates, with excesses more like β Pic at 12μm than Vega. Despite being further away, the estimated disc sizes for these new candidates were similar to those found for the prototypes. They also used a 25μm/60μm criterion for stars additionally in the Gliese catalogue and found 12 new candidates, four of which were in common with the list of Aumann (1985). Backman & Gillett (1987) dropped the criterion about having all the fluxes in the IRAS Point Source Catalog, and used the IRAS data themselves to determine weak fluxes at wavelengths other than 12μm. They found 25 new Vega-like stars with excesses at 25μm, 60μm or 100μm, including 7 from Aumann's list.

All these studies confirmed an initial characteristic from the four prototypes, that the dust discs most often occur around A stars. Aumann (1988) investigated the spectral-type distribution of stars showing the Vega-like phenomenon, and confirmed that this was the case. A stars most often show Vega-like flux excesses due to a bias in the IRAS database which favours nearby bright stars (which are usually A or F stars), and the material orbiting luminous A stars is most favoured for detection by IRAS.

Aumann & Probst (1991) studied the 12μm characteristics of nearby stars (using the Gliese catalogue), looking for new Vega-like stars that could be further investigated using ground-based telescopes. Of 548 main sequence stars, they found one suitable candidate (β Pic), and one doubtful one!

4 The follow-up of the prototypes at other wavelengths

Harper *et al* (1984) observed Vega at 193μm with the KAO, and found that their datum fell below the simple black-body model for the dust, showing that a more sophisticated model was needed. Most follow-up has been done on β Pic, because its dust disc is edge-on and can be seen optically. However, the disc around β Pic is unusual in several respects and so this may not reveal much about the 'typical' parameters for the dust

discs generally. Optical imaging enabled the disc to be seen in scattered light by Smith & Terrile (1984), Gradie *et al* (1987), and Paresce & Burrows (1987). The disc was found to be asymmetric, and the size of the dust grains were greater than 1μm. Polarisation in disc was measured by Gledhill *et al* (1991), and found to be 17% at R, suggesting large grains in disc. The dust disc was resolved at 10μm and 20μm by Telesco *et al* (1988), suggesting grains less than 1μm in size were present. Observations at 800μm (Becklin & Zuckerman, 1990) and 1300μm (Chini *et al*, 1991) of all the prototypes suggest large and small grains are present.

Silicate emission at 10μm has been observed by Telesco & Knacke (1991), in β Pic dust disc. They suggested dust grains around 0.2μm were present. Absorption lines from metal ions in low stages of ionisation have been detected in the β Pic system by Hobbs, Vidal-Madjar, Lagrange-Henri and others, showing that there is gas present, in the inner dust-free zone (*e.g.* Lagrange-Henri *et al*, 1988). Boggess *et al* (1991), used HST and IUE data to confirm the suggestion by Lagrange-Henri *et al* that 2 – 3 clumps of gas fall into the system each week. Hobbs (1986) failed to find any evidence of similar gas in the other prototype systems (Vega, α PsA).

5 Follow-up of other Vega-like stars

There has not been much work done on stars other than the prototypes, either to establish their nature, or further investigate their properties. A search for CO (115GHz) in Aumann and Walker & Wolstencroft sources to look for evidence of mass loss was negative apart from four stars, δ Cas, HD35187, HD155826, HD221354 (Walker *et al*, 1988; Walker & Butner, 1992). In these cases it was suspected that the CO emission came from molecular material in the line of sight, and that the same might be true of the IRAS data. Skinner *et al* (1992) have detected silicate emission from one of the stars in the Walker & Wolstencroft list (see papers by Sylvester and by Barlow in this volume). Several sources in the Walker & Wolstencroft list have been detected in mm/sub-mm by Barlow & Skinner and Walker & Butner.

6 Conclusions

From the various searches and follow-up work, the common features that make a Vega-like star can be defined. The essential requirements for a Vega-like star are:–

1. **A normal, main-sequence star**, (no B or M stars, or emission-line stars), but binary systems are acceptable.
2. **A cool excess**; a 60μm excess is essential, but an excess at any IRAS wavelength is acceptable.
3. **The dust disc should have a small mass** (but not necessarily small size).

There are several other inferred, or desirable, properties.

- There should probably be no mass loss and 'no' gas in the system, although β Pic has atomic gas present.
- The dust grain size should be larger than ISM grains, but there appear to be several populations of dust grain in the discs.
- An inner dust free zone seems usual, but ϵ Eri appears not to have one.

There is still a lot of work to be done in understanding the dust discs around these normal main-sequence stars. It is not certain that the four prototypes even define one type of dust disc. Data at wavelengths other than IRAS are essential for the interpretation of the dust disc (especially for determining the disc size and grain populations), but the discs are unlikely to be observed at optical wavelengths; the work must be done at different wavelengths for stars other than β Pic.

References

Aumann, H.H., 1985. Publ. Astr. Soc. Pacific **97**, 885.

Aumann, H.H., 1988. Astron. J. **96**, 1415.

Aumann, H.H., *et al*, 1984. Astrophys. J. **278**, L23.

Aumann, H.H., and Probst, R.G., 1991. Astrophys. J. **368**, 264.

Backman, D.E., and Gillett, F.C., 1987. In *5th Cool Stars Workshop* ed. J. Linsky and R. Stencel, p. 291.

Becklin, E.E., and Zuckerman, B., 1990. In *Submillimeter Astronomy*, ed. G.D. Watt and A.S. Webster, p. 147.

Boggess, A., *et al*, 1991. Astrophys. J. **377**, L49.

Chini, R., Krügel, E., Shustov, B., Tutukov, A., and Kreysa, E., 1991. Astron. Astrophys. **252**, 220.

Gillett, F.C., 1986. In *Light on Dark Matter*, ed. F Israel, p. 61.

Gledhill, T.M., Scarrott, S.M., and Wolstencroft, R.D., 1991. Mon. Not. R. Astr. Soc. **252**, 50p.

Gradie, J., Hayashi, J., Zuckerman, B., Epps, H., and Howell, R., 1987. Proc. 18th Lunar and Planetary Science Conference (part I), p. 351.

Harper, D.A., Loewenstein, R.F., and Davidson, J.A., 1984. Astrophys. J. **285**, 808.

Hobbs, L.M., 1986. Astrophys. J. **308**, 854.

Lagrange-Henri, A.M., Vidal-Madjar, A., and Ferlet, R., 1988. Astron. Astrophys. **190**, 275.

Paresce, F., and Burrows, C., 1987. Astrophys. J. **319**, L23.

Telesco, C.M., Becklin, E.E., Wolstencroft, R.D., and Decher, R., 1988. Nature **335**, 51.

Telesco, C.M., and Knacke, R.F., 1991. Astrophys. J. **372**, L29.

Sadakane, K., and Nishida, M., 1986. Publ. Astr. Soc. Pacific **98**, 685.

Selby, M.J., Mountain, C.M., Blackwell, D.E., Petford, A.D., and Leggett, S.K., 1983. Mon. Not. R. Astr. Soc. **203**, 795.

Skinner, C.J., Barlow, M.J., and Justtanont, K., 1992. Mon. Not. R. Astr. Soc. **255**, 31p.

Smith, B.A., and Terrile, R.J., 1984. Science **224**, 1421.

Walker, H.J., and Butner, H.M., 1992. In preparation.

Walker, H.J., Butner, H.M., and Wolstencroft, R.D., 1988. Bull. Am. Astron. Soc. **20**, 643.
Walker, H.J., and Wolstencroft, R.D., 1988. Publ. Astr. Soc. Pacific **100**, 1509.
Wolstencroft, R.D., and Walker, H.J., 1988. Phil. Trans. R. Soc. London A, **325**, 423.

Dust Discs around Vega-excess Stars

R.J. Sylvester M.J. Barlow
Department of Physics and Astronomy
University College London
Gower Street, London WC1E 6BT, England

C.J. Skinner
Institute for Geophysics and Planetary Physics
Lawrence Livermore National Laboratory
7000 East Avenue, L-413, Livermore CA94550, USA.

Abstract

The observational evidence for dusty discs around main sequence stars is reviewed, and the discs discussed in terms of their fractional luminosity $L_{dust}/L_{\star}$. New values of this quantity indicate that a substantial range (10^{-5}–0.5) exists among Vega-excess stars. The observational requirements for determining dust masses are outlined. Details of a modelling method developed by the authors are given, and results presented. It is shown that photometry over a wide range of wavelengths as well as infrared spectroscopy are needed in order to constrain the models uniquely.

1 Introduction

One of the most interesting discoveries made by the *IRAS* satellite was the presence of excess infrared emission above the extrapolated photospheric flux from a number of main-sequence stars (Aumann *et al.*, 1984), notably α Lyr (Vega), β Pic, α PsA (Fomalhaut) and ε Eri. The excess emission is thought to be due to the presence of cool dust grains around the stars. It is widely accepted that main-sequence stars do not produce dust in significant quantities, so the most plausible explanation is that the dust is material remaining from the time the stars originally formed. The dynamics of cloud collapse and star formation make a disc geometry more probable than any other, such as a spherical shell.

Confirmation of the disc hypothesis was obtained when β Pic was imaged by Smith and Terrile (1984) in the near-IR (890nm), and subsequently by Paresce and Burrows (1987) using optical coronography in the B, V, R, and I bands. The images showed a fairly thin, edge-on, disc which was scattering the light from the star, and which extended to at least 25 arcsec from the star. At the distance of β Pic (16 pc), this corresponds to a disc diameter of around 800AU. Telesco *et al.* (1988) resolved the β Pic disc at 10μm and 20μm using a bolometer array at the 3.0m IRTF on Mauna Kea, showing that the thermally emitting dust is indeed physically associated with the optically scattering material.

The *IRAS* fluxes of Vega-excess stars cannot be adequately modelled by a single temperature blackbody energy distribution (see e.g. Walker & Wolstencroft, 1988 or Becklin

& Zuckerman, 1990); this is to be expected, as the material orbiting the star is likely to be at a range of temperatures corresponding to the different grain sizes and the differing distances of the grains from the star. The best-fitting single-temperature models for the four 'prototype' Vega-excess stars have temperatures of around 100K (Walker & Wolstencroft, 1988, Gillett, 1986). Typical distances for classical Vega-excess stars are in the range 7–30 pc, i.e. about a factor of ten closer than the nearest pre-main sequence stars with circumstellar discs (Gillett, 1986).

A number of groups have found other Vega-excess candidates by searching the *IRAS* database, for example Aumann (1985), Sadakane & Nishida (1986), Coté (1987)and Stencel & Backman (1991). Probably the most complete list yet produced is that of Walker and Wolstencroft (1988), which contains over 30 SAO stars selected on the basis of their 60μm/100μm flux ratios and evidence of spatial extension in at least one of the *IRAS* bands. Several of the objects in their list appear qualitatively different from the Vega /β Pictoris prototypes in that they are optically much fainter (with V magnitudes typically between 8 and 9) and more distant, yet their 60 and 100μm fluxes are as large as those emitted from α Lyr and β Pic. In addition, not only their 25–100μm fluxes but also their 12μm fluxes are dominated by dust emission.

The ratio of the total energy radiated by the dust in the IR to the stellar luminosity, $L_{dust}/L_{\star}$, gives a useful indication of the optical depth of the disc material. For optically thin emission, $L_{dust}/L_{\star}$ is in fact equal to the fraction of the sky, as seen from the star, which is occupied by dust. For a flat disc, the maximum value it can obtain is 1/4, while for a 'flared' disc, i.e. one in which the azimuthal thickness increases with distance from the star, $L_{dust}/L_{\star}$ can reach values of approximately 1/2 (Kenyon & Hartmann, 1987). 'Typical' Vega-excess stars have $L_{dust}/L_{\star} \sim 10^{-5}$–$10^{-3}$ (e.g. β Pic $= 2.6 \times 10^{-3}$) — a very low value, which indicates that the dust shells are very optically thin at all wavelengths. We find that a number of the objects in the Walker & Wolstencroft sample have substantially larger values of $L_{dust}/L_{\star}$, some of which exceed the 'flat disc' maximum of 0·25. Table 1 presents the values of $L_{dust}/L_{\star}$ for a number of Vega-excess stars, which we have calculated by integrating under a smooth curve fitted to the photometric points in the infrared region, after subtraction of an optically normalised Kurucz model atmosphere having an effective temperature taken from the spectral type versus T_{eff} tables of Schmidt-Kaler (1982). The photometry was dereddened by an amount determined from the derived E($B-V$) for each star. Figure 1 shows a typical continuum fit to the photometry for β Pic, as well as for two of the stars from the Walker and Wolstencroft list.

2 Properties of the dust-discs

Telesco and Knacke (1991) obtained photometry of β Pic in four narrow bands ($\delta\lambda \approx 1\mu$m) in the 10$\mu$m region. The 9.7$\mu$m silicate feature was detected, implying the presence of silicate grains less than $\sim$10μm in size.

In May 1991, Skinner, Barlow and Justtanont (1992) observed the K5 star SAO 179815, one of the objects in the Walker & Wolstencroft list, with CGS3, the UCL common-user 10 and 20μm spectrometer on UKIRT. A 10μm spectrum was obtained, with a resolving power of $\sim$60, which clearly showed the presence of a broad 9.7μm silicate feature, conclusively demonstrating the presence of small silicate grains around the star. The shape of the silicate feature, along with the spectral energy distribution, allowed

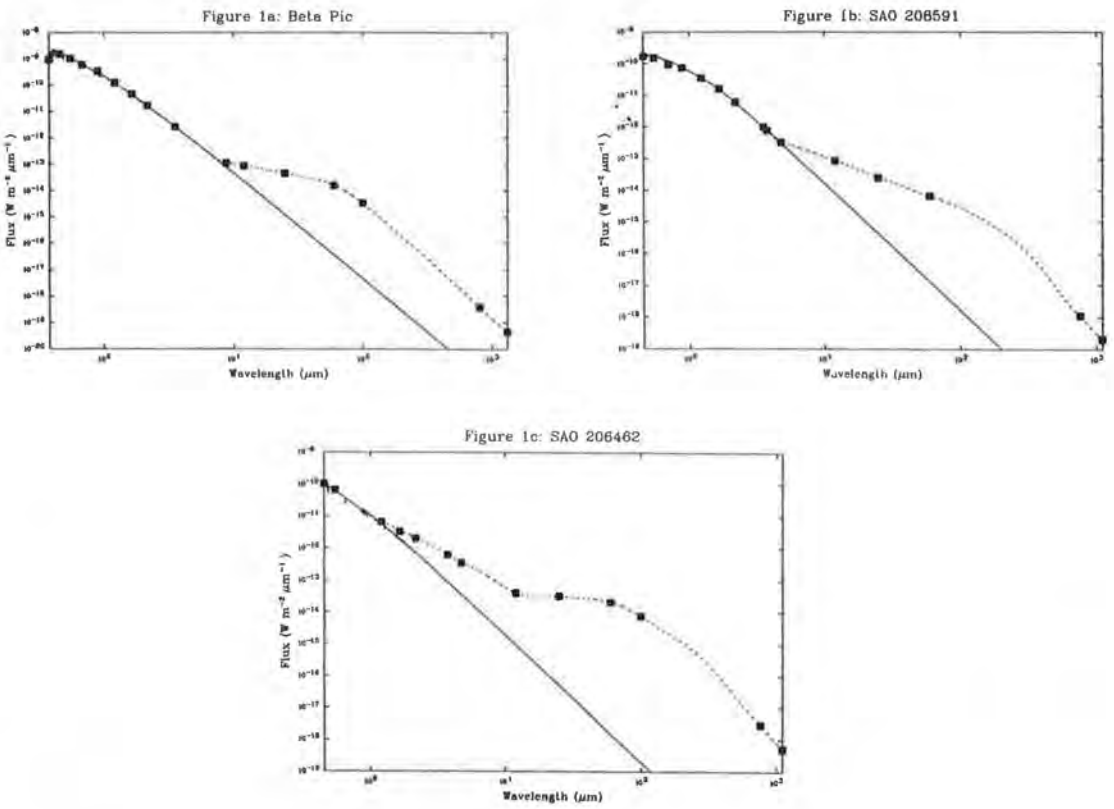

Figure 1: Continuum fits for calculating excess emission (dotted curves). **(a)** β Pic **(b)** SAO 208591 **(c)** SAO 206462. The Kurucz models (solid curves) for the three stars have T_{eff} of 8250K, 6000K and 9500K respectively. All three have log g = 4.

Star	Spec. Type	$L_{dust}/L_\star$
α Lyr	A0V	2.3×10^{-5}
β Pic	A5V	2.6×10^{-3}
ε Eri	K2V	2.6×10^{-5}
τ^1 Eri	F5/F6V	4.6×10^{-5}
Gl 217.1	A3V	$\leq 6.1 \times 10^{-5}$
SAO 140789	A0V	0.010
SAO 208591	G0V	0.018
SAO 158350	K5	9.7×10^{-3}
SAO 183986	G5Ve	0.44
SAO 186777	B9V	0.21
SAO 206462	A0V	0.13
SAO 179815	K5V	0.084
SAO 226057	A7V	0.39
SAO 26804	K2	0.036

Table 1: Values of the fractional IR excess luminosity $L_{dust}/L_\star$ for a number of Vega-excess stars.

them to constrain the size and density distributions of the grains in models of the disc.

The total mass of dust in a power-law size distribution $n(a) \propto a^{-\gamma}$ is determined by a_{max} for $\gamma < 4$, which is the case for most interstellar or solar-system grain size distributions. A power-law grain size distribution has been predicted for asteroidal fragments and micrometeoroids by Dohnanyi (1969, 1970) and for grains in molecular clouds and red giant winds by Biermann and Harwit (1988). Power-law distributions have been found to fit asteroidal size distributions, the particles in Saturn's rings, and interstellar extinction curves (Mathis *et al.* 1977). They are a natural product of grain-grain collisions. It is therefore important to determine the value of a_{max} for Vega-excess stars.

For a dust grain of radius a, there is a turnover wavelength, λ_T (where $\lambda_T \approx 2\pi a$), shortwards of which the extinction by the grain is grey (i.e. independent of λ), and longwards of which, the dust grain emissivity varies as $\lambda^{-\beta}$ (or ν^{β}) where β is typically 1–2 (see Figure 2).

A widely used formula for determining dust masses in different environments is due to Hildebrand (1983), and is applicable in the Rayleigh-Jeans emission limit for grains.

$$M_d \propto \frac{F_\nu D^2}{B(\nu,T)} \frac{(\nu_{ref}/\nu)^\beta}{\kappa_\nu(\nu_{ref})}$$

where $\kappa_\nu(\nu_{ref})$ is the known opacity (cm^2 g^{-1}) of small grains at some reference frequency ν_{ref} and the grains are assumed to have a ν^β frequency dependence. One must observationally confirm that the spectrum has reached the $F_\nu \propto \nu^{2+\beta}$ region at the wavelength for which the formula is used.

For typical power-law grain size distributions, the spectrum will not approach its limit of $\nu^{2+\beta}$ (i.e. the product of the Rayleigh-Jeans blackbody limit and the grain emissivity law) until $\lambda > 20 a_{max}$ where a_{max} is the maximum grain size.

Becklin and Zuckerman (1983) and Chini *et al.* (1991) have made measurements of the submillimetre and millimetre flux from Vega, Fomalhaut, and β Pic, amongst others,

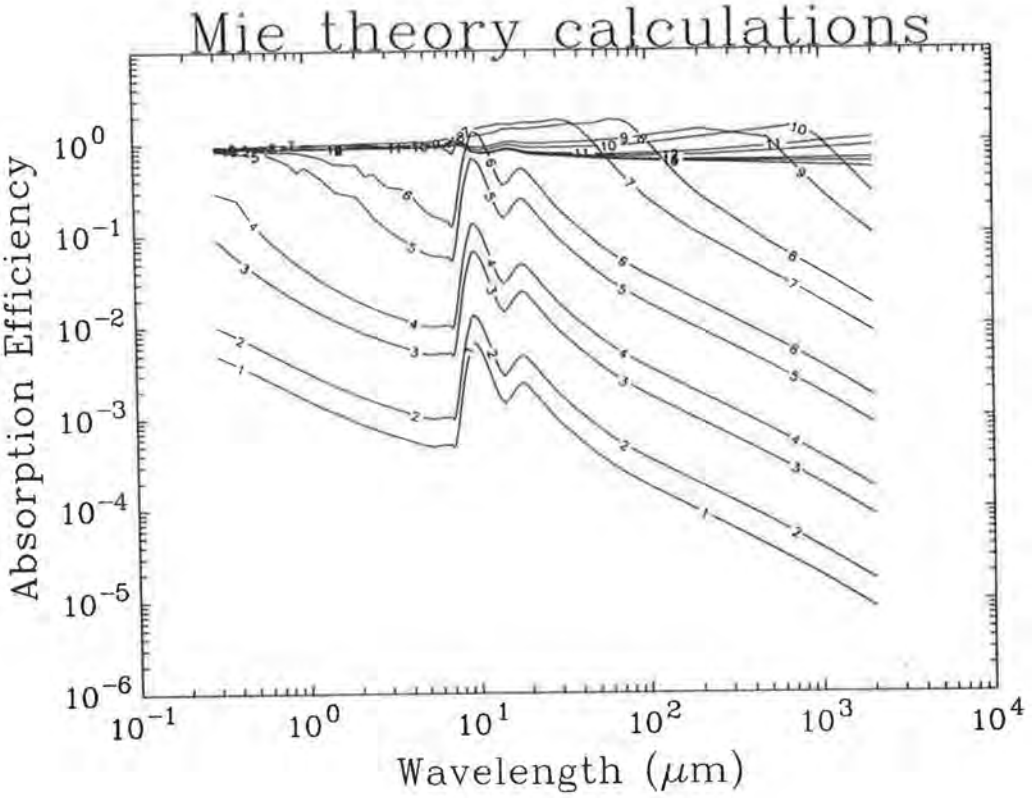

Figure 2: Absorption efficiency, Q_{abs} for grains of various sizes calculated with Mie theory. Curves labelled 1, grain radius = 0.005μm; 2, radius = 0.01μm; 3, radius = 0.05μm; 4, radius = 0.1μm; 5, radius = 0.5μm; 6, radius = 1.0μm; 7, radius = 5.0μm; 8, radius = 10μm; 9, radius = 50μm; 10, radius = 100μm; 11, radius = 500μm; 12, radius =1.0mm; 13, radius = 5.0mm 14, radius =10mm; 15, radius =50mm.

using the JCMT, IRAM and SEST. As shown in Table 2, the spectral indices for α Lyr and α PsA in the 800–1300μm region are both greater than 3, — the spectra appear to be in the $\nu^{2+\beta}$ region at submillimetre wavelengths. This implies a maximum grain size of less than 50μm for these two stars. Barlow, Skinner and Sylvester obtained 760μm and 1100μm fluxes for a number of stars from the Walker & Wolstencroft list (Table 3). The spectral indices show that turnover has not been reached for at least four of these stars. The maximum grain size for these stars must therefore be significantly larger than 50μm.

Star	F_ν(100μm) Jy	F_ν(800μm) mJy	F_ν(1300μm) mJy	α(100–800)	α(800–1300)
α Lyr	7.54	22	4.5	2.81	3.3
β Pic	11.3	80	25	2.38	2.4
α PsA	11.2	35	7.3	2.77	3.2

Table 2: Submillimetre fluxes for three 'prototype' Vega-excess stars, from Becklin & Zuckerman (1983) and Chini *et al.*(1991).

Star	Sp. type	F_ν(100μm) Jy	F_ν(800μm) mJy	F_ν(1100μm) mJy	α(100–800)	α(800–1100)
SAO 179815	K5V	4.5		63		
SAO 206462	A0V	25.7	570	209	1.88	2.72
SAO 226057	A7V	13.9	608	264	1.54	2.26
SAO 183956	A8V	5.5	351	167	1.35	2.00
SAO 183986	G5e	4.8	233	114	1.49	1.92
SAO 186777	B9V	23.4		302		

Table 3: Submillimetre fluxes for six Vega-excess stars obtained by the authors at the JCMT in February 1992.

A number of the stars in the Walker & Wolstencroft list have characteristics which suggest that they may provide a link between relatively old main-sequence stars with discs (e.g. α Lyr) and pre-main sequence stars with discs, such as 'naked' T Tauri stars. These intermediate objects are not located in regions of star formation but their spectral indicators (in some cases) and their relatively large infrared fluxes and dust masses appear to indicate that they are young main sequence stars. For example, the spectrum of the A0Ve star SAO 140789 shows OI in emission at wavelengths of 7772Å and 8446Å, which is unusual for B9–A2 stars. Andrillat *et al.* (1990) speculated that the object is a quiescent Herbig Ae-Be star (that is, an inactive pre-main sequence star).

1–5μm photometry obtained by the authors at UKIRT in June 1992, combined with *IRAS* and submillimetre fluxes, appears to show that in some cases there is a separate near-infrared excess, implying the presence of two distinct distributions of matter around the star — one much warmer, and hence closer to the star, than the other. There has been speculation that the apparent absence of dust at intermediate distances, emitting in the mid-IR, implies that these regions are being 'swept clean' by planets. A less exotic

explanation for the near-IR excess is temperature fluctuations of very small grains, where very small grains, which have a low heat capacity, absorb an energetic ultraviolet photon, which causes the grain temperature to transiently increase greatly until it re-radiates the energy away as near-infrared photons (see Guhathakurta and Draine, 1989). Alternatively, the presence of icy mantles on the more distant grains would affect their optical properties, and could give rise to two temperature distributions from a single spatial distribution of material.

3 Modelling

A programme of modelling the observations of Vega-excess stars from the Walker & Wolstencroft catalogue is being undertaken by the authors. The first such star to be modelled was SAO 179815, whose 10μm spectrum was found by Skinner, Barlow and Justtanont (1992) to show the silicate feature. The results of that modelling are summarised later in this section. Other stars are presently being modelled.

The observational data used are the *IRAS* 12–100μm fluxes, ground-based optical and 1–5μm photometry, CGS3 10 and 20μm spectra, and submillimetre and millimetre photometry. In the future, it is also hoped to include optical coronagraphic and 10 and 20μm infrared images, as well as radio fluxes in the cm region, to further constrain the models.

The model is based on that developed for α Ori by Skinner and Whitmore (1987), but modified to work in disc geometry, rather than that of a spherical shell. The disc is treated as being optically thin, hence there are no shadowing or self-heating effects taken into account.

The model is axially symmetric and equally valid for flat discs or 'flared' discs (which get thicker as the distance from the star increases). The only difference is in the interpretation given to the parameter representing density in the disc.

The dust mass per unit area (in the disc plane) at a distance r from the star is taken to vary as $r^{-\beta}$: for a flat disc, this is equivalent to a power law density distribution in the disc; for flared discs account must be taken of the variation in disc thickness before describing the actual density in the disc. The dust is modelled with the optical constants of Draine and Lee (1984), which appeared to give the best fit to the observed spectrum of SAO 179815 of all the optical constants available (Skinner & Whitmore 1987). Absorption coefficients for grains of different sizes are calculated using Mie theory from the optical constants.

The temperature of the dust grains at any position in the disc is found by applying the condition of radiative equilibrium. The energy absorbed by a grain is given by:

$$E_{in} = \int_{\lambda} Q_{abs}(\lambda) \pi a_g^2 B_{\lambda}(T_{\star}) \frac{r^2}{R_{\star}^2} \, d\lambda$$

whilst the energy radiated by the grain is

$$E_{out} = \int_{\lambda} Q_{abs}(\lambda) 4\pi a_g^2 B_{\lambda}(T_{grain}) \, d\lambda$$

where Q_{abs} is the absorption efficiency, a_g the grain radius, $T_{\star}$ the stellar temperature, $R_{\star}$ the stellar radius, r the distance of the grain from the star and T_{grain} the grain

temperature. By equating E_{in} and E_{out}, the temperature of a grain of a given size at a given distance from the star can be found.

The model calculates the flux from the object at 69 wavelengths, ranging from 0.3μm to 2mm. Up to fifteen grain sizes can be used, varying in radius between 0.005μm (50 Å) to 5cm.

The free parameters in the model are

- γ — the index for the power law grain size distribution $n(a) \propto a^{-\gamma}$
- β — the index for the dust density distribution $N(r) \propto r^{-\beta}$
- Maximum / minimum grain sizes
- Inner disc radius
- Outer disc radius
- Total dust mass

The effects of the parameters are relatively easy to predict. Increasing the value of γ increases the proportion of small grains in the distribution. As Figure 2 shows, smaller grains have more pronounced 9.7 and 18μm features, and a shorter 'turnover' wavelength. Increasing γ therefore increases the contrast of the observed silicate feature, while reducing the flux level at longer wavelengths (see Figure 3a). From Figure 3a, one can see that when $\gamma = 3.0$, the contrast in the silicate feature is very large indeed — there is an increase in flux of more than an order of magnitude between wavelengths of 7 and 10μm. For $\gamma = 1.0$, the excess emission is completely smooth and featureless — the 'grey' emission from grains larger than about 10μm (see Figure 2) dominates. At long wavelengths, we again see the effect of having a greater proportion of large grains: there are more grains whose emission has not yet 'turned over' at the wavelengths shown, so the long-wavelength flux is greatest for $\gamma = 1$ and least for $\gamma = 3$. Also, since the area of a grain varies as a_g^2, but the volume (and hence the mass) varies as a_g^3, small grains give more emission per unit mass than large grains at wavelengths shorter than the turnover wavelength. Increasing the value of γ thus can be expected to decrease the dust mass required to produce sufficient flux at 12μm and 25μm. Increasing the value of β increases the proportion of dust in the inner, warmer regions of the disc, and thus increases the 12μm and 25μm fluxes relative to those at longer wavelengths. This is illustrated in Figure 3b, where we see that the effect on the model spectrum of increasing β — and thereby bringing material into the inner parts of the disc — is that the 'average' temperature of the grains goes up, and so the peak of the dust emission moves shortwards, without affecting the contrast of the silicate feature. The relative strengths of the 10 and 20μm features are, however, affected by the slope of the underlying emission in that region. Since hotter grains emit more at all wavelengths than cooler ones, the overall flux for a given dust mass increases with an increase in β.

Increasing the inner radius of the disc decreases the maximum temperature attained by the grains; this reduces the flux at shorter wavelengths, while having little effect for wavelengths longer than $\sim$ 60μm. (See Figure 3c) By altering R_{in}, but renormalising the 60μm flux by changing the mass of dust present, one is effectively adding or removing dust from the inner edge of the disc, without greatly changing the amount of dust in the outer parts of the disc. The result of this is to alter the flux level in the shorter-wavelength parts

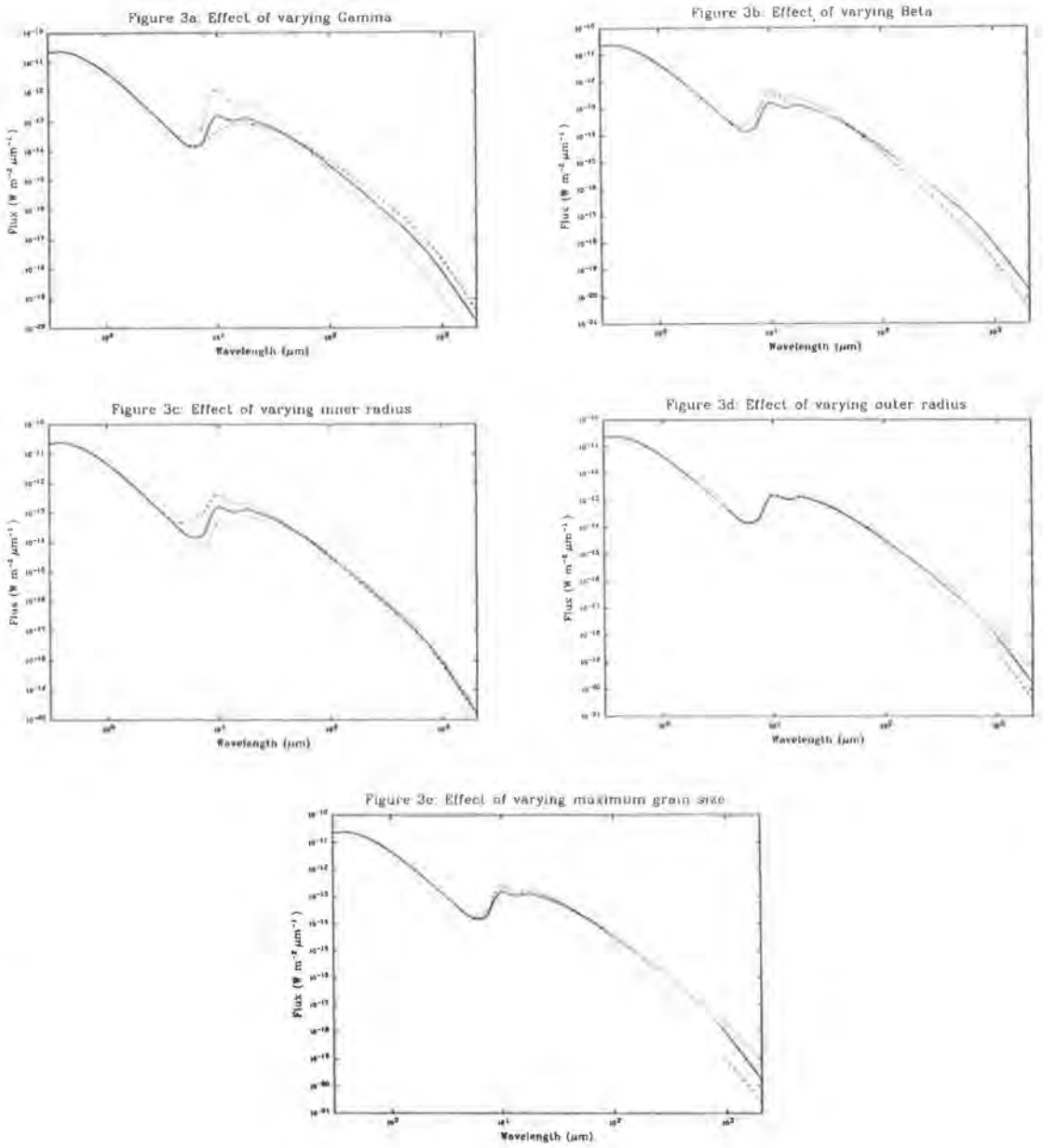

Figure 3: **Figure 3:** Effects of varying the parameters of the disc model. All curves are normalised to the same flux at 60μm. **(a)** Index for power law size distribution. Dashed curve, $\gamma = 1.0$; solid curve, $\gamma = 2.0$; dotted curve, $\gamma = 3.0$ **(b)** Power law index for density distribution. Solid curve, $\beta = 1.0$; dashed curve, $\beta = 2.0$; dotted curve, $\beta = 3.0$ **(c)** Disc inner radius. Dashed curve, $R_{in} = 2.7$AU; solid curve, $R_{in} = 5.3$AU; dotted curve, $R_{in} = 10.7$AU. **(d)** Disc outer radius. Dashed curve, $R_{out} = 160$AU; solid curve, $R_{out} = 2400$AU; dotted curve, $R_{out} = 24000$AU. **(e)** Maximum grain size. Dashed curve, $a_{max} = 10\mu$m; solid curve, $a_{max} = 100\mu$m; dotted curve, $a_{max} = 50$mm.

of the excess, where the hottest grains have their peak emission, while having little effect longwards of about 60μm. In the modelling, the central star is treated as a blackbody at the effective temperature determined by the observed spectral type of the star.

Conversely, increasing the outer radius of the disc effectively adds grains at the outer edge of the system, where the dust is coolest. This increases the flux at the very longest wavelengths, where the emission from cold grains peaks, while having little effect on the flux at wavelengths shorter than about 100μm (See Figure 3d). Since the most distant grains are only weakly illuminated by the star, a large change in outer radius, and consequently in the total mass of the disc, produces only a relatively minor change in the flux, even at the longest wavelengths.

Altering the maximum grain radius affects the wavelength by which the emission from all the grains has turned over. This affects the flux and spectral index at long wavelengths (See Figure 3e). It is worth comparing the effects of the outer radius of the disc and of the maximum grain size, both of which are greatest at long wavelengths. As we have already discussed, the amount of radiation emitted by a grain at a given wavelength is proportional to product of the black-body emission and the grain (absorption) efficiency, both taken at the wavelength of interest. By varying the disc outer radius, we are changing the temperature of the coldest grains, and hence the wavelength by which all of the grains are in the Rayleigh-Jeans region of the black-body curve. On the other hand, by altering the maximum grain size, we change the wavelength by which all of the grains have left the 'grey' part of their emission curves, and are radiating with an efficiency $\sim \lambda^{-1}$ or λ^{-2}. In Figure 3d, we see that from 60μm onwards, the curves diverge slowly, but by about 700μm, they are parallel to one another, indicating that more or less all of the grains' emission is in the Rayleigh-Jeans domain. In Figure 3e, however, the curves diverge from one another at different wavelengths, depending on the turnover wavelength of the largest grains. The dotted curve is for a maximum grain radius of 50mm, so turnover is not reached in the wavelength region plotted. The practical implication of this in terms of modelling observations is that at least two photometric points are required longwards of 100μm to constrain these two disc parameters. If, for instance, all one had were the *IRAS* 100μm flux, and the flux at one submillimetre wavelength, a range of models could be constructed that fit the data points well, with a range of different values of these parameters. The models with a large outer radius, which tends to give large long-wavelength fluxes, would have a small maximum grain size — hence a short turnover wavelength and less long-wavelength flux — to compensate, and *vice versa*. Turning to the mid-infrared, increasing the minimum grain radius has the effect of decreasing the contrast in the silicate features, since small grains have a greater contrast in their absorption efficiency (see Figure 2). Since all plausible models have γ positive, i.e. more small grains than large ones, a very small change in a_{min} will have a noticeable effect, especially in the region between 1 and 5μm, where the silicate feature becomes 'washed out' (Figure 2).

Figures 4a and 4b show combined optical, 1–5μm, *IRAS* and millimetre photometry for SAO 179815 and SAO 226057, after dereddening by $E(B-V) = 0.2$ and 0.03 respectively, together with the relevant Kurucz (1991) models for each star. These models, for a wide range of effective temperatures and surface gravities, take much more complete account of line blanketing than did previous models. There is extremely good agreement between the model atmosphere fit and the photometry for SAO 179815 between approximately 0.3 and 3.5μm, showing that there is negligible dust emission shortwards of about 5μm. There is

excess emission at all four *IRAS* points and also at the two sub-mm points. SAO 226057, however shows an excess from at least the H-band (1.65μm) onwards, and possibly even from J (1.22μm). SAO 226057 has a significantly larger value of $L_{dust}/L_{\star}$ (= 0.39) than does SAO 179815 ($L_{dust}/L_{\star} = 0.084$), indicating that there are larger quantities of dust around SAO 226057.

Figure 4a shows the results of modelling SAO 179815. This is the model M5A of Skinner *et al.*, extended to longer wavelengths for comparison with the recently obtained JCMT photometry. The CGS3 spectrum, rescaled to the *IRAS* 12μm point is included in the plot (small filled squares). The model fit is very good, in close agreement with the data points for wavelengths shortwards of 100μm. The JCMT photometry, obtained after the modelling was performed, shows, however, that the model underestimates the flux at mm wavelengths. This puts a better constraint on the maximum grain size in the disc than was previously available. The maximum grain size in the model was 1mm: the JCMT photometry shows that it should be considerably larger than this. Photometry at still longer wavelengths is required to determine the maximum grain size.

Figure 4b shows two model fits to SAO 226057. The model parameters for both stars are given in Table 4. It was found that no single set of parameters could simultaneously give a good fit to the excess at 1-5μm and the long-wavelength data. It was necessary to have two distinct populations of dust, represented by different grain-size and density distributions to fit the photometry from 1μm–1.3mm. Fitting the observed energy distribution in the 1-5μm region requires grain temperatures of the order of 1000K, about a factor of 5 higher than those needed to model the excess in the *IRAS* bands.

	Star	γ	β	R_{in} AU	R_{out} AU	a_{min} μm	a_{max} μm	M_{disc} $M_{\odot}$
(a)	SAO 179815	2.0	3.0	1.46	640	0.005	1000	1.0×10^{-8}
(b)	SAO 226057	2.0	1.0	5.33	2400	0.005	100	1.5×10^{-6}
(c)	SAO 226057	1.0	2.0	8.00	6400	0.005	500	1.2×10^{-5}
(d)	SAO 226057	2.0	4.0	0.09	320	0.005	500	3.0×10^{-11}

Table 4: Parameters for the models described in the text. **(a)** Model for SAO 179815. **(b)**,**(c)** Two models for the excess of SAO 226057 from ~8μm longwards. **(d)** A 'hot dust' model for the 1–5μm excess of SAO 226057.

The model of SAO 179815 defines the parameters of the disc within a very small range of values. Any substantial variation in one of the parameters causes the model fluxes to deviate from the observed values; one cannot compensate by varying the other parameters in such a way as to restore the quality of the fit. The only parameter not completely constrained is the maximum grain size, for which there is a lower limit, but no upper limit. By contrast, the lack of 10 and 20μm spectra for SAO 226057 makes this object harder to model uniquely. The two models shown in Figure 4b provide equally good fits to the observational data, but it can be seen that they have substantially different levels of contrast in the 9.7μm and 18μm silicate features. 10 and 20μm spectra of this object should enable one to distinguish easily between these two models. The available data do still constrain the parameters of the disc to lie close to those of the two models shown.

Figure 4a: SAO 179815

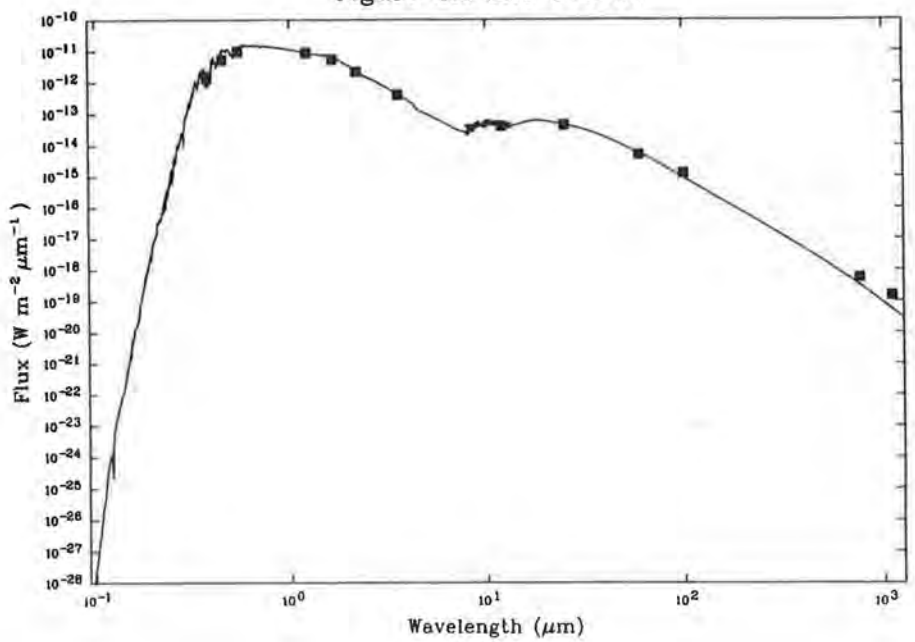

Figure 4b: SAO 226057

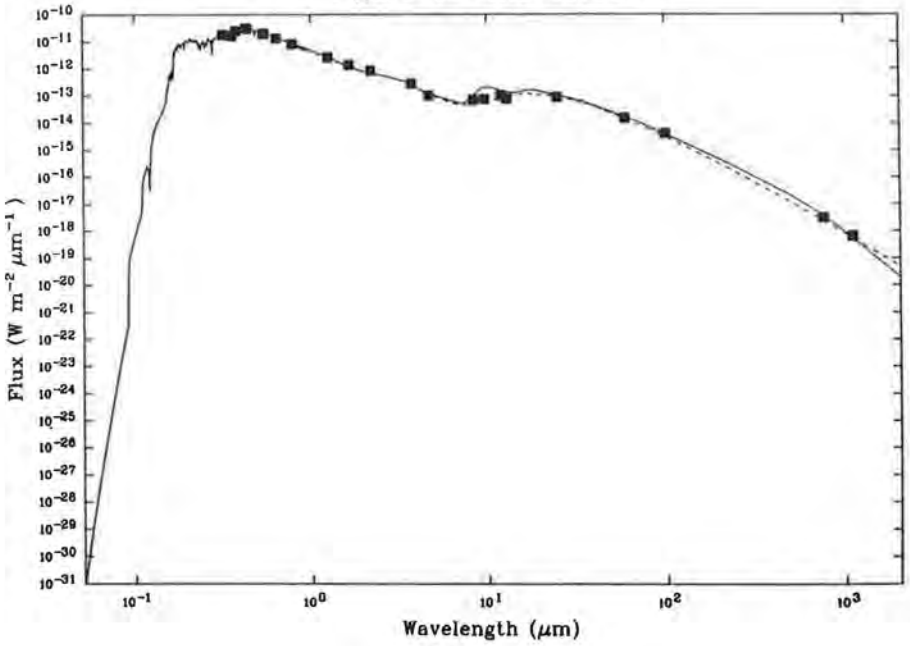

Figure 4: Model spectra. **(a)** SAO 179815. The Kurucz model atmosphere has T_{eff} = 4250K, log g=4.0. **(b)** Two models for SAO 226057. Both include a 'hot dust' component to model the photometry in the 1–5μm region. The Kurucz model atmosphere has T_{eff} = 7750K, log g=4.0.

4 Conclusions

A large number of main-sequence stars exhibit the 'Vega-excess phenomenon'. The so-called prototype Vega-excess stars could be said to be atypical, due to their low dust luminosities, and lack of an excess at 12 and sometimes even 25μm. Two Vega-excess systems have been demonstrated to contain silicate dust, which is of interest not least because the Earth and the other terrestrial planets are composed largely of silicates. The modelling of Vega-excess systems shows that, using a combination of optical, infrared and submillimetre photometry and infrared spectroscopy, one can determine the parameters of the disc reasonably well. Further observational data are clearly needed before a sufficiently large number of Vega-excess objects can be satisfactorily modelled to allow one to draw conclusions about these objects as a class.

References

Andrillat, Y., Jaschek, M., 1990, Astron. Astrophys., **233**, 474.

Aumann, H. H., 1985, Publs Astr. Soc. Pacif., **97**, 885.

Aumann, H. H., Gillett, F. C., Beichman, C. A., de Jong, T., Houck, J. R., Low, F. J., Neugebauer, G., Walker, R. G. & Wesselius, P. R., 1984. Astrophys. J., **278**, L23.

Becklin, E. E., Zuckerman, B., 1990, in *Submillimetre Astronomy*, p. 147, eds G. D. Watt & A. S. Webster, Kluwer, Holland.

Biermann, P., Harwit, M., 1980, Astrophys. J., **241**, L105.

Chini, R., Krügel, E., Shustov, B., Tutukov, A., Kreysa, E., 1991, Astron. Astrophys., **252**, 220.

Coté J., 1987, Astron. Astrophys., **181**, 77.

Dohnanyi, J. S., 1969, J. Geophys. Res., **74**, 2531.

Dohnanyi, J. S., 1970, J. Geophys. Res., **75**, 3468.

Draine, B. T., Lee, H-M., 1984, Astrophys. J., **285**, 89.

Gillett, F. C., 1986, in *Light on Dark Matter*, p. 61 ed. F. P. Israel, Reidel, Dordrecht.

Hildebrand, R. H., 1983, Quart. J. R. astr. Soc., **24**, 267.

Kenyon, S.J., Hartmann, L., 1987, Astrophys. J., **323**, 714.

Kurucz, R.L., 1991, "New lines, new models, new colors", in proceedings of the workshop on "Precision Photometry: Astrophysics of the Galaxy", held at Union College, Schenectady, New York, October 3–5, 1990, ed. A.G. Davis Philip, A.R. Upgren and K.A. Janes (L. Davis Press, Schenectady), p.27

Mathis, J. S., Rumpl, W., Nordsieck, K. H., 1977, Astrophys. J., **217**, 425.

Paresce, F., Burrows, C., 1987, Astrophys. J., **319**, L23.

Sadakane, K., Nishida, M., 1986, Publs Astr. Soc. Pacif., **98**, 685.

Schmidt-Kaler, Th., 1982, in *Landolt-Börnstein, Numerical Data and Functional Relationships in Science and Technology, Group VI, Astronomy, Astrophysics and Space Research*, Vol. 2b, ed. K. Schaifers and H. H. Voigt, Berlin, Springer-Verlag.

Skinner, C. J., Barlow, M. J., Justtanont, K., 1992, Mon. Not. R. astr. Soc., **255**, 31P.

Skinner, C. J., Whitmore, B., 1987, Mon. Not. R. astr. Soc., **224**, 335.

Smith, B. A., Terrile, R. J., 1984, Science, **226**, 1421.

Stencel, R. E., Backman, D. E., 1991, Astrophys. J. Suppl. Ser., /bf 75, 905.

Telesco, C. M., Becklin, E. E., Wolstencroft, R. D., Decher, R., 1988, Nature, **335**, 51.

Telesco, C. M., Knacke, R. F., 1991, Astrophys. J., **372**, L29.

Telesco, C. M., Knacke, R. F., 1991, Astrophys. J., **372**, L29.
Walker, H. J., Wolstencroft, R. D., 1988, Publs Astr. Soc. Pacif., **100**, 1509.

The Interaction between Dust Disks and the Interstellar Medium

Daniel P. Whitmire, John J. Matese and Patrick G. Whitman
Department of Physics,
The University of Southwestern Louisiana
Lafayette, LA 70504-4210 ,USA.

Abstract

The optically thin Vega-like particulate disks believed to exist around many main sequence stars will be rapidly processed by interstellar dust grains, unless they are shielded by the magnetic fields associated with stellar winds. When not shielded, the time scale for interstellar collisional processing is much less than the time scale for Poynting-Robertson and internal-collision depletion. We show that magnetic fields associated with stellar winds of solar magnitude will shield the disks in interstellar voids but not inside clouds of gas density ≥ 1 cm^{-3}. When exposed to the cloud flux, multiple impact fragmentation of the larger circumstellar grains will result in a significant increase in the disk area and optical depth. The brightning of the disk could persist for millions of years after the star emerges from the cloud. This model can explain the observed velocity streaming of the brightest disk stars, whose centroid passed through the massive Sco Oph cloud complex some 6 Myr ago, and the dearth of late A type dwarfs with particulate disks.

1 Introduction

There are 22 A-type main-sequence dwarf stars within 22 pc of the Sun. Of these, half have been found to exhibit some level of nonphotospheric IR emission in one or more IRAS bands (Aumann, 1985; Backman and Gillett, 1987; Backman and Paresce, 1992, hereafter BP). The source of this emission is generally believed to be orbiting circumstellar grains which have most likely collisionally relaxed to a flattened disk. It is expected theoretically that most of the observed IR emission is from particles near the blow-out sizes (1 - 15 μm). This expectation has been confirmed in the case of β Pic where detailed modeling of the IR excess requires inefficient small grains (Gillett, 1986; Matese *et al.*, 1987; BP). The disk stars are in general not young and therefore the observed grains must have larger sources (BP).

Circumstellar grains within these optically thin particulate disks will strongly interact with interstellar dust and will be rapidly processed by multiple-impact fragmentation, *unless magnetically shielded* (Whitmire *et al.*, 1992, hereafter WMW). Initially, this will result in an increase in disk area and IR optical depth. On the other hand, erosion of circumstellar grains by interstellar dust would only decrease disk area (Lissauer and Griffith, 1989). However, if fragmentation can occur, either via multiple impacts of ~ 0.15 μm interstellar dust or by single impacts of an unknown larger component of interstellar dust, it will dominate erosion. The time scale for multiple impact fragmentation of ~ 100

μm circumstellar grain by interstellar dust corresponding to a hydrogen number density n = 1 cm^{-3} and relative velocity V = 25 km s^{-1} is $\sim 5\times10^4$ yr (WMW). The corresponding erosion time scale is $\sim 4\times10^6$ yr (Lissauer and Griffith, 1989).

2 Magnetic Shielding

In the case of the Sun, interstellar grains of size $\sim$ 0.15 μm do not penetrate through the heliosphere, located at $\sim$50 AU, because they are deflected by the perpendicular component of the solar wind magnetic field (Levy and Jokipii, 1976). Dust grains in the heliosphere are charged to $\sim$5 volt and the resulting Lorentz force is 100 times larger than the gravitational force (Holzer, 1989). If A-type main-sequence stars have stellar winds comparable to that of the Sun ($\sim 3\times10^{-14}$M$_\odot$ yr^{-1}) we can estimate the radius of the heliospheric barrier, r_h, by equating the stellar and interstellar wind pressures (Begelman and Rees, 1976),

$$n(r)V^2(r) = \frac{n_1 V_1^2}{(r/1\mathrm{AU})^2} \quad ,$$

where the stellar wind parameters are scaled to the solar values at 1 AU. The density of the interstellar wind as a function of r is

$$n(r) = n_\infty(\frac{V(r)}{V_\infty}) \quad ,$$

where the subscript ∞ refers to cloud parameters. Making the approximation

$$V(r) \approx V_\infty \quad ,$$

gives

$$r_h \approx \sqrt{\frac{n_1}{n_\infty}}\frac{V_1}{V_\infty} \quad .$$

Inserting the solar parameters n_1 = 5 cm^{-3}, V_1 = 450 km s^{-1} and $V_\infty \approx$ 25 km s^{-1} yields

$$r_h \approx \frac{40\mathrm{AU}}{\sqrt{n_\infty/1\mathrm{cm}^{-3}}} \quad .$$

It was shown in WMW that the centroid of the 5 brightest particulate disk stars passed through the Sco Oph cloud complex $\approx$ 6 Myr ago. The mean density of this complex is $\sim$ 1 cm^{-3} while the mean density of the void between the cloud and the Sun today is $\sim$ 0.05 cm^{-3} (Frisk and York, 1983, 1986). Inserting these values into the heliospheric radius formula gives a variation of $r_h \sim 40 - 180$ AU, which is similar to the radial range of the dominant IR emission from the particulate disk stars. Modeling of the IR excess in the 3 prototype disk stars (α Lyr, α Psa and β Pic) gives a mean inner disk edge radius of 40 AU (BP). The outer edge is not constrained by the IR models but, based on negative optical observations, it is not likely to extend more than a few hundred AU. Even in the case of β Pic, whose disk can be seen optically to extend beyond 400 AU, most of the radiating material lies well inside this distance.

3 Fragmentation Model

We assume that main-sequence dwarfs have Kuiper belts of residual cometary material whose inner edges begin either at distances corresponding to stable ice, $\approx$ 5 AU in the Solar System, or somewhat beyond the last major planet, whichever is further. If all protoplanetary nebula were optically thin, the former distance would scale like $\sqrt{\text{luminosity}}$. It is more likely that this is not true and that temperatures in nebulae depend on the internal disk viscosity and other parameters. Nonetheless, we expect that stellar luminosity scaling is likely to be accurate to within a factor of two.

In the Solar System, the mass distribution of interplanetary grains has a broad peak at a size corresponding to $\approx 100\mu$m (Grün *et al.*, 1985). The peak in the area (and the zodiacal optical depth) distribution corresponds to a somewhat smaller size of $\approx 30\mu$m. A significant source of many of these grains, even in the inner Solar System, is cometary outgasing. Grains in the outer Solar System beyond the orbit of Neptune would be almost exclusively cometary in origin. In addition to sublimation, collisions in Kuiper belts between cometary bodies of all sizes (Weissman, 1984) could also contribute to the population of $\geq 100\mu$m size grains. A quasi-equilibrium of these large grains may exist, depending on the time scales of sources, sinks and (as discussed below) interstellar cloud encounters.

Stars spend most of their lives in interstellar voids of density $n \sim 0.01 - 0.1\text{cm}^{-3}$. During these periods of typically tens of millions of years, the large grain population increases or comes into equilibrium. The large grains, once produced, are protected from external fragmentation by the heliospheric barrier at 130 - 400 AU. Upon entering a cloud of density $n \geq 1$ cm^{-3}, the heliosphere collapses to $\leq$ 40 AU and the large circumstellar grains are then exposed to the interstellar wind. Multiple impact fragmentation will rapidly ($\leq 5 \times 10^4$ yr) increase the disk area and IR luminosity. This time scale is much less than the Poynting-Robertson and internal-collision time scales (BP). Circumstellar grains of size $\leq 100\mu$m will be fragmented to smaller sizes and subsequent fragmentation will lead to the rapid multiplication of internal projectiles of sizes ≥ 1 μm which are capable of fragmenting grains larger than $\sim$100 μm. The ultimate enhancement of disk area and optical depth at the time the star leaves the cloud is difficult to estimate quantitatively. Once in the void again, only internal collisions and Poynting-Robertson drag will determine the evolution of the disk area. The numerous small new grains produced at distances $\geq$ 40 AU will slowly evolve inward due to Poynting-Robertson drag, further enhancing the optical depth. This general picture of how particulate disks interact with the interstellar medium can readily explain two observational features of the particulate disk stars: velocity streaming of the stars with the brightest particulate disks, and the absence of any detectable disks around A dwarfs later than A5.

4 Velocity Streaming

The criteria used to select the set of the 5 most significant disk stars is discussed in WMW. This conservatively chosen set consists of α Lyr, α Psa, β Pic, β Leo, and ζ Lep. Monte Carlo simulations were used to compare the velocity dispersions of sets chosen at random from the remaining 17 main sequence A stars listed in the Gliese catalog ($\leq$ 22 pc). It was found that dispersion velocities less than those of the particulate disk star set occurred

by chance in only 2% of the cases. Small dispersion velocities are normally indicative of streaming clusters of stars originating from the same birth cloud, or young field stars from unrelated clouds. However, we argued in WMW that neither interpretation is consistent with the low velocity dispersion of the disk star set.

Although the disk stars did not originate in any known cloud, the trajectory of the centroid of this group was shown (within velocity uncertainties) to pass through the massive Sco Oph cloud complex some 6 Myr ago. WMW suggested that the observed velocity streaming is a kinematical selection artifact of a model in which observable particulate disks are produced or greatly enhanced by episodic passages through interstellar clouds. As randomly moving stars pass through the cloud they are 'tagged' with disks of high optical depth (due to multiple fragmentation). But the only stars we are (currently) observing are those within 22 pc of the Sun. All of these tagged stars had to be aimed in the same general direction toward this relatively small volume and therefore their transverse velocity dispersions would necessarily be small. Of the 17 control stars, three passed through the Sco Oph cloud. Two of these controls are listed as stars with Vega-like IR excess by Backman and Gillett (1987). The third is a late A7 star and therefore this anomaly may be explained by magnetic shielding, which we consider next. Further discussion and details of this model are given in WMW.

5 Early - Late Asymmetry

There have been no positive measurements of stellar winds from main sequence A dwarfs, only limits of $\leq 10^{-10}$ $M_\odot$ yr^{-1}. Decreased stellar winds and therefore decreased magnetic shielding is indicated by the gap in X-ray emission between spectral types B8 and A5 (Rosner *et al.*, 1985). In the set of the 5 brightest disk stars none are later than A5. In the set of 11 A dwarfs which have been reported to have some IR excess by either Backman and Gillett (1987) or Aumann (1988), none are later than A5. In the set of 12 A dwarfs for which no IR excess was reported (Backman and Gillett, 1987) there are 4 stars later than A5, which is consistent with an unbiased sample. This striking bias against late A dwarfs having particulate disks is compatible with the X-ray evidence. The reduced heliospheric shielding in the early A spectral types implies more fragmentation of disk grains by interstellar cloud grains, while fragmentation is suppressed in the well shielded late spectral types. An early-late asymmetry is not apparent, nor necessarily expected, in the F and G dwarf data. This argues against the possibility that the A star asymmetry is due to observational selection.

Acknowledgements

We thank Drs. Dana Backman and Olin Eggen for helpful suggestions. This work was supported by grants from the Louisiana Educational Quality Support Fund and the NASA-Ames Research Center University Consortium.

References

[1] Aumann, H.H. 1985, PASP, **97**, 885.

[2] Aumann, H.H. 1988, AJ, **96**, 1415.

[3] Backman, D.E. and Gillett, F.C. 1987, in *Cool Stars, Stellar Systems and the Sun*, ed. J.L. Linsky and R.E. Stensel (Berlin:Springer), 340.

[4] Backman, D.E. and Paresce, F. 1992, in *Protostars and Planets III* (Tucson: Univ. Arizona Press), in press.

[5] Begelman, M.G. and Rees, M.J. 1976, Nature, **261**, 298.

[6] Frisch, P.C. and York, D.G. 1983, ApJ (Letters), **271**, L59.

[7] Frisch, P.C. 1986, in *The Galaxy and the Solar System*, ed. R. Smoluchowski, J.N. Bahcall and M.S. Matthews (Tucson: Univ. Arizona press), 83.

[8] Gillett, F.C. 1986, in *Light on Dark Matter*, ed. F.P. Israel (Dordecht: Reidel), 61.

[9] Grün, E., Zook, H.A., Fechtig, H., and Giese, R.H. 1985, Icarus, **62**, 244.

[10] Holzer, T.E. 1989, ARAA, **27**, 199.

[11] Levy, E.H. and Jokipii, J.R. 1976, Nature, **264**, 423.

[12] Lissauer, J.J. and Griffith, C.A. 1989, ApJ, **340**, 468.

[13] Matese, J.J., Whitmire, D.P., Lafleur, L.D., Reynolds, R.T., and Cassen, P.M. 1987, BAAS, **19**, 830.

[14] Rosner, R., Golub, L., and Vaiana, G.S. 1985, ARAA, **23**, 413.

[15] Weissman, P.R. 1984, Science, **224**, 987.

[16] Whitmire, D.P., Matese, J.J., and Whitman, P.G. 1992, ApJ, **388**, 190.